**University of Alberta**

# Numerical and Physical Modelling of Reciprocating Pumps for use in Gas Wells

by

**Jeffrey Jonathan Rudolf**

A thesis submitted to the Faculty of Graduate Studies and Research in partial fulfillment of the requirements for the degree of Master of Science.

Department of Mechanical Engineering

Edmonton, Alberta
Spring 2003

National Library of Canada
Acquisitions and Bibliographic Services
395 Wellington Street
Ottawa ON K1A 0N4
Canada

Bibliothèque nationale du Canada
Acquisitions et services bibliographiques
395, rue Wellington
Ottawa ON K1A 0N4
Canada

Your file Votre référence

Our file Notre référence

The author has granted a non-exclusive licence allowing the National Library of Canada to reproduce, loan, distribute or sell copies of this thesis in microform, paper or electronic formats.

L'auteur a accordé une licence non exclusive permettant à la Bibliothèque nationale du Canada de reproduire, prêter, distribuer ou vendre des copies de cette thèse sous la forme de microfiche/film, de reproduction sur papier ou sur format électronique.

The author retains ownership of the copyright in this thesis. Neither the thesis nor substantial extracts from it may be printed or otherwise reproduced without the author's permission.

L'auteur conserve la propriété du droit d'auteur qui protège cette thèse. Ni la thèse ni des extraits substantiels de celle-ci ne doivent être imprimés ou autrement reproduits sans son autorisation.

0-612-82340-7

Canada

**University of Alberta**

**Library Release Form**

**Name of Author:** Jeffrey Jonathan Rudolf

**Title of Thesis:** Numerical and Physical Modelling of Reciprocating Pumps for use in Gas Wells

**Degree:** Master of Science

**Year this Degree Granted:** 2003

Permission is hereby granted to the University of Alberta to reproduce single copies of this thesis and to lend or sell such copies for private, scholarly, or scientific research purposes only.

The author reserves all other publication and other rights in association with the copyright in the thesis, and except as hereinbefore provided, neither the thesis nor any substantial portion thereof may be printed or otherwise reproduced in any material form whatever without the author's prior written permission.

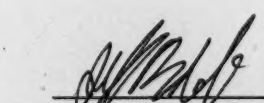

Jeffrey Jonathan Rudolf
19-111 Fairbrother Cr
Saskatoon, Saskatchewan
Canada, S7S 1L3

2003/3/17

*The heights by great men reached and kept*
*Were not attained by sudden flight,*
*But they while their companions slept*
*Were toiling upward in the night.*

—Longfellow

*Physics is like sex: sure, it may give some practical results, but that's not why we do it.*

—Richard Feynman

**University of Alberta**

**Faculty of Graduate Studies and Research**

The undersigned certify that they have read, and recommend to the Faculty of Graduate Studies and Research for acceptance, a thesis entitled Numerical and Physical Modelling of Reciprocating Pumps for use in Gas Wells submitted by Jeffrey Jonathan Rudolf in partial fulfillment of the requirements for the degree of Master of Science.

Dr. T.R. Heidrick (Supervisor)

Dr. B.A. Fleck (Co-Supervisor)

Dr. M. Polikar

Dr. P.C. Flynn

Date March 17/03

To my family and friends, especially my Parents.

# Abstract

## ABSTRACT

The production of natural gas from petroleum reservoirs often involves two-phase flow (gas and liquid phases). As the reservoir matures, its pressure becomes insufficient to sustain gas flow in this two-phase configuration. A new pumping concept has been patented by the Alberta Research Council in which gas and liquid phases flow separately and gas pressure is used to power a down-hole device to pump the liquid phase to the surface. The merit of this pumping concept for application to gas wells in Alberta has been investigated through the construction of a mathematical model for both two-phase flow and separate phases flow gas well configurations.

The applicability of using reciprocating pumps to perform this new pumping concept has also been investigated. Results from mathematical and physical modelling of a reciprocating pump have been used to modify and improve the separate phases gas flow model. This improved model was used to determine opti-

mum design parameters for implementation into a field application. The results of this research could now be used to design a prototype pumping device for field testing.

# Acknowledgements

I thank my research Supervisors Dr. Ted Heidrick, Dr. Raj Rajan and Dr. Brian Fleck for their guidance throughout this endeavour. I also thank Mr. Rod Ridley for providing helpful advice along the way.

I thank Mr. Gerard Korpany and Mr. Mario DeRocco of the Alberta Research Council as well as the U of A Mechanical Engineering Machine Shop for providing valuable technical support.

I also thank my lab partners Marty Lastiwka, Mike Wojcichowsky and Chris Sideroff whose research projects were always enlightening distractions from my own work.

Thanks goes out to all my friends currently working in the "Patch". Their practical advice was greatly appreciated.

Finally, I am grateful for the financial support provided to me by the Alberta Research Council and the Natural Science and Engineering Research Council of Canada.

# CONTENTS


**1 Introduction** **1**

1.1 Natural Gas Production . . . . . 1

1.1.1 Natural Gas Production in Canada . . . . . 3

1.1.2 Natural Gas Production in United States . . . . . 3

1.2 Liquid Loading Problems in Natural Gas Wells . . . . . 4

1.2.1 Current Practice . . . . . 5

1.3 ARC Pumping Concept . . . . . 7

1.4 Objectives of the Research Work . . . . . 9

**2 Mathematical Model of Flow in a Natural Gas Well** **12**

2.1 Mathematical Model of a Gas Well in a Two-Phase Flow Configuration . . . . . 13

2.1.1 Calculation Methodology . . . . . 13

2.1.2 Minimum Gas Flow Model . . . . . 14

2.1.3 Two-Phase Flow Model . . . . . 17

2.1.4 Reservoir Inflow Model . . . . . 21

2.2 Mathematical Model of a Gas Well in a Separate Phases Flow Configuration . . . . . 22

2.2.1 Calculation Methodology . . . . . 23

2.2.2 Gas Flow Model . . . . . 23

2.2.3 Liquid Work Model . . . . . 28

2.2.4 Pump Model . . . . . 29

2.3 Selected Gas Well . . . . . 30

2.4 Model Results . . . . . 31

2.4.1 Calculation Procedure . . . . . 32

2.4.2 Constant Liquid Rate . . . . . 34

2.4.3 Constant Gas-Liquid Ratio . . . . . 39

2.5 Effect of Field Conditions . . . . . 42

2.5.1 Gas Well Depth . . . . . 42
2.5.2 Reservoir Inflow Resistance . . . . . 44
2.5.3 Gas Well Liquid Production . . . . . 47
2.6 Summary . . . . . 50

**3 Mathematical Model of a Reciprocating Pump 51**
3.1 Direct-Acting Reciprocating Pumps . . . . . 51
3.2 Description of a Direct-Acting Pump used in the ARC Pumping Concept . . . . . 54
3.2.1 Description of Pump Operation . . . . . 54
3.3 Mathematical Model of the Direct Acting Pump Performance 56
3.3.1 Definitions and Assumptions . . . . . 57
3.3.2 Gas Utilization . . . . . 59
3.3.3 Pump Friction . . . . . 60
3.3.4 Thermodynamic Efficiency . . . . . 62
3.4 Summary . . . . . 67

**4 Physical Model of a Reciprocating Pump 69**
4.1 Description of the Apparatus . . . . . 69
4.1.1 Physical Pump Model . . . . . 69
4.1.2 Test Facility . . . . . 77
4.1.3 Instrumentation and Data Acquisition . . . . . 81
4.2 Test Procedure . . . . . 83
4.3 Results . . . . . 85
4.3.1 Gas Utilization . . . . . 85
4.3.2 Friction . . . . . 88
4.3.3 Thermodynamic Efficiency . . . . . 102
4.4 Summary . . . . . 108

**5 Application of Reciprocating Pumps in Gas Wells 109**
5.1 Implementation of a Mathematical Model for Reciprocation Pump Application . . . . . 110
5.1.1 Mathematical Model of Field Application . . . . . 110
5.1.2 Simplifying Assumptions . . . . . 112
5.2 Model Results . . . . . 117
5.2.1 Effect of Pump Area Ratio . . . . . 117
5.2.2 Optimum Area Ratio . . . . . 123
5.2.3 Effect of Pump Friction . . . . . 130

5.3 Effect of Field Parameters . . . . . 137
5.3.1 Gas Well Depth . . . . . 137
5.3.2 Reservoir Inflow Resistance . . . . . 139
5.3.3 Gas Well Liquid Production . . . . . 141
5.4 Summary . . . . . 144

**6 Conclusion** **146**
6.1 Conclusions . . . . . 146
6.2 Recommendations for Future Work . . . . . 150

**A Selection of a "Typical" Alberta Natural Gas Well** **153**
A.1 Classification of Alberta Gas Wells . . . . . 153
A.2 Selection of a "Typical" Alberta Gas Well . . . . . 157
A.2.1 Gas Well Properties . . . . . 157
A.2.2 Reservoir Inflow Properties . . . . . 157
A.2.3 Composition of Natural Gas Mixture . . . . . 158
A.2.4 Properties of Gas and Liquid Phases . . . . . 161

**B Estimation of Properties of Natural Gas Mixture** **162**
B.1 Molecular Weight of Gas Mixture . . . . . 162
B.2 Pseudocritical Properties . . . . . 163
B.3 Calculation of z-Factor . . . . . 164
B.4 Viscosity of Natural Gas Mixture . . . . . 167
B.5 Specific Heat Ratio for Gas Mixture . . . . . 168

**C Numerical Techniques Used in the Gas Well Model** **169**
C.1 Numerical Integration of Two-Phase Flow Pressure Gradient . 170
C.2 Numerical Integration of the Dry Gas Flow Pressure Gradient 172
C.3 Minimum Reservoir Pressure for Constant Liquid Production Rate . . . . . 173
C.4 Optimum Area Ratio for Constant Liquid Production Rate . . 178

**D Tests Performed** **182**

**E Test Data Analysis** **184**
E.1 Analysis of Steady Data . . . . . 184
E.2 Analysis of Transient Data . . . . . 186
E.3 Correction to Determine Pump Intake Pressure . . . . . 188

# List of Figures


| | | |
|---|---|---|
| 1.1 | Diagram of a Wellbore for a typical Natural Gas Well | 2 |
| 1.2 | Schematic of the Progression of Liquid Loading in a Gas Well | 4 |
| 1.3 | Schematic of Application of the ARC Pumping Concept | 8 |
| 1.4 | Thesis Methodology | 11 |
| 2.1 | Logic of Mathematical Model for Gas Well Experiencing Liquid Loading Problems | 14 |
| 2.2 | Schematic of Flow in a Rectangular Porous Medium | 21 |
| 2.3 | Logic of Mathematical Model for Separate Flow of Natural Gas and Reservoir Liquid | 24 |
| 2.4 | Diagram of a Pipeline Element | 25 |
| 2.5 | Minimum Reservoir Pressures for Constant Liquid Production of 7 $m^3$/day | 36 |
| 2.6 | Normalized Minimum Reservoir Pressures for Constant Liquid Production of 7 $m^3$/day | 37 |
| 2.7 | Gas Flow Rates at Minimum Reservoir Pressures for Constant Liquid Production of 7 $m^3$/day | 38 |
| 2.8 | Minimum Reservoir Pressures for Constant Gas-Liquid Ratio of 3671 | 40 |
| 2.9 | Normalized Minimum Reservoir Pressures for Constant Gas-Liquid Ratio of 3671 | 41 |
| 2.10 | Effect of Gas Well Depth on $\Delta P_{RES}$ for Constant Liquid Production Rate of 7 $m^3$/day | 43 |
| 2.11 | Effect of Gas Well Depth on $\Delta P_{RES}$ for Constant Gas-Liquid Ratio of 3671 | 44 |
| 2.12 | Effect of Reservoir Inflow Resistance on $\Delta P_{RES}$ for Constant Liquid Production of 7 $m^3$/day | 45 |
| 2.13 | Effect of Reservoir Inflow Resistance on $\Delta P_{RES}$ for Constant Gas-Liquid Ratio of 3671 | 46 |

2.14 Effect of Liquid Production on $\Delta P_{RES}$ for Constant Liquid Production Rate Scenario . . . . . 48
2.15 Effect of Changing Gas-Liquid Ratio on $\Delta P_{RES}$ . . . . . 49

3.1 Schematic of Direct-Acting Reciprocating Pump Operation 53
3.2 Schematic of Direct-Acting Reciprocating Pump Application in the ARC Technology . . . . . 55
3.3 Schematic of Direct-Acting Reciprocating Pump . . . . . 57
3.4 Thermodynamic Efficiency as a Function of Normalized Pressure for a Gas-Powered, Direct-Acting Reciprocating Pump . . . . . 65
3.5 Effect of Friction on Pump Thermodynamic Efficiency . . . 67

4.1 Schematic of Test Reciprocating Pump . . . . . 71
4.2 Photograph of Test Reciprocating Pump . . . . . 72
4.3 Schematic of Pumping Element in Physical Pump Model . . 73
4.4 Photograph of Test Pump Components . . . . . 74
4.5 Close-up of Liquid and End Section . . . . . 75
4.6 Schematic of Gas Flow Loop . . . . . 78
4.7 Schematic of Liquid Flow Loop . . . . . 80
4.8 Experimental and Mathematical Model Gas-Liquid Volume Ratios for Physical Pump Model . . . . . 87
4.9 Pump Friction Results for Single and Two-Stage Pump Operation($P_{PUMP}$ = 925 kPag) . . . . . 90
4.10 Pump Friction Results for Single and Two-Stage Pump Operation($P_{PUMP}$ = 215 kPag) . . . . . 91
4.11 $\Delta P_{GAS}$ Trace For Test No. 19 at a Liquid Flowrate of 4 mL/s 92
4.12 $\Delta P_{GAS}$ Trace For Test No. 19 at a Liquid Flowrate of 12.6 mL/s . . . . . 93
4.13 $\Delta P_{GAS}$ Trace For Test No. 19 at a Liquid Flowrate of 33 mL/s . . . . . 94
4.14 $P_{FRICTION}$ Repeatability Test Results for Single Stage Operation . . . . . 95
4.15 $P_{FRICTION}$ Repeatability Test Results for Two Stage Operation . . . . . 96
4.16 Friction Coefficient Results for Single and Two-Stage Pump Operation ($P_{PUMP}$ = 925 kPag) . . . . . 97

4.17 Friction Coefficient Results for Single and Two-Stage Pump Operation ($P_{PUMP}$ = 215 kPag) . . . . . 98
4.18 Gas Differential Pressure Measurement for Single Stage(Bottom) (a) and Two-Stage Pump (b) Operation . . . . . 99
4.19 Comparison of Single Stage (Top) and Single Stage (Bottom) $P_{FRICTION}$ Results . . . . . 101
4.20 Thermodynamic Efficiency of Experimental Pump at $P_{PUMP}$ = 215 kPag . . . . . 104
4.21 Thermodynamic Efficiency of Experimental Pump at $P_{PUMP}$ = 925 kPag . . . . . 106
4.22 Thermodynamic Efficiency of Experimental Pump at $\tilde{P}_{PUMP}$ = 0.14 . . . . . 107

5.1 Force Balance on Pumping Element . . . . . 111
5.2 Estimate of Differential Pressure From Pump Intake to Wellhead . . . . . 116
5.3 Schematic of Model Solution Procedure to Examine Effect of Area Ratio . . . . . 119
5.4 Effect of Area Ratio on Normalized Minimum Reservoir Pressure for Constant Liquid Production Rate of 7 $m^3$/day 120
5.5 Effect of Area Ratio on Normalized Minimum Reservoir Pressure for Constant Gas Liquid Production Ratio of 3671 122
5.6 Schematic of Solution Procedure to Determine Optimum Area Ratio for Constant Liquid Rate . . . . . 125
5.7 Optimum Area Ratio for Typical Alberta Gas Well at Constant Gas Liquid Production Rate of 7 $m^3$/day . . . . . 126
5.8 Normalized Reservoir Pressure for Optimum Pump Area Ratio at Constant Gas Liquid Production Rate of 7 $m^3$/day 127
5.9 Optimum Pump Area Ratio at Constant Gas Liquid Production Ratio of 3671 . . . . . 129
5.10 Normalized Reservoir Pressure for Optimum Pump Area Ratio at Constant Gas Liquid Production Ratio of 3671 . . 131
5.11 Optimum Area Ratio With and Without Friction at Constant Gas Liquid Production Rate of 7 $m^3$/day . . . . . 132
5.12 Effect of Friction on Normalized Reservoir Pressure for Optimum Area Ratio at Constant Gas Liquid Production Rate of 7$m^3$/day . . . . . 133

5.13 Effect of Friction on Normalized Minimum Reservoir Pressure for Optimum Area Ratio at Constant Gas to Liquid Production Ratio of 3671 . . . . . 136
5.14 Effect of Gas Well Depth on Optimum Area Ratio for Constant Liquid Production Rate of 7 $m^3$/day . . . . . 138
5.15 Effect of Reservoir Inflow Resistance on Optimum Area Ratio for Constant Liquid Production Rate of 7 $m^3$/day . . . . 140
5.16 Effect of Liquid Production on Optimum Area Ratio for Constant Liquid Production Rate . . . . . 142
5.17 Effect of Liquid Production on Optimum Area Ratio for Constant Gas to Liquid Production Ratio . . . . . 143

A.1 Number of Alberta Gas Wells by Depth . . . . . 155

C.1 Diagram of a Pipeline Element . . . . . 171
C.2 Schematic of Models Used to Calculate Reservoir Pressure . 174
C.3 Reservoir Pressure as a Function of Gas Flowrate for the Typical Alberta Gas Well at $P_{WH} = 1000$ kPa . . . . . 175
C.4 Schematic of Minimization Algorithm to Determine Minimum Reservoir Pressure . . . . . 176
C.5 Schematic of Solution Procedure to Determine Optimum Area Ratio for Constant Liquid Rate . . . . . 180
C.6 Wellhead Pressure as a Function of Gas Flowrate for Gas Well in Appendix B at Reservoir Pressure of 1200 kPa . . . 181

E.1 Typical Sample of Steady Raw Data . . . . . 185
E.2 Typical Sample of Transient Raw Data . . . . . 187
E.3 Schematic of Gas Flow Loop used to Determine Pressure Correction . . . . . 190
E.4 Experimental Results for Determining Empirical Constant 'B' to Correct the Gas Tank Intake Pressure . . . . . 191
E.5 Experimental Results for Validating Empirical Constant 'B' to Correct the Gas Tank Intake Pressure . . . . . 192

# List of Tables


4.1 Gas and Liquid Flow Loop Instrumentation . . . . . 81

A.1 Alberta Gas Wells Sorted by Depth . . . . . 156
A.2 Properties of "Typical" Alberta Gas Well . . . . . 158
A.3 Reservoir Inflow Properties . . . . . 159
A.4 Composition of Gas Mixture . . . . . 160
A.5 Gas Mixture and Liquid Properties . . . . . 161

B.1 Critical Properties of Natural Gas Components . . . . . 165
B.2 Values of Coefficients in Equation B.7 . . . . . 166

D.1 Test Matrix . . . . . 183

# NOMENCLATURE

## LATIN SYMBOLS

| | |
|---|---|
| $A$ | Cross-Sectional Area |
| $A_G$ | Cross-Sectional Area of a Gas-Side of Reciprocating Pump |
| $A_L$ | Cross-Sectional Area of a Liquid-Side of Reciprocating Pump |
| $A_R$ | Area Ratio of a Gas-Driven Reciprocating Pump |
| $C$ | Constant in Back-Pressure Equation |
| $C_D$ | Drag Coefficient on Spherical Particle |
| $C_F$ | Friction Coefficient of Reciprocating Pump |
| $d_p$ | Diameter of Liquid Droplet Modelled as a Rigid Spherical Particle |
| $d_t$ | Diameter of Production Tubing |
| $\frac{dP}{dL}$ | Pressure Gradient |
| $\left.\frac{dP}{dL}\right\|_{lo}$ | Pressure Gradient of Liquid Flow Only |
| $E$, $F$ *and* $H$ | Dimensionless Parameters in Freidel Correlation |

$E_1$ *and* $E_2$ ..... Dimensionless Parameters in CISE Correlation

$f$ ..... Pipe Flow Friction Factor

$f_{go}$ ..... Pipe Flow Friction Factor of Gas Flow Only

$f_{lo}$ ..... Pipe Flow Friction Factor of Liquid Flow Only

$F_{Friction}$ ..... Net Friction Force Acting On Pumping Element

$Fr_h$ ..... Froude Number Based on Homogeneous Two-Phase Flow

$G$ ..... Mass Flux of Fluid Flow

$G_g$ ..... Mass Flux of Gas Phase in Two-Phase Fluid Flow

$G_l$ ..... Mass Flux of Liquid Phase in Two-Phase Fluid Flow

$g$ ..... Gravitational Acceleration

$k$ ..... Ratio of Gas Specific Heats at Constant Pressure and Constant Volume

$k_P$ ..... Permeability of Porous Media

$L$ ..... Length Coordinate

$L_W$ ..... Length of the Gas Well

$M_W$ ..... Molecular Weight

$\dot{m}$ ..... Mass Flow Rate

$n$ ..... Exponent in Back-Pressure Equation

$P$ ..... Pressure (kPa)

$P_{BH}$ ..... Bottomhole Pressure(Pressure at Bottom of the Gas Well)

$P_c$ ..... Critical Pressure

$P_{DIS}$ ..... Pump Drive Gas Discharge Pressure

$P_{FRICTION}$ ..... Pump Friction Pressure (Equivalent Pumping Pressure)

$P_{IN}$ ..... Pump Drive Gas Intake Pressure

$P_{pc}$ ..... Pseudo-Critical Pressure

$P_{PUMP}$ ..... Pumping Pressure

$\tilde{P}_{PUMP}$ ..... Normalized Pumping Pressure

$P_r$ ..... Reduced Pressure

$P_{sc}$ ..... Pressure at Standard Conditions (101.325 kPa)

$P_{RES}$ ..... Pressure of Petroleum Reservoir

$P_{WH}$ ..... Wellhead Pressure

$Q_g$ ..... Volumetric Flowrate of Gas Phase

$Q_{g,sc}$ ..... Volumetric Flowrate of Gas at Standard Conditions

$Q$ ..... Volumetric Flowrate

$Q_l$ ..... Volumetric Flowrate of Liquid

$R$ ..... Ideal Gas Constant (=8.3154 kJ/kmol/K)

$Re_p$ ..... Reynolds Number based on Diameter of a Spherical Particle

$Re_t$ ..... Pipe Flow Reynolds Number based on Diameter of a Production Tubing

$R_{gl}$ ..... Gas-Liquid Volume ratio at Standard Conditions

$S$ ..... Slip Ratio of Two-Phase Mixture(Gas to Liquid Velocity)

$S_g$ ..... Specific Gravity of the Gas Mixture with Respect to Air

$S_L$ ..... Stroke Length of a Reciprocating Pump

$T$ ..... Temperature

$T_c$ ..... Critical Temperature

$T_{pc}$ ..... Pseudo-Critical Temperature

$T_{RES}$ ..... Temperature of Petroleum Reservoir

$T_r$ ..... Reduced Temperature

$T_{sc}$ ..... Temperature at Standard Conditions (288.8K)

$v$ ..... Specific Volume of Fluid

$V$ ..... Fluid Velocity

$V_g$ ..... Gas flow Velocity

$\hat{V}_g$ ..... Volume of Gas per Stroke

$V_{gmin}$ ..... Minimum Velocity of the Gas Phase

$\hat{V}_l$ ..... Volume of Liquid per Stroke

$V_l$ ..... Liquid flow Velocity

$V_P$ ..... Pump Piston Velocity

$W$ ..... Rate of Work or Pump Power

$W_l$ ..... Rate of Work Required to Bring Liquid Phase to the Surface

$W_g$ ..... Rate of Work Obtained from Gas Phase

$We_p$ ..... Weber Number Based on Diameter of Spherical Liquid Droplet

$We_h$ ..... Weber Number Based on Homogeneous Two-Phase Flow

$x$ ..... Quality (Mass Fraction) of Gas in Two-Phase Mixture

$Y$ ..... Mass Fraction of Gas Component in Gas Mixture

$Z$ ..... Depth Coordinate

$Z_W$ ..... Depth of Gas Well

$z$ ..... Gas Compressibility Factor

GREEK SYMBOLS

$\alpha$ ..... Void Fraction of Two-Phase Mixture

$\beta$ ..... Dimensionless Parameters in CISE Correlation

$\Delta P$ ..... Change in Pressure

$\Delta P_{RES}$ ..... Difference in Minimum Reservoir Pressure from Two-Phase to Separate Phases Gas Well Operation

$\Delta P_{TL}$ ..... Friction Losses in the Liquid Tubing

$\epsilon$ ..... Roughness Height

$\varepsilon$ ..... Wichert and Aziz Correction

$\Phi^2$ ..... Two-Phase Multiplier

$\Phi^2_{lo}$ ..... Two-Phase Multiplier based on Liquid Phase Only

$\eta$ ..... Thermodynamic Efficiency

$\mu_g$ ..... Dynamic Viscosity of the Gas Phase

$\mu_l$ ..... Dynamic Viscosity of the Liquid Phase

$\rho_g$ ..... Density of the Gas Phase

$\rho_l$ ..... Density of the Liquid Phase

$\rho_r$ ..... Reduced Density

$\sigma$ ..... Surface Tension of Liquid

ACRONYMS

*ARC* ..... Alberta Research Council

*DARP* ..... Direct-Acting Reciprocating Pump

*GLR* ..... Gas to Liquid Volume Ratio at Standard Conditions

*SLPM* ..... Standard Liters per Minute (1 Atm and 0°)

CHAPTER 1

# Introduction

## 1.1 Natural Gas Production

Natural gas is a mixture of hydrocarbons (primarily methane) and non-hydrocarbons such as carbon dioxide ($CO_2$), nitrogen ($N_2$), hydrogen sulphide ($H_2S$) and water vapour. Natural gas is primarily obtained from petroleum reservoirs located beneath the earth and is brought to the surface using natural gas wells. The structure of a typical natural gas well is shown in Figure 1.1.

A typical natural gas well consists of a hole drilled into the ground from the surface to a depth where a natural gas reservoir is present. The hole, commonly referred to as the wellbore, is lined with a steel pipe called the casing. The casing is usually perforated at the depth at which the natural gas reservoir is present. The perforations in the casing allow the natural gas to flow from the reservoir into the bottom of the wellbore. Typically, a second pipe is set in the wellbore, known as the production tubing, and is

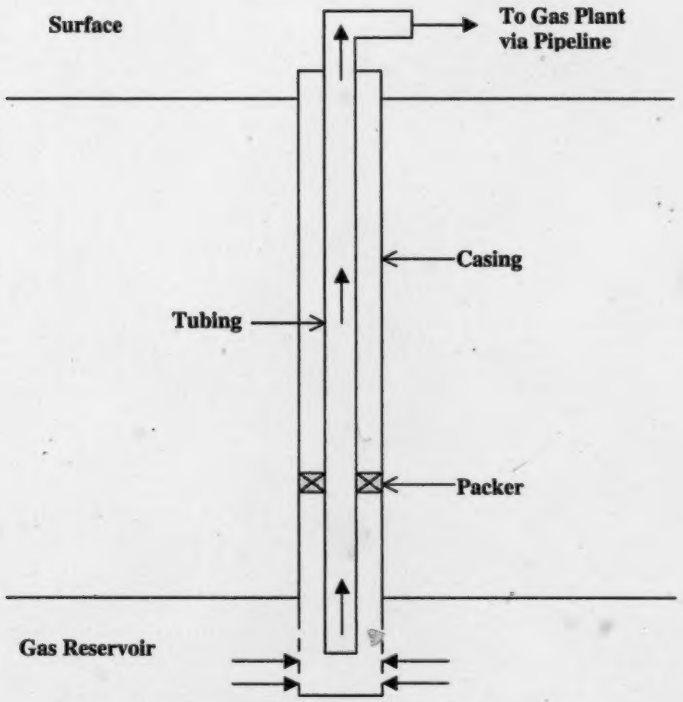


**Figure 1.1: Diagram of a Wellbore for a typical Natural Gas Well**

usually sealed in the wellbore by a packer.

In most gas wells, some liquids are produced (either water or hydrocarbon condensate) as droplets in the gas stream. In a typical situation, reservoir fluids (natural gas and some amount of liquid phase) flow from the natural gas reservoir into the bottom of the wellbore, from the bottom of the wellbore to the surface via the tubing. From the surface the reservoir fluids travel to

a gas plant where they are processed (to remove desired and undesired components of the gas mixture) through compression, fractionation, separation, dehydration and/or desulphurization equipment.

### 1.1.1 Natural Gas Production in Canada

Canada is the world's third largest producer of natural gas. Each year Canada produces approximate 6 trillion cubic feet (TCF) from approximately 73,000 flowing gas wells. Each year, approximately 4,000 gas wells are drilled to maintain this production level. Natural gas production is based primarily in Western Canada with approximately 3,000 flowing gas wells in British Columbia, 7,000 flowing gas wells in Saskatchewan and approximately 60,000 gas wells flowing in Alberta [3].

### 1.1.2 Natural Gas Production in United States

The United States is the world's second largest producer of natural gas and produces about 20 TCF annually. To maintain this level of production the United States consistently drills about 10,000 new gas wells each year. As well, there are currently approximately 311,000 flowing gas wells in the United States. Natural gas wells are spread throughout the United States, with large numbers of wells in Texas (57,000), Ohio (34,000) and West Virginia (31,000) [1].

## 1.2 Liquid Loading Problems in Natural Gas Wells

A common production problem in natural gas wells is liquid loading. The process of liquid loading is shown schematically in Figure 1.2. In the early

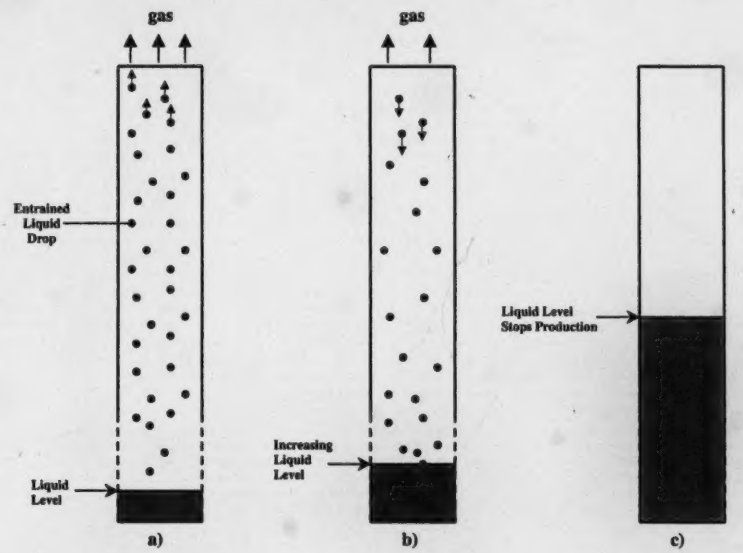


**Figure 1.2: Schematic of the Progression of Liquid Loading in a Gas Well**

life of a natural gas well, the reservoir pressure allows the gas wells to produce at a rate sufficient to carry the liquid phase (primarily as dispersed droplets) to the surface along with the gas phase (Figure 1.2a)). As the reservoir matures, its pressure decreases and subsequently the gas flowrate becomes insufficient to carry the produced liquids to the surface. The produced liquids subsequently fall back into the wellbore and begin to build up at the bottom of the well (Figure 1.2 b)). As liquid loading progresses, the

column of liquid built up in the wellbore exerts back-pressure on the natural gas reservoir. Production for the well decreases until the reservoir fluids no longer flow into the bottom of the wellbore (Figure 1.2 c)). Liquid loading is a phenomenon experienced by all natural gas wells at some point in their producing life. Coleman et al. [5] points out that liquid loading problems are generally controlled by the wellhead pressure and the diameter of the production tubing. If liquid loading problems are not addressed, the life of the natural gas well and overall recovery from the petroleum reservoir can be severely compromised [14].

### 1.2.1 Current Practice

Current practice in industry to solve liquid loading problems utilizes a number of different methods, but some of the more common techniques are described below.

One method is to stop the flow of gas at the surface (or shut-in the well) for some time. Gas pressure then builds up in the well and in the nearby reservoir region. After the well has been shut-in for some time, the gas is allowed to flow from the well at a velocity high enough to carry the liquid phase to the surface due to the built up pressure. This incremental gas velocity is temporary and decreases as the gas pressure in the well and nearby reservoir region is depleted to some quasi-steady value. Liquid will begin to build up in the wellbore and thus subsequent shut-in cycles will be required to keep the gas well flowing. This method is commonly known as intermittent flow and is described by Lea and Tighe [18].

An improvement over intermittent flow is plunger lift. In plunger lift, a plunger is placed in the production tubing to act as interface between the built up liquid and gas phase to carry liquid to the surface. In essence, the plunger acts like a pipeline pig. The gas well is operated in the same manner as intermittent flow by operating the gas well with shut-in and flowing cycles. A thorough description a plunger operation is given by Beauregard and Ferguson [2]. The weakness of both plunger lift and intermittent flow is that the gas well is operated periodically, rather than in a continuous fashion.

Another method used to solve liquid loading problems is to replace the original production tubing with a smaller diameter pipe. The smaller diameter results in a higher gas velocity in the well which is sufficient to carry the liquid phase to the surface [14]. The drawback with this method is that it is costly to change out the production tubing in a gas well and installing a small diameter tubing initially, leads to excessive pressure losses due to viscous friction.

Liquid loading problems are often solved through injection of a surfactant into the gas well. This surfactant mixes with the gas and liquid phases to create a foam with a density lower than that of the liquid phase. Because of the foam's lower density, much lower gas velocities are required to carry it to the surface [28]. A drawback with surfactants is that they do work well when water is the liquid phase, but have had less success when hydrocarbon condensate is present [30].

Liquid loading problems are also addressed by reducing the back-pressure at the wellhead (or surface). By lowering the wellhead pressure, the gas flowrate and hence flow velocity increases to a value sufficient to carry the liquid phase to the surface. This is usually done by placing a compressor at the surface to raise the gas pressure high enough so it can flow to a gas processing facility. This method, however, has operating costs to power the compressor and keep the gas well flowing.

## 1.3 ARC Pumping Concept

A new pumping concept has been developed and patented by the Alberta Research Council [25, 26, 27] aimed at solving liquid loading problems in natural gas wells producing from mature reservoirs.

This concept comprises of a down-hole pump that uses gas pressure from the gas reservoir as the driver to bring the produced liquid (water and/or condensate) phase from the reservoir to the surface separate from gas phase. By producing a natural gas well in this manner, the reservoir pressure (and hence reservoir energy) could be used more efficiently and production from the natural gas well can be restored. This will increase the overall recovery from the reservoir. A schematic of this pumping concept is shown in Figure 1.3.

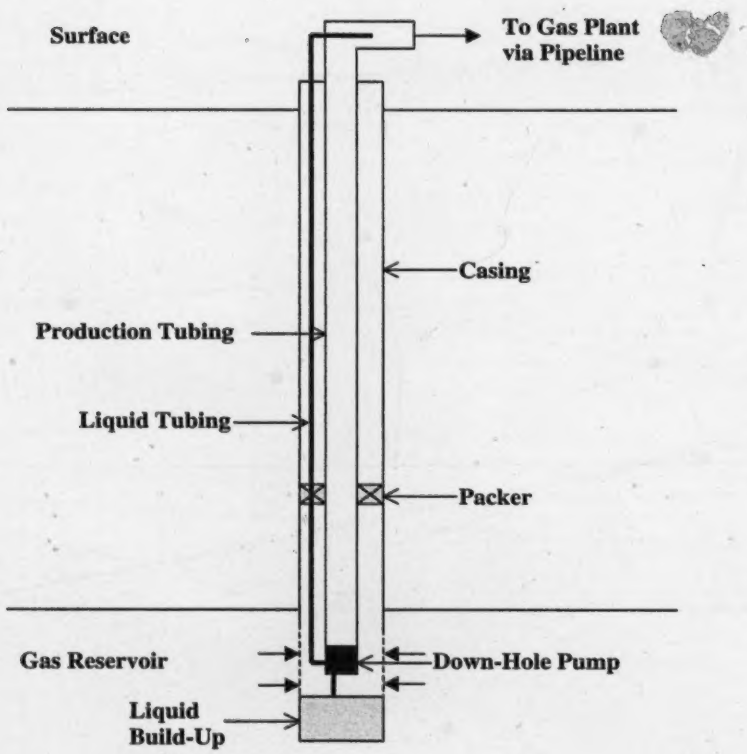


Figure 1.3: Schematic of Application of the ARC Pumping Concept

The gas and liquid phases enter the bottom of the wellbore where the two phases are separated by gravity. The gas phase then enters the down-hole pump placed at the bottom of the production tubing, does some work and then exits the pump up the production tubing. The liquid phase flows into the bottom of the wellbore, builds up and enters the down-hole pump where it is pumped up a second tubing string, called the liquid tubing. In the preferred embodiment of the Alberta Research Council (ARC) patents, the pump is of a direct-acting reciprocating type, but the downhole pump could be any type of pump that is driven by gas pressure to pump the liquid built up in the wellbore.

## 1.4 Objectives of the Research Work

The purpose of this research work was to determine the applicability of reciprocating pumps for use in the pumping concept proposed by the ARC to solve liquid loading problems in natural gas wells. The methodology used in this work is shown in Figure 1.4 and consisted of the following stages:

- Before any type of pump was investigated for use in the pumping concept patented by the ARC, justification was required for operating a gas well with liquid loading problems in a separated phases flow configuration. To obtain this, mathematical flow models of a gas well operating in a conventional two-phase flow, and operating with gas and liquid phases flowing separately were constructed. In the separate phases flow model, gas pressure is used in the most efficient manner

possible to power a device to pump the liquid phase to the surface. Both gas well flow models were then analyzed using data from a "typical" Alberta gas well to determine and compare the minimum reservoir pressure required to sustain gas flow in each configuration.

- An understanding of reciprocating pumps and their possible application in the ARC pumping concept was then obtained. This provides the base required for the development of mathematical models to predict pump performance characteristics.

- A physical model of a reciprocating pump application was constructed and its performance is tested in a low-pressure air and water flow loop. The results of these tests were compared with the predictions by the mathematical models to give further insight into pump performance.

- Results from the mathematical and physical pump modelling were used to construct a field model application of a reciprocating pump to operate a gas well with liquid loading problems in a separate flow configuration. This model was used to determine the minimum reservoir pressure required to sustain gas flow and to determine optimum design and field conditions for solving liquid loading problems.

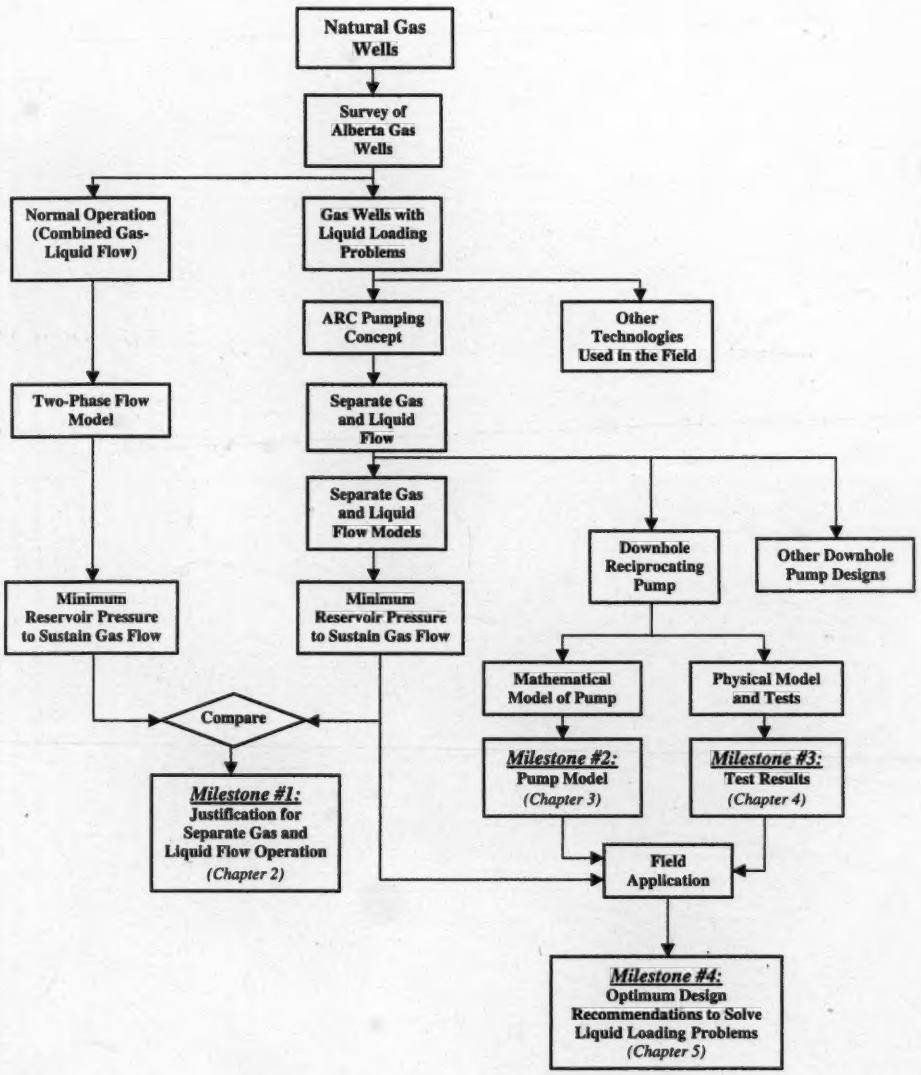
Natural Gas Wells
Survey of Alberta Gas Wells
Normal Operation (Combined Gas-Liquid Flow)
Gas Wells with Liquid Loading Problems
ARC Pumping Concept
Other Technologies Used in the Field
Two-Phase Flow Model
Separate Gas and Liquid Flow
Separate Gas and Liquid Flow Models
Downhole Reciprocating Pump
Other Downhole Pump Designs
Minimum Reservoir Pressure to Sustain Gas Flow
Minimum Reservoir Pressure to Sustain Gas Flow
Mathematical Model of Pump
Physical Model and Tests
Compare
Milestone #2: Pump Model (Chapter 3)
Milestone #3: Test Results (Chapter 4)
Milestone #1: Justification for Separate Gas and Liquid Flow Operation (Chapter 2)
Field Application
Milestone #4: Optimum Design Recommendations to Solve Liquid Loading Problems (Chapter 5)

**Figure 1.4: Thesis Methodology**

# CHAPTER 2

# Mathematical Model of Flow in a Natural Gas Well

The purpose of this chapter is determine the applicability of the pumping concept proposed by the Alberta Research Council, which is to operate a natural gas well by producing the liquid and gas phases separately and pressure from the gas phase is used to power a device to pump the liquid phase to the surface.

To accomplish this, a mathematical model of a gas well operating in a conventional two-phase flow will be developed. Then, a mathematical model is introduced where a gas well operates with the gas and liquid phases produced separately and if the liquid phase is pumped by some "device" that uses gas pressure in the most efficient manner possible. These models are then be used to determine the minimum reservoir pressure required to keep a "typical" Alberta natural gas well flowing. A comparison of the minimum reservoir pressures will indicate the applicability of the concept proposed by the ARC. As well, the effect of gas well depth, liquid production rate and

reservoir flow resistance will be investigated in order to better understand natural gas well characteristics where the ARC concept is best applied.

## 2.1 Mathematical Model of a Gas Well in a Two-Phase Flow Configuration

In this model, the natural gas well is assumed to be operated in a standard configuration, shown previously in Figure 1.1. In this configuration, production from the natural gas well has both gas and reservoir liquids flow from the reservoir to the bottom of the wellbore. From the bottom of the wellbore the gas and liquids flow to the surface as a two-phase mixture.

### 2.1.1 Calculation Methodology

To model this configuration, the following sequence (shown schematically in Figure 2.1) was followed. Starting from the wellhead pressure, the minimum gas flowrate required to bring the produced liquids to the surface is calculated. This gas flowrate and corresponding liquid production rate are entered into a two-phase flow model to estimate the pressure of the gas well at the bottom (bottomhole pressure or $P_{BH}$). Then, the bottomhole pressure and minimum gas flowrate are entered into a reservoir inflow model, which determines the reservoir pressure. Each segment of this model is explained in detail in the following sections.

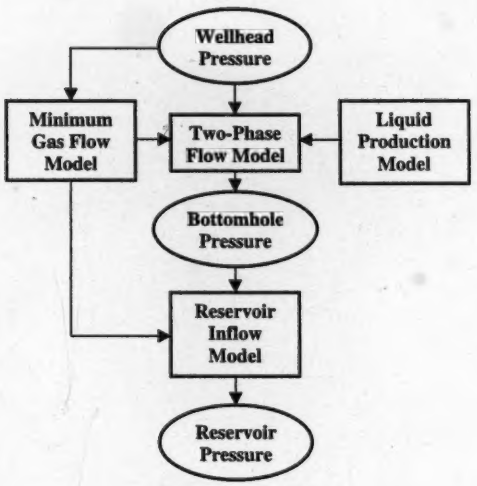


**Figure 2.1: Logic of Mathematical Model for Gas Well Experiencing Liquid Loading Problems**

### 2.1.2 Minimum Gas Flow Model

The minimum gas flowrate required to carry the produced liquids to the surface was determined using a model based on the method of Turner et al. [29]. This model predicts that the flow velocity required to carry the liquids to the surface is equal to the terminal velocity of the liquid drops. Using this model, the terminal (or minimum gas velocity) velocity of the liquid drop is given by:

$$V_{gmin} = \left[\frac{40g\sigma(\rho_l - \rho_g)}{\rho_g^2 C_D}\right]^{1/4} \tag{2.1}$$

Equation 2.1 determines the terminal velocity of a rigid, spherical droplet in a stagnant fluid. Turner assumes a flow regime with a moderately high

Reynolds number where the drag coefficient does not vary significantly. Thus, Turner used a constant drag coefficient with a value of 0.44. Since the drag coefficient is not actually constant, a correlation to account for the variability in the drag coefficient given by White [34] was chosen. This correlation has the form:

$$C_D = \frac{24}{Re_p} + \frac{6}{1+\sqrt{Re_p}} + 0.4 \tag{2.2}$$

where $Re_p$ is the droplet Reynolds number in the flow. This equation is valid for the range of Reynolds number from 1 to 200,000 (which is the range of Reynolds number expected for this type of flow) with an accuracy of $\pm$ 10 percent. The Reynolds number is defined in this case by the equation:

$$Re_p = \frac{\rho_g V_g d_p}{\mu_g} \tag{2.3}$$

In order to determine the Reynolds number, a model for the size of liquid droplets is required. Hinze [12] found that for liquid droplets the maximum diameter is governed by the Weber number. Weber number is a ratio of the stagnation pressure of the flowing fluid to surface tension in the droplet and has the following form:

$$We_p = \frac{\rho_g V_g^2 d_p}{\sigma} \tag{2.4}$$

Large Weber numbers cause the droplet to disintegrate into smaller droplets. Turner et al. [29] used a Weber number equal to 30 in Equation 2.4, which yields a maximum droplet diameter to be equal to:

$$d_p = \frac{30\sigma}{\rho_g V_g^2} \tag{2.5}$$

Using this droplet size, the Reynolds number was then calculated using the equation:

$$Re_p = \frac{30\sigma}{\mu_g V_g} \tag{2.6}$$

The density of the gas of the gas phase was determined from the modified ideal gas equation of state, which has the form:

$$\rho_g = \frac{PM_W}{zRT} \tag{2.7}$$

Pressure and temperature vary throughout a flowing gas well. Therefore the appropriate conditions need to be selected in order to predict the onset of liquid loading. Wellhead temperature and pressure conditions are used in this model because it will predict the maximum terminal velocity of the liquid droplet. Also, using the wellhead conditions is common practice in industry, as described by Coleman et al. [5].

Production data from natural gas wells are typically given for a flowrate at standard conditions. The minimum gas velocity determined in Equations 2.1 can be converted into a minimum flowrate at standard conditions as function of pressure and temperature. The flowrate of gas is determined by the equation:

$$Q_g = V_g \pi \frac{d_t^2}{4} \tag{2.8}$$

This gas flowrate is then converted to a standard flowrate by using the ideal gas equation of state relation:

$$Q_{g,sc} = Q_g \frac{P z_{sc} T_{sc}}{P_{sc} z T} \tag{2.9}$$

The standard conditions used here are 15.6°C (60°F) and 101.325 kPa (1 Atmosphere). These standard conditions are consistent with industry practice. At standard conditions, $z_{sc}$ is approximately 1. Combining Equations 2.8 and 2.10 and converting them to a daily standard flowrate yields:

$$Q_{g,sc} = V_g \pi \frac{d_t^2}{4} \frac{PT_{sc}}{P_{sc} z T} \tag{2.10}$$

### 2.1.3 Two-Phase Flow Model

To determine the bottom flowing pressure, a model was used to predict the pressure drop of a two-phase flow moving upwards inside a vertical pipe. Assuming one-dimensional flow and a constant pressure gradient, the pressure drop in the pipe can be expressed by the equation:

$$\Delta P = \frac{dP}{dL} \Delta L \tag{2.11}$$

where P is the pressure of the two-phase mixture, $\frac{dP}{dL}$ is the pressure gradient in the pipe and L is the pipe length. The pressure gradient can be broken down into three components; acceleration (subscript a), friction (subscript f) and gravity (subscript g) shown in the following equation:

$$\frac{dP}{dL} = \left(\frac{dP}{dL}\right)_a + \left(\frac{dP}{dL}\right)_f + \left(\frac{dP}{dL}\right)_g \tag{2.12}$$

For the purposes of simplifying the analysis, the pressure gradient due to acceleration is assumed negligible compared to the contribution due to gravity and friction. In this model it is assumed that liquid is transported to the surface using an annular/mist two-phase flow regime.

### Frictional Pressure Gradient $\left(\frac{dP}{dL}\right)_f$

The frictional pressure gradient was estimated assuming a well mixed two-phase flow using a Lockhart-Martinelli [20] multiplier. This can be shown mathematically by the equation:

$$\left(\frac{dP}{dL}\right)_f = \Phi_{lo}^2 \left(\frac{dP}{dL}\right)_{lo} \tag{2.13}$$

where $\left(\frac{dP}{dL}\right)_{lo}$ is the liquid single-phase pressure gradient based on the total mass flow rate of the two-phase mixture and $\Phi_{lo}^2$ is the corresponding two-phase multiplier. The liquid only pressure gradient is determined by the equation:

$$\left(\frac{dP}{dL}\right)_{lo} = \frac{fG^2}{2d_t\rho_l} \tag{2.14}$$

The friction factor was determined by using the Colebrook equation taken from White [33]. This equation is valid for turbulent flow in a duct and is modified for smooth pipes with the implicit form:

$$\frac{1}{\sqrt{f}} = -2.0\log_{10}\left(\frac{2.51}{\sqrt{f}Re_t}\right) \tag{2.15}$$

where $Re_t$ is the Reynolds number of the fluid flow in a duct and is:

$$Re_t = \frac{Gd_t}{\mu_l} \tag{2.16}$$

The two-phase multiplier is determined using the Friedel correlation [8, 11]. This correlation was recommended by Hewitt [11] for horizontal and upward vertical flows when the dynamic viscosity ratio of the liquid phase to the gas phase($\frac{\mu_l}{\mu_g}$) is less than 1000, which is the case for most natural gas wells

producing water and/or condensate. The Friedel correlation for two-phase multiplier has the form:

$$\Phi_{lo}^2 = E + \frac{3.24FH}{Fr_h^{0.045} We_h^{0.035}} \tag{2.17}$$

The dimensionless factors E, F and H are respectively calculated by the equations:

$$E = (1-x)^2 + x^2 \frac{\rho_l f_{go}}{\rho_g f_{lo}} \tag{2.18}$$

$$F = x^{0.78}(1-x)^{0.224} \tag{2.19}$$

$$H = \left(\frac{\rho_l}{\rho_g}\right)^{0.91} \left(\frac{\mu_g}{\mu_l}\right)^{0.19} \left(1 - \frac{\mu_g}{\mu_l}\right)^{0.7} \tag{2.20}$$

Both friction factors in Equation 2.18 are calculated using Equation 2.15 for the total mass flux flowing with their respective properties. The quality of the two-phase mixture is the mass fraction of gas flowing in the two-phase mixture. This is described mathematically in the equation:

$$x = \frac{G_g}{G_g + G_l} \tag{2.21}$$

The Froude number is the ratio of inertial forces to gravitational forces in the fluid and in this case is evaluated by the equation:

$$Fr_h = \frac{(G_g + G_l)^2}{g d_t \rho_h^2} \tag{2.22}$$

The density of the two-phase mixture if it was homogeneous is determined by the equation:

$$\rho_h = \left(\frac{x}{\rho_g} + \frac{1-x}{\rho_l}\right)^{-1} \tag{2.23}$$

The Weber number in this case is based on the properties of the flow if it was homogeneous and are determined by the equation:

$$We_h = \frac{(G_g + G_l)^2 d_t}{\rho_h \sigma} \tag{2.24}$$

### Gravitational Pressure Gradient $\left(\frac{dP}{dL}\right)_g$

The gravitational pressure gradient is estimated using a model given by Wallis [31] by the equation:

$$\left(\frac{dP}{dL}\right)_g = \frac{Z_W}{L_W}\Big(\alpha\rho_g + (1-\alpha)\rho_l\Big)g \tag{2.25}$$

The void-fraction was determined by the equation from Whalley [32]:

$$\alpha = \frac{1}{1 + (S\frac{1-x}{x}\frac{\rho_l}{\rho_g})} \tag{2.26}$$

To determine slip-ratio, Whalley [32] recommends the use of the CISE [23, 11] correlation. The CISE correlation determines slip-ratio using the equation:

$$S = 1 + E_1\Big(\beta - \frac{\beta}{1-\beta}E_2\Big)^{0.5} \tag{2.27}$$

Parameters $\beta$, $E_1$ and $E_2$ are respectively determined:

$$\beta = \frac{\rho_l x}{\rho_l x + \rho_g(1-x)} \tag{2.28}$$

$$E_1 = 1.578 Re_t^{-0.19}\Big(\frac{\rho_l}{\rho_g}\Big)^{0.22} \tag{2.29}$$

$$E_2 = 0.0273 We Re_t^{-0.51}\Big(\frac{\rho_l}{\rho_g}\Big)^{-0.08} \tag{2.30}$$

where $We$ is defined in this case by the equation:

$$We = \frac{(G_g + G_l)^2 d_t}{\rho_l \sigma} \tag{2.31}$$

and $Re_t$ is defined by Equation 2.16 using the viscosity of the liquid phase.

The resulting two-phase flow pressure gradient is expressed mathematically as:

$$\frac{dP}{dL} = \Phi_{lo}^2\left(\frac{dP}{dL}\right)_{lo} + \frac{Z_W}{L_W}\Big(\alpha\rho_g + (1-\alpha)\rho_l\Big)g \tag{2.32}$$

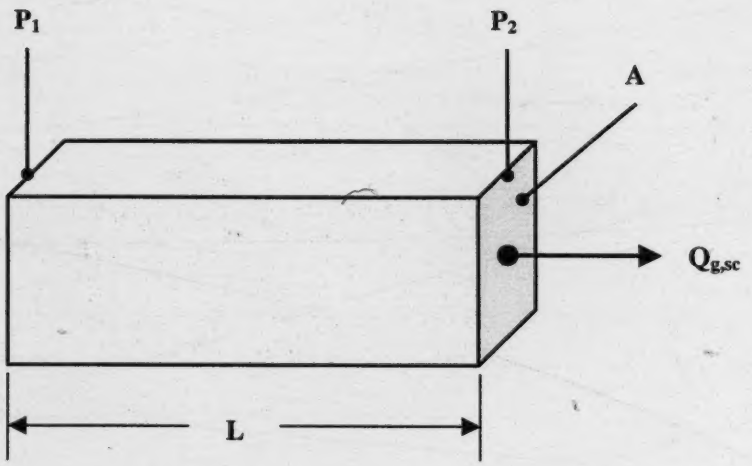


**Figure 2.2: Schematic of Flow in a Rectangular Porous Medium**

### 2.1.4 Reservoir Inflow Model

Petroleum reservoirs are often modelled as porous media and the Darcy's equation is the starting point of these models. Darcy's equation for one-dimensional fluid flow in an isotropic, homogeneous porous medium is:

$$V = -\frac{k_P}{\mu}\frac{dP}{dL} \tag{2.33}$$

where $k_P$ is the permeability of the porous medium and $\mu$ is the viscosity of the fluid. For isothermal flow of an ideal gas (at temperature $T_{RES}$) in a one-dimensional reservoir in cartesian coordinates (shown in Figure 2.1.4), Katz and Lee [16] gives the gas flowrate at standard conditions as:

$$Q_{g,sc} = \frac{k_P A}{2L\mu_g P_{sc}}\frac{T_{sc}}{T_{RES}}(P_{RES}^2 - P_{BH}^2) \tag{2.34}$$

where $A$ is the cross-sectional area of the medium and $L$ is its length. In applying Equation 2.34 to a natural gas well, a condition of quasi-steady flow is required.

Rawlins and Schellhardt [24] found that gas flow from the reservoir to the bottomhole of a gas well is given by:

$$Q_{g,sc} = C(P_{RES}^2 - P_{BH}^2)^n \tag{2.35}$$

$C$ and $n$ are empirical parameters determined from production tests performed on natural gas wells. Comparing Equation 2.34 with Equation 2.35 coefficient $C$ represents the effective permeability, Area and Length of the petroleum reservoir as the gas well sees it. As well, coefficient '$C$' contains a correction for the deviation from ideal gas behaviour of the gas at reservoir conditions. Therefore coefficient '$C$' can be considered as an effective wellbore admittance factor. A higher value of '$C$' allows for greater flow of gas from the reservoir to the well. Also, if exponent '$n$' in Equation 2.35 is equal to unity it will correspond to Darcy's Equation (Equation 2.34) as well. Therefore, Equation 2.35 was chosen because it is simple and it is also widely used in practice.

## 2.2 Mathematical Model of a Gas Well in a Separate Phases Flow Configuration

In this scenario, natural gas and reservoir liquids are produced separately, shown previously in Figure 1.3. The liquid is produced using a pump that extracts work from the natural gas in the most efficient way possible. This

configuration should operate a lower reservoir pressure for two reasons. First, the friction and hydrostatic pressure losses in a gas well are higher in a two-phase flow. As well, it is anticipated that the gas well will be able to operate at lower gas flowrates than required to prevent the onset of liquid loading if each phase is produced separately.

### 2.2.1 Calculation Methodology

To model this scenario, the following sequence was followed and is shown schematically in Figure 2.3. Starting from the wellhead pressure, for a given gas flow rate the gas discharge pressure (or pressure just above the pump) is determined using the gas flow model. The amount of work required to deliver the liquid to the surface is estimated and employed in the model for gas work, which then determines the bottom hole flowing pressure. The gas flow rate and bottomhole flowing pressure are then used in the reservoir inflow model to determine the reservoir pressure. Each segment of this modelling will be explained below in detail. Both the liquid production rates and reservoir inflow model (Equation 2.35) used the same models as for the model of a gas well in the two-phase flow configuration described earlier.

### 2.2.2 Gas Flow Model

The gas flow model used is based on the method of Cullender and Smith [6] technique to estimate the flowing bottomhole pressure of a natural gas well. The Cullender and Smith technique uses a generalized form of the mechanical energy balance and assumes that the gas contains no free liquids. The general form of the Mechanical Energy Balance is expressed mathematically (from

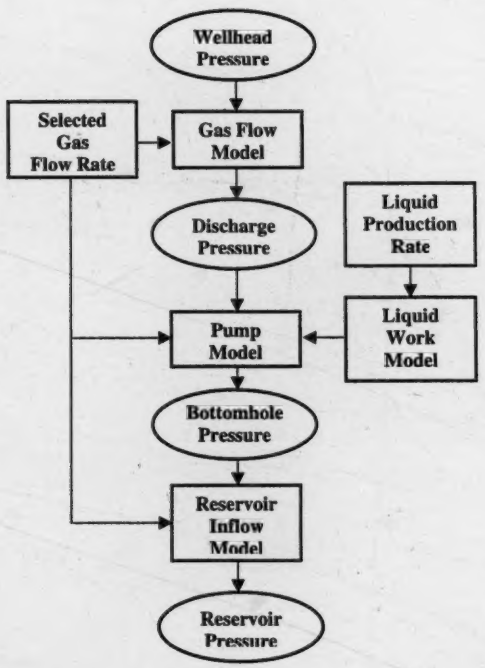


**Figure 2.3: Logic of Mathematical Model for Separate Flow of Natural Gas and Reservoir Liquid**

Brodkey and Hershey [4]) as:

$$\frac{dP}{\rho} + gdZ + VdV + dF + dW_s = 0 \tag{2.36}$$

Each term in Equation 2.36 is described as follows. The first term is due volume-pressure, the second is potential energy due to gravity, the third is kinetic energy, the fourth is the friction term and the fifth is the shaft work term. Shaft work in Equation 2.36 is neglected. Kinetic energy is generally neglected but is retained here for completeness and because Young et al. [36]

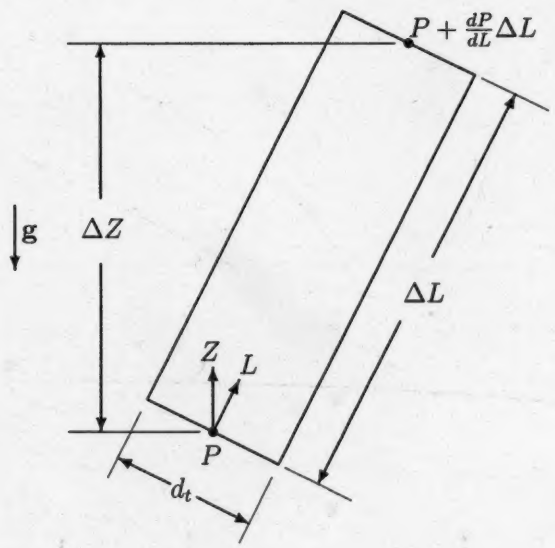


**Figure 2.4: Diagram of a Pipeline Element**

found that kinetic energy effects should be included for wells less than 4,000 ft (1167 m) deep or with wellhead pressures less than 100 psia (690 kPa). In this work it assumed that these conditions may occur when then is model is applied. In deriving this model, consider the drawing given in Figure 2.4. For the volume-pressure term, the density of the gas is determined using the modified ideal gas equation of state used earlier (Equation 2.7). The resulting term becomes:

$$\frac{dP}{\rho} = zRT\frac{dP}{PM_W} \tag{2.37}$$

For the potential energy due to gravity, lengths $\Delta Z$ and $\Delta L$ are assumed proportional resulting in:

$$gdZ = -g\frac{\Delta Z}{\Delta L}dL \tag{2.38}$$

To evaluate the kinetic energy term, a relation for the fluid velocity($V$) must be applied. First the concept of constant mass flow is utilized where:

$$\dot{m} = \rho V A \tag{2.39}$$

Area($A$) is the cross-section of the pipe element and is denoted by:

$$A = \frac{\pi d_t^2}{4} \tag{2.40}$$

and combining Equations 2.40, 2.7 and 2.48 to solve for gas velocity results in:

$$V = \frac{4\dot{m}zRT}{PM_W\pi d_t^2} \tag{2.41}$$

To solve for $dV$, it is assumed that isothermal flow conditions exist over the length of the element and that the z-factor remains constant over the length of the pipeline element. Therefore $V$ becomes a function of P only over the length of the pipeline element and thus $dV$ becomes:

$$dV = -\frac{4\dot{m}zRT}{\pi M_W d_t^2}\frac{dP}{P^2} \tag{2.42}$$

Combining Equations 2.41 and 2.42, the kinetic energy term becomes:

$$VdV = -\left(\frac{4\dot{m}zRT}{\pi M_W d_t^2}\right)^2\frac{dP}{P^3} \tag{2.43}$$

The friction in the pipeline element is modelled using the local friction factor:

$$dF = -\frac{f}{d_t}\frac{V|V|}{2}dL \tag{2.44}$$

Applying Equations 2.41 and 2.7, the friction term becomes:

$$dF = -\frac{8f\dot{m}|\dot{m}|}{\pi^2 d_t^5}\left(\frac{zRT}{PM_W}\right)^2 dL \tag{2.45}$$

The friction factor is calculated using implicit form of the Colebrook equation taking pipe roughness into account. This form of the equation is given by White [33] as:

$$\frac{1}{\sqrt{f}} = -2.0\log_{10}\left(\frac{2.51}{\sqrt{f}Re_t} + \frac{\epsilon}{3.7d_t}\right) \tag{2.46}$$

and is valid for the turbulent duct flow assumed in this model. Combining Equations 2.37, 2.38, 2.43 and 2.45, applying the chain rule and re-arranging to solve for the pressure gradient in the pipe element results in:

$$\frac{dP}{dL} = -\frac{\frac{8f\dot{m}|\dot{m}|}{\pi^2 d_t^5}\left(\frac{zRT}{P}\right)^2 + g\frac{\Delta Z}{\Delta L}}{\frac{zRT}{P} - \left(\frac{4\dot{m}zRT}{\pi d_t^2}\right)^2 \frac{1}{P^3}} \tag{2.47}$$

Equation 2.47 can be altered by making a few substitutions. First, the top and bottom equation can be multiplied by square of the gas density (Equation 2.7). Second, it is recognized that mass will flow in the direction of dL (upwards towards the surface), therefore the absolute value can be dropped. As well, the mass flow is converted gas flowrate at standard condition using the equation:

$$\dot{m} = Q_g \rho_g \tag{2.48}$$

and solving for $Q_g$. The standard flowrate is then calculated using Equation 2.10. Making these substitutions Equation 2.47 becomes:

$$\frac{dP}{dL} = -\frac{\frac{8fQ_{g,sc}^2 P_{sc}^2 M_W^2}{R^2 T_{sc}^2 \pi^2 d_t^5} + g(\frac{PM_W}{zRT})^2 \frac{\Delta Z}{\Delta L}}{\frac{PM_W}{zRT} - \left(\frac{4Q_{g,sc}P_{sc}M_W}{RT_{sc}\pi d_t^2}\right)^2 \frac{1}{P}}. \tag{2.49}$$

Further simplification can be obtained by multiplying the top and bottom by the square of the ideal gas constant ($R/M_W$). The gas flow pressure gradient becomes:

$$\frac{dP}{dL} = -\frac{\frac{8fQ_{g,sc}^2P_{sc}^2}{T_{sc}^2\pi^2d_t^5} + g(\frac{P}{zT})^2\frac{\Delta Z}{\Delta L}}{\frac{PR}{zM_WT} - \left(\frac{4Q_{g,sc}P_{sc}}{T_{sc}\pi d_t^2}\right)^2\frac{1}{P}} \tag{2.50}$$

### 2.2.3 Liquid Work Model

In modelling the work required to bring the liquid phase to the surface, the flow was assumed steady. The liquid phase is pumped from the gas well bottomhole pressure to the pressure at wellhead. In addition, it is assumed that the liquid tubing is placed in the casing annulus so that it does not restrict the flow of gas in the production tubing. Using the principles of thermodynamics, the rate of work done on the liquid can be estimated by the equation:

$$W_l = \dot{m}\int\frac{dP}{\rho_l} \tag{2.51}$$

Since the liquid is incompressible, Equation 2.51 becomes:

$$W_l = \frac{\dot{m}}{\rho_l}\int dP = \frac{Q_l\rho_l}{\rho_l}\int dP = Q_l\Delta P \tag{2.52}$$

The change in pressure consists of three parts: change in pressure due to elevation, change in pressure due to friction and the pressure difference between the wellhead pressure ($P_{WH}$) and the pressure at the gas well bottomhole pressure ($P_{BH}$).

Friction in the liquid tubing is neglected because this model is meant to

be an idealization. The pressure difference between the wellhead and bottom of the gas well is also neglected. This second assumption compensates for neglecting the friction because in a flowing gas well, pressure at the bottom of the well will be higher than at the wellhead. Therefore, the change in pressure assumed for the liquid work model is:

$$\Delta P = \rho_l g Z_W \tag{2.53}$$

Thus, the work to bring the liquid to the surface is:

$$W_l = Q_l(\rho_l g Z_W) \tag{2.54}$$

### 2.2.4 Pump Model

The purpose of this model is to determine the bottomhole pressure, which is at the intake (or start) of the gas work extraction process. This model will take the required liquid work, the gas flowrate, and the gas discharge pressure of the tubing and determine the bottomhole pressure.

Thermodynamically, the rate of work that can be obtained by expansion of a gas is given by the equation:

$$W_g = -\dot{m}_g \int v dP \tag{2.55}$$

If the gas is assumed ideal and is expanded isentropically fashion, the rate of work extracted per kg of gas, neglecting potential and kinetic energy, is given by Moran and Shapiro [22] as:

$$\frac{W_g}{\dot{m}_g} = T_1 \frac{R}{M_W} \frac{k}{k-1} \left(1 - \left(\frac{P_1}{P_2}\right)^{\frac{k-1}{k}}\right) \tag{2.56}$$

where $k$ is the ratio of specific heats of the gas. In this case, state 1 is at the conditions just below the pump (subscript BH) and state 2 is the conditions at the bottom of the production tubing (subscript DIS) just above the pump. The mass flow rate of the gas can be expressed in terms of a gas flowrate at standard condtions using Equation 2.48. The density of the gas at standard conditions was determined using Equation 2.7. Taking Equation 2.48 and inserting it into Equation 2.56, the rate of work achieved by expansion of the gas becomes:

$$W_g = Q_{g,sc}\frac{P_{sc}}{T_{sc}}T_{BH}\frac{k}{k-1}\left(1-\left(\frac{P_{BH}}{P_{DIS}}\right)^{\frac{k}{k-1}}\right) \tag{2.57}$$

In the model, the liquid work required in Equation 2.54 equals the work done by expanding the gas in Equation 2.58. Knowing this, and rearranging to solve for the bottomhole pressure:

$$P_{BH} = P_{DIS}\left(1+\frac{Q_l}{Q_{g,sc}}\frac{(k-1)g\rho_l Z_W T_{sc}}{kP_{sc}T_{BH}}\right)^{\frac{k}{k-1}} \tag{2.58}$$

## 2.3 Selected Gas Well

The gas well models developed for two-phase flow and separate phases flow were tested using data from a "typical" Alberta natural gas well. In order to select this "typical" Alberta gas well, a survey of Alberta natural gas wells was performed. The details from this survey are given in Appendix A. Based on the results of this survey, most natural gas wells were found to range in depth from 300 m to 1250 m. Therefore a gas well with a depth of approximately 700 m was considered typical and a 715 m deep Alberta natural gas well was selected.

At the time of selection, the "typical" gas well produced approximately 25,700 $m^3$ of gas and 7 $m^3$ of water per day. For the selected gas well, its properties (such as depth, gas composition and reservoir inflow model), given in Appendix A, were implemented into the two gas well models. A production tubing size of 50.6 mm was chosen because it is the typical size for a flowing gas well in Alberta. To estimate properties of the gas mixture such as z-factor, viscosity and specific heat ratio, various correlations were used and are given in greater detail in Appendix B.

## 2.4 Model Results

The gas well models were tested using the "typical" Alberta gas to determine the minimum reservoir pressure for each flow configuration. This was done for two different liquid production conditions:

- a constant liquid production rate of 7 $m^3$/day and
- a constant gas-liquid ratio of 3671.

The constant liquid production rate is meant to simulate a gas well with liquid production rate that is independent of the amount of gas produced.

Gas-liquid ratio is defined as ratio of the volume of natural gas at standard conditions to the volume of liquid produced and is defined mathematically as:

$$R_{gl} = \frac{Q_{g,sc}}{Q_l} \tag{2.59}$$

In essence gas-liquid ratio is a mass flow ratio of gas to liquid. A constant gas-liquid ratio simulates a situation where a gas well is producing from a reservoir with a relative resistance to gas and liquid flow (on a per mass basis) that remains constant. This liquid production model was used by Gasbarri and Wiggins [9] to model the dynamics of plunger lift, a technology mentioned earlier that is used to solve liquid loading problems in natural gas wells. Both liquid production scenarios investigated here are idealizations, but will still provide useful information from the results.

The gas well models were tested for wellhead pressures from 100 to 4,000 kPa. This range is consistent with the expected operation of the "typical" Alberta gas because its initial reservoir pressure was 4200 kPa.

### 2.4.1 Calculation Procedure

#### Two-Phase Flow Gas Well Configuration

Reservoir pressure was calculated in the two-phase flow gas well model using the following sequence:

1. Starting from a given wellhead pressure, the minimum gas velocity is calculated iteratively using Equation 2.1 (which is implicit). The minimum gas velocity is then converted to a gas flowrate at standard conditions using Equation 2.10.

2. The wellhead pressure, gas flowrate and corresponding liquid production are used to calculate the two-phase flow pressure gradient. The pressure gradient (Equation 2.32) is integrated numerically from the

wellhead to bottom of the gas well to determine the bottomhole pressure. Details of the numerical integration are given in Appendix C.

3. Reservoir pressure is then calculated from the bottomhole pressure and gas flowrate using Equation 2.35.

### Separate Phases Flow Gas Well Configuration

Reservoir pressure was calculated in the separate phases flow gas well model using the following sequence:

1. Using a "selected" gas flow rate at a given wellhead pressure the dry-gas flow pressure gradient is calculated (Equation 2.50). The pressure gradient is integrated numerically from the wellhead to bottom of the gas well to determine the pump gas discharge pressure. Details of the numerical integration are given in Appendix C.

2. The corresponding liquid production rate is used to determine the rate of work required to bring the liquid to the surface (Equation 2.54). This value is then entered into the gas work equation (Equation 2.58) to determine the bottomhole pressure.

3. Reservoir pressure is then calculated from the bottomhole pressure and gas flowrate using Equation 2.35.

In obtaining the minimum reservoir pressure for the case of separate liquid and gas production, a different methodology was required for each liquid production scenario to determine the appropriate "selected" gas flow rate. For the constant liquid rate, regardless of the amount of gas produced, there

will always be a finite amount of work required to be done in order to bring the liquid to the surface. Examining Equation 2.58, the pressure drop from the bottom of the well to the pump gas discharge pressure ($P_{BH}$-$P_{DIS}$) will be very large if the gas flowrate is small, and very small if the gas flowrate is large. However, if a large amount of gas is produced, then the pressure drop from the reservoir to the bottom of the gas well (using Equation 2.35) becomes very large. Therefore, there exists an optimum gas flowrate between these two extremes where the reservoir pressure is at a minimum. Details regarding on how this optimum gas flow rate is determined are given in Appendix C.

To obtain the appropriate "selected" gas flowrate for the constant gas-liquid ratio, recall that liquid production is directly proportional to gas production. Therefore, inserting Equation 2.59 into Equation 2.58 yields

$$P_{BH} = P_{DIS}\left(1 + \frac{1}{R_{gl}}\frac{(k-1)g\rho_l Z_W T_{sc}}{kP_{sc}T_{BH}}\right)^{\frac{k}{k-1}} \tag{2.60}$$

which is independent of gas flow rate. The required bottomhole pressure is minimized if the required discharge gas pressure is minimized. For a given wellhead pressure, gas discharge pressure is minimized if there is zero flow. Thus, the required bottomhole pressure is minimized when the gas flowrate is zero and this will correspond to the minimum reservoir pressure for this type of liquid production scenario.

### 2.4.2 Constant Liquid Rate

For the constant liquid production rate, a comparison of the two operating scenarios is given in Figure 2.5. For comparison, the static pressure of the

gas well as a function of wellhead pressure is also shown. Static pressure is calculated by integrating the dry-gas flow pressure gradient (Equation 2.50) at zero flow from the wellhead to the bottom of the well. In Figure 2.5, the two-phase curve shows the minimum reservoir pressure required to keep the gas well flowing in a two-phase flow at a given wellhead pressure. The separate phases curve is the minimum reservoir pressure required to keep the gas well flowing using the reservoir energy as efficiently as possible.

The results in Figure 2.5 show that operating this gas well with separate liquid and gas phases, the well can be operated to much lower reservoir pressures than required to keep the well flowing in a two-phase flow configuration. The significance of these curves is given as follows. Referring to Figure 2.5, assuming a constant wellhead pressure, the reservoir pressure at point A is above the two-phase curve and thus will flow without experiencing liquid-loading problems.

As the reservoir pressure drops (point B), due to the removal of gas over time, it becomes less than the two-phase curve and will experience liquid loading problems and will stop producing if nothing is done. However, since point B is above the separate phases curve a "device" that uses the reservoir pressure more efficiently could be used to keep the well flowing in a separate phases flow configuration. Alternatively, the operator of the gas well could reduce the pressure at the wellhead to keep the gas well flowing. This, however would require additional compression power to get the natural gas to a processing facility. As well, reducing the wellhead pressure may

have an effect on production from other gas wells tied into the same pipeline.

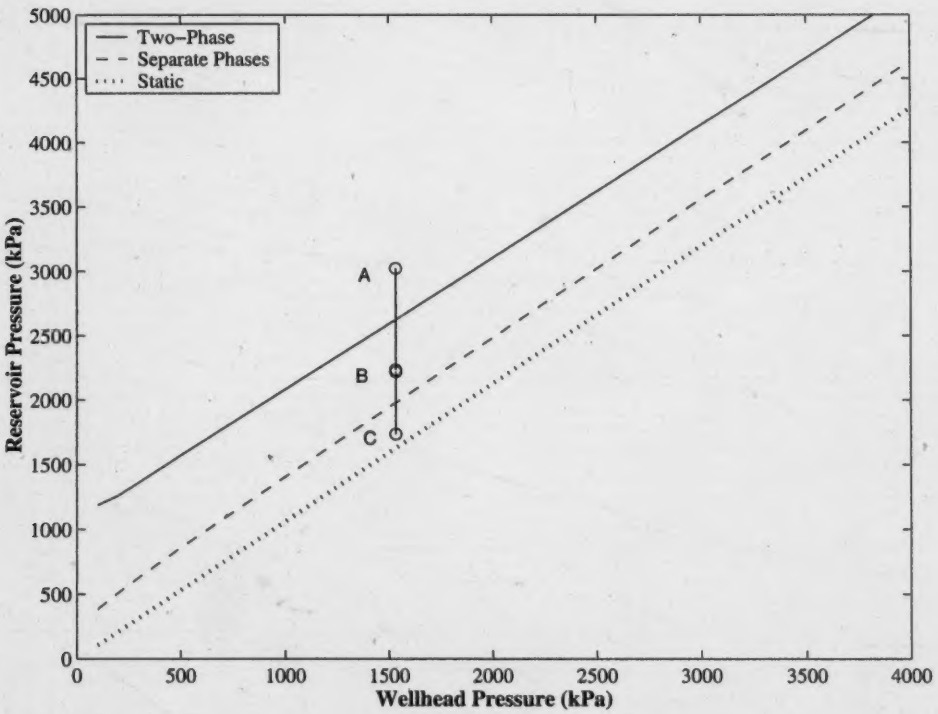


**Figure 2.5: Minimum Reservoir Pressures for Constant Liquid Production of 7 $m^3$/day**

As the reservoir pressure decreases further (point C), the well will keep flowing only if wellhead pressure is decreased. Therefore, the region between the two-phase and the separate-phases curve is where a "device" based on the ARC pumping concept would be applicable.

In order to obtain a more meaningful comparison between the two operating scenarios, the results for the two-phase and separated phases are normalized by subtracting the static reservoir pressure. These results are shown in Figure 2.6. These results show that the two-phase flow configuration requires

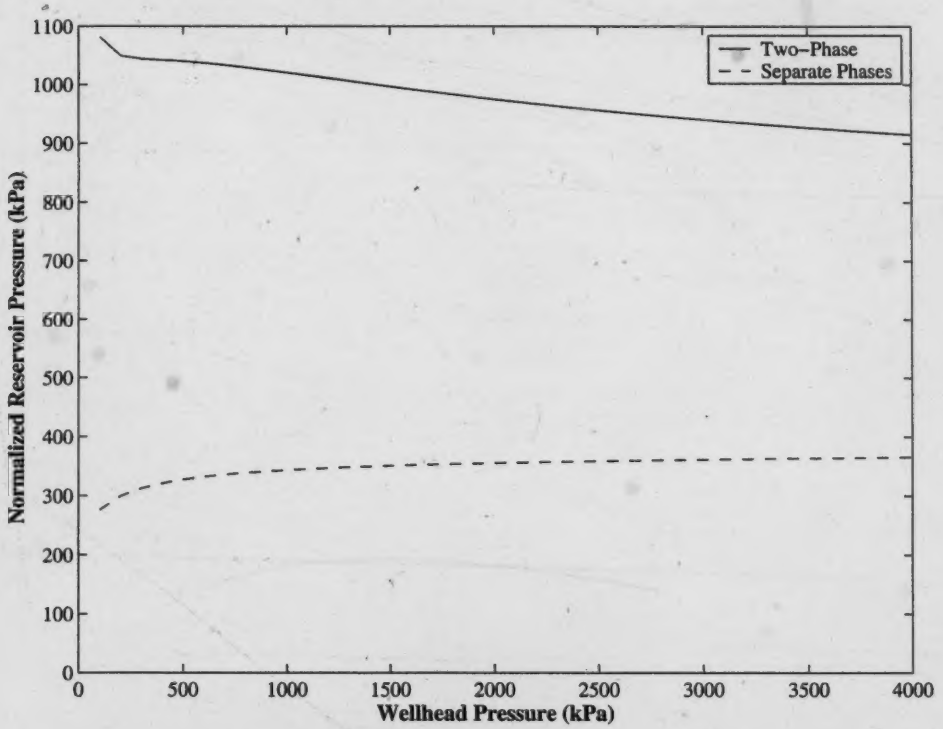


**Figure 2.6: Normalized Minimum Reservoir Pressures for Constant Liquid Production of 7 $m^3$/day**

more reservoir pressure to keep the gas well flowing when compared to the separate phases configuration. This effect is more prominent at lower wellhead pressures and decreases as the wellhead pressure increases.

A main reason for the lower reservoir pressures required to operate the gas well in the separate phases configuration is because a smaller gas flowrate is required. To demonstrate this a comparison of the gas flow rates required to operate each gas well at their minimum reservoir pressure is given in Figure 2.7. These results show that gas flow rate required to keep the gas well flowing

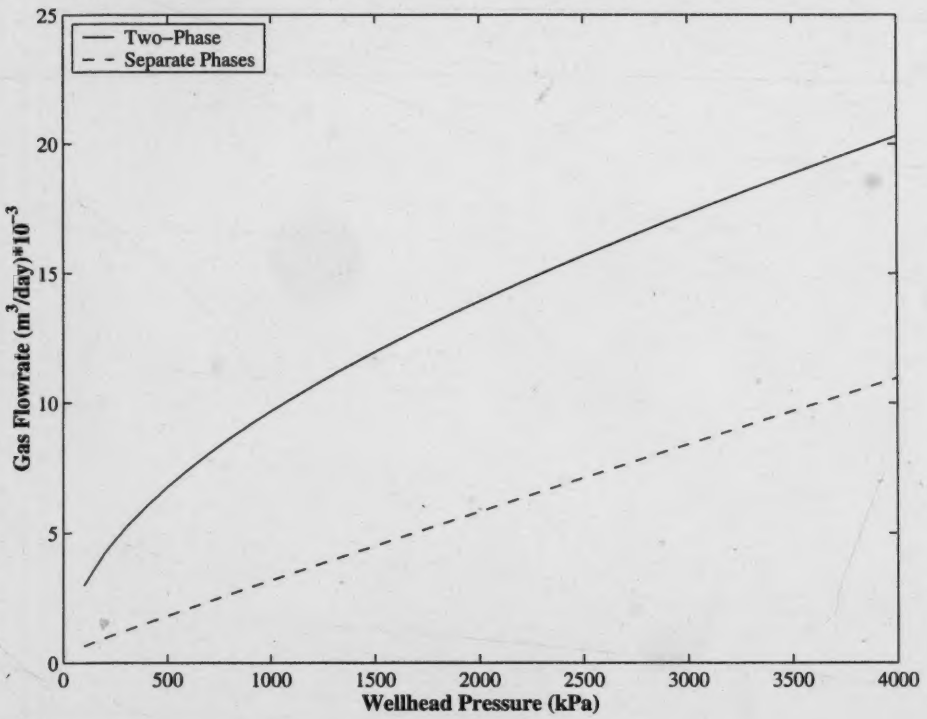


**Figure 2.7: Gas Flow Rates at Minimum Reservoir Pressures for Constant Liquid Production of 7 $m^3$/day**

in a separate phases configuration is much less than required for a two-phase

flow configuration. The flow rate required for the separate phases increases almost linearly with wellhead pressure and the two-phase flow configuration is proportional to $(P_{WH})^{0.5}$. Because of this smaller flowrate, pressure drops in the production tubing and in the reservoir are also smaller allowing the well to be operated at lower reservoir pressures.

### 2.4.3 Constant Gas-Liquid Ratio

For the constant gas-liquid ratio, a comparison of the two operating scenarios is given in Figure 2.8. As in the constant liquid rate case, the reservoir pressure required to keep the gas well flowing in a two-phase flow configuration is much larger than required for the separate phases configuration. Here, the separate phases curve is only slightly higher than the static pressure curve. This is because the minimum gas flow required to keep the well flowing is zero and therefore differs from the static pressure by a factor determined by Equation 2.60 to account for the bringing the corresponding liquid to the surface.

Again for a more detailed comparison, the reservoir pressures were normalized by subtracting the static pressure and these results are shown in Figure 2.9. Once again, as in the constant liquid rate case, there is a large gap between the two-phase and separate phases operating curves. The gap is largest at lower wellhead pressures and decreases as the wellhead pressure increases for the range shown in Figure 2.9. Based on these results it appears that the concept of producing the liquid and gas phases separately has a significant advantage compared with two-phase flow operation. This

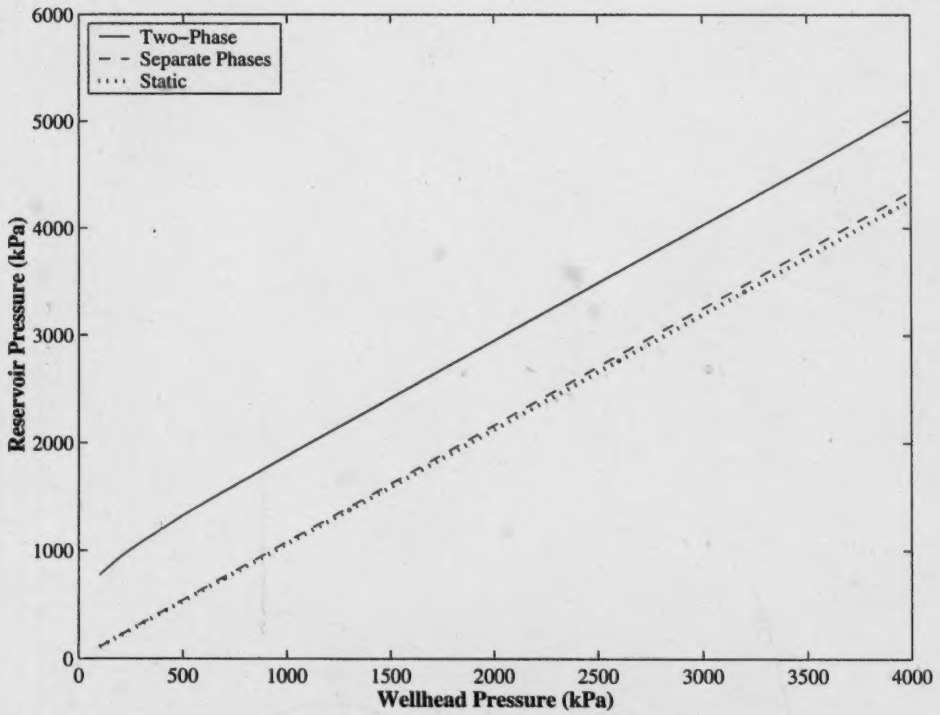


**Figure 2.8: Minimum Reservoir Pressures for Constant Gas-Liquid Ratio of 3671**

advantage is greatest at lower wellhead pressures and decreases somewhat with wellhead pressure, but still remains significant for the range wellhead pressures investigated.

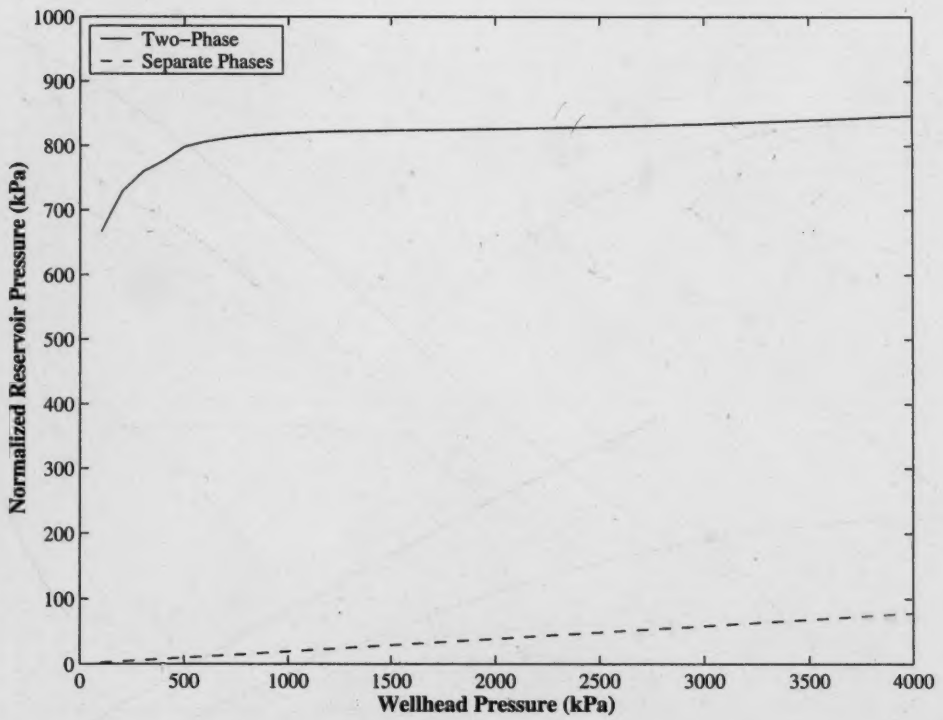


**Figure 2.9: Normalized Minimum Reservoir Pressures for Constant Gas-Liquid Ratio of 3671**

## 2.5 Effect of Field Conditions

To gain greater insight as to the applicability of the concept of producing the gas and liquid phases separately, the effect of some field conditions used in the modelling was investigated. The field conditions investigated in this research work are, gas well depth, reservoir inflow resistance and gas well liquid production.

### 2.5.1 Gas Well Depth

As mentioned earlier, the majority of natural gas wells in Alberta range in depth from about 300 m to 1250 m. To investigate this range, the model was tested using a gas well depth 1430 m (twice as deep as 715 m gas well investigated initially) and a gas well with a depth 357 m (half as deep as the initial gas well).

#### Constant Liquid Production Rate

To evaluate the effect of gas well depth, the results were determined in terms of a new parameter $\Delta P_{RES}$ which is the difference in minimum reservoir pressure for the two-phase and separate phases operating curves. For the constant liquid production rate case, these results are given in Figure 2.10. These results show that for all three depths, $\Delta P_{RES}$ has a large value indicating a significant advantage in producing the gas and liquid phases separately. $\Delta P_{RES}$ is greatest at lower wellhead pressures and increases with the depth of the gas well. However, even with the shallower case, $\Delta P_{RES}$ remains significant for the wellhead pressures investigated here.

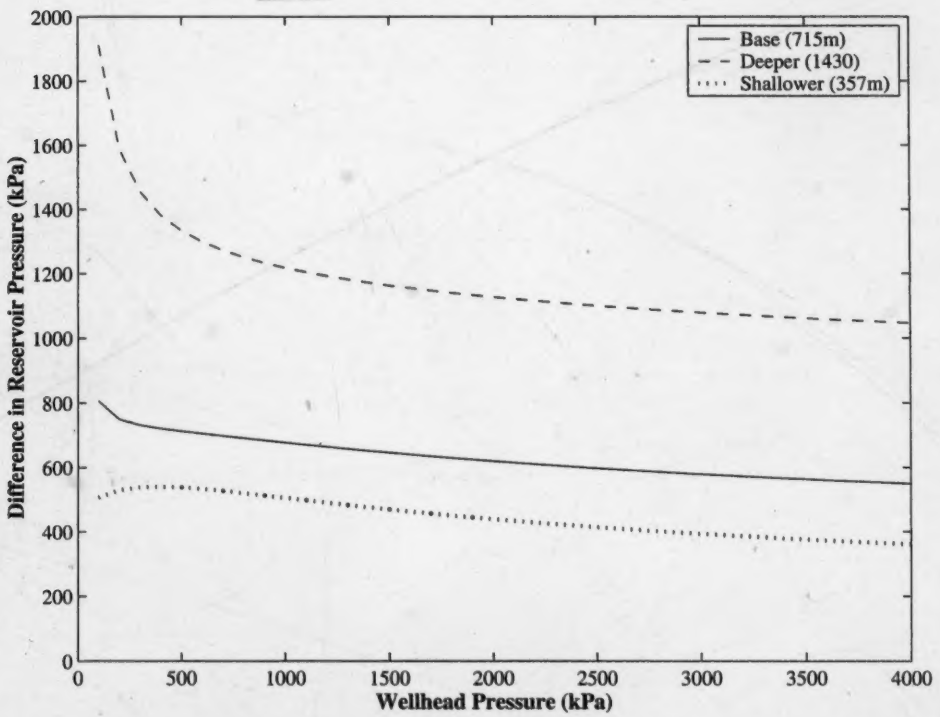


**Figure 2.10: Effect of Gas Well Depth on $\Delta P_{RES}$ for Constant Liquid Production Rate of 7 $m^3$/day**

### Constant Gas-Liquid Ratio

For the constant gas-liquid ratio case the results are given in Figure 2.11. As in the constant liquid production rate case, the results show that $\Delta P_{RES}$ has a positive value, indicating a significant advantage in producing the gas and liquid phases separately. Of the three conditions, $\Delta P_{RES}$ has the largest value in a deeper well, because pressure losses (both frictional and gravitational)

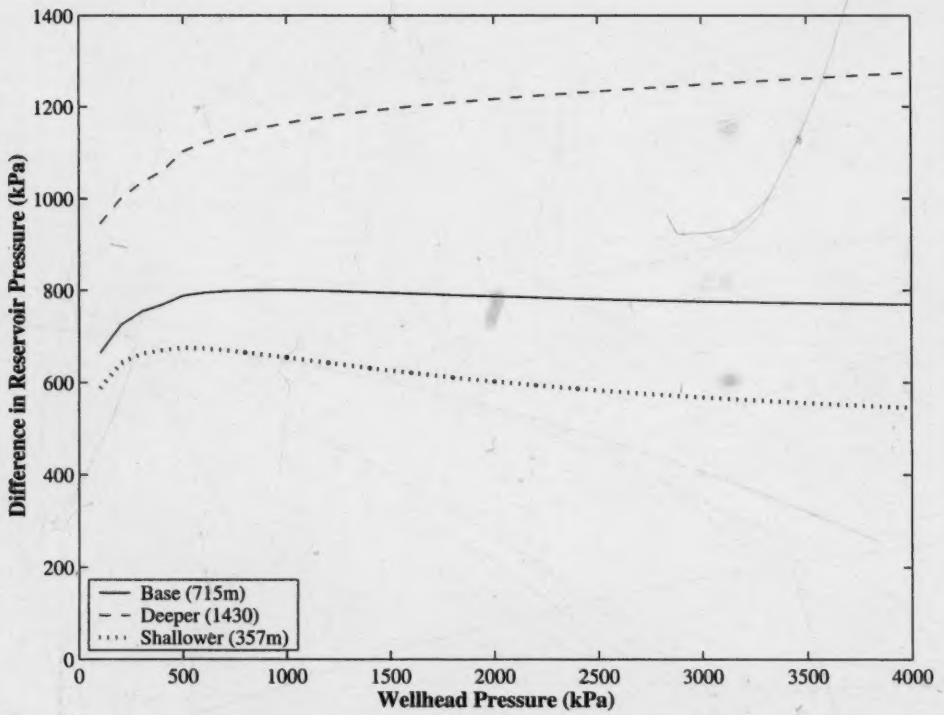


**Figure 2.11: Effect of Gas Well Depth on $\Delta P_{RES}$ for Constant Gas-Liquid Ratio of 3671**

in a two-phase flow are greater.

### 2.5.2 Reservoir Inflow Resistance

To investigate the effect reservoir inflow resistance, Equation 2.35 was modified. Recall that coefficient 'C' in Equation 2.35 represents an effective gas flow admittance factor. This coefficient was modified by doubling its original value to examine the effect of smaller inflow resistance, and halved to

examine the effect of greater inflow resistance.

### Constant Liquid Production Rate

For the constant liquid production rate, the results for the effect reservoir inflow resistance are given in Figure 2.12. Based on these results it appears

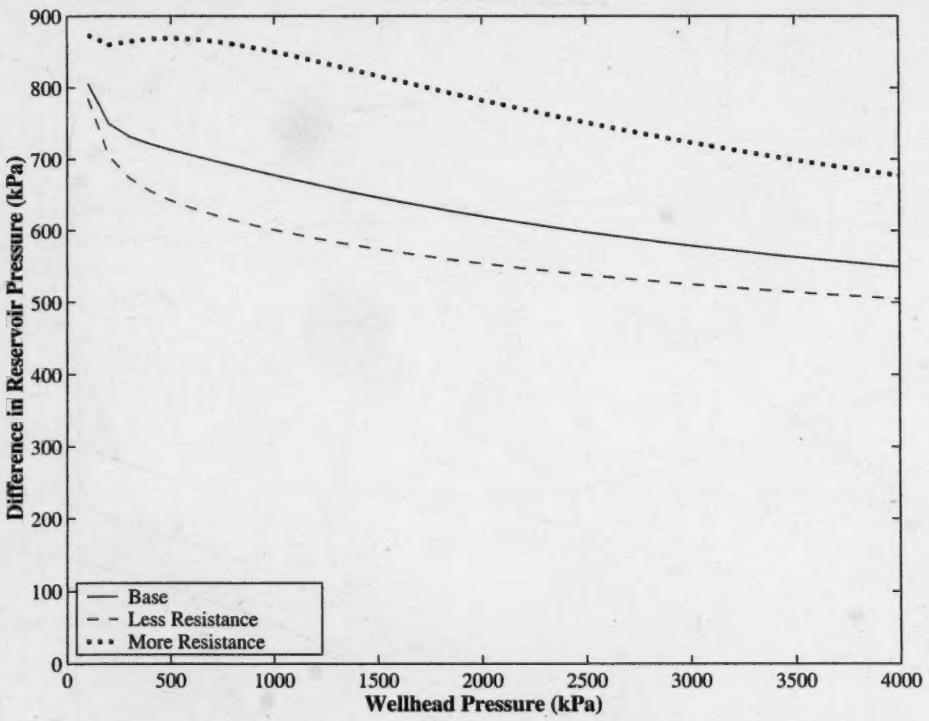


**Figure 2.12: Effect of Reservoir Inflow Resistance on $\Delta P_{RES}$ for Constant Liquid Production of 7 $m^3$/day**

that $\Delta P_{RES}$ increases with reservoir inflow resistance.

### Constant Gas-Liquid Ratio

For the constant gas-liquid Ratio case, the results are given in Figure 2.13. These results show the same effect as in Figure 2.12 that $\Delta P_{RES}$ is higher

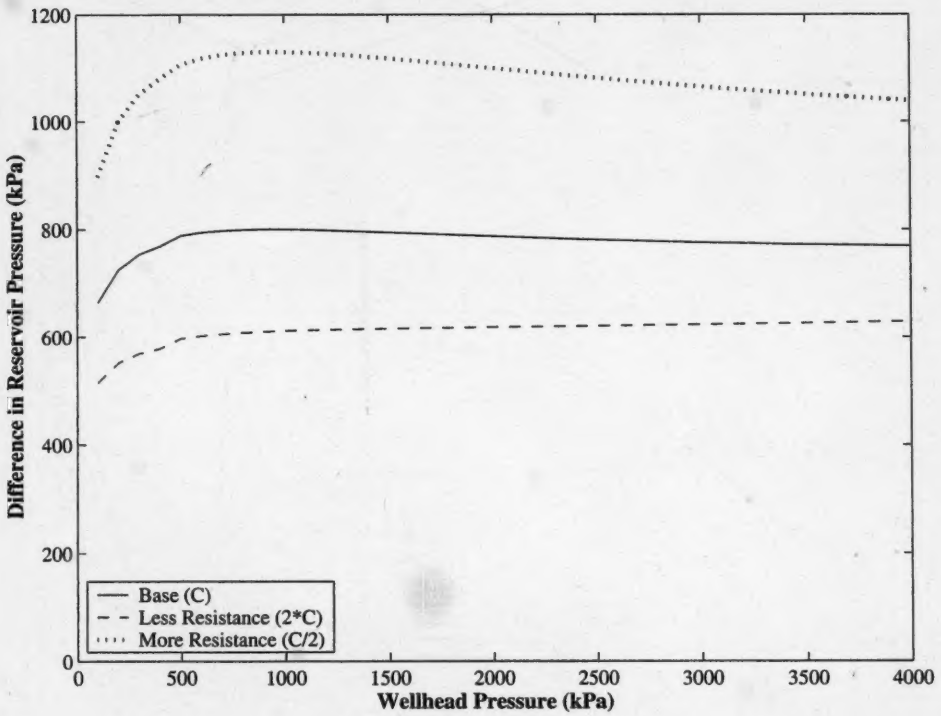


**Figure 2.13: Effect of Reservoir Inflow Resistance on $\Delta P_{RES}$ for Constant Gas-Liquid Ratio of 3671**

when there is a larger inflow resistance. The reason for this increase is because pressure drop in the reservoir will be much higher for the two-phase flow configuration due to the higher gas flow rate required to keep the gas well

flowing. As before, $\Delta P_{RES}$ appears to decrease somewhat at higher wellhead pressures.

### 2.5.3 Gas Well Liquid Production

To examine the effect of liquid production, changes were made for both the constant liquid rate and constant gas-liquid ratio cases. For the constant liquid rate, liquid production rates of 14 $m^3$/day (more liquid) and 3.5 $m^3$/day (less liquid) were compared to base case of 7 $m^3$/day. For the constant gas-liquid ratio case, a ratio of 7342 (more liquid) and 1835 (less liquid) were compared to the base case of 3671.

#### Constant Liquid Production Rate

For the constant liquid production rate, the results for the effect reservoir inflow resistance are given in Figure 2.14. These results show that $\Delta P_{RES}$ is increases if the gas well produces higher amounts of liquid.

#### Constant Gas-Liquid Ratio

For the constant gas-liquid ratio case, the results are given in Figure 2.15. These results show the same effect as in Figure 2.14, that $\Delta P_{RES}$ is slightly higher when there is a higher gas-liquid ratio. The increase in $\Delta P_{RES}$ is due to the higher amount of liquid creating a larger pressure drop in the production tubing when the gas well is produced in a two-phase flow configuration. As before, $\Delta P_{RES}$ decreases as the wellhead pressure increases.

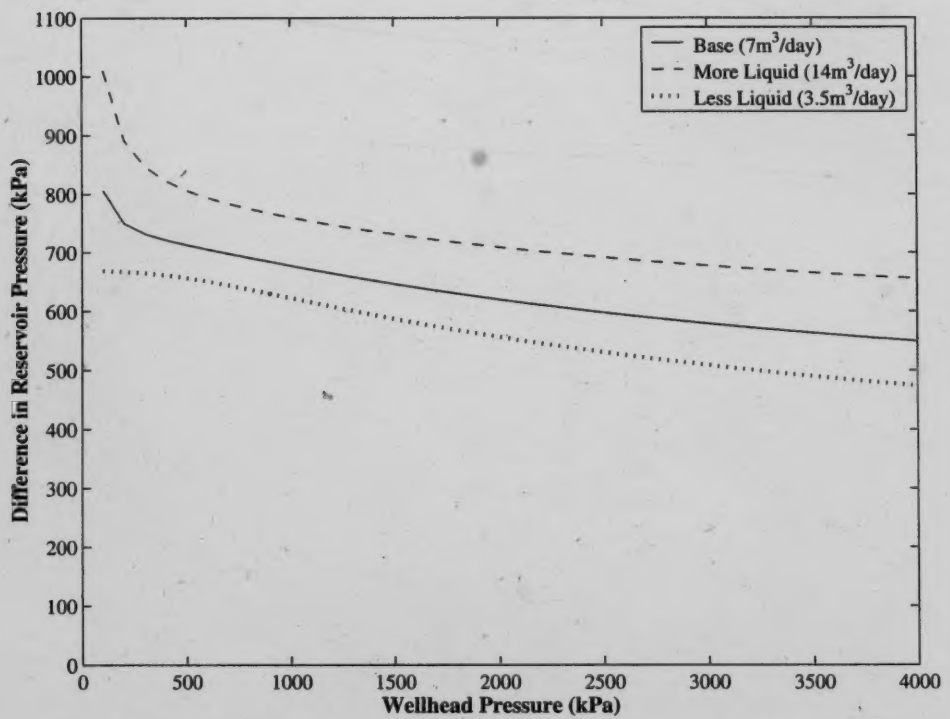


**Figure 2.14: Effect of Liquid Production on $\Delta P_{RES}$ for Constant Liquid Production Rate Scenario**

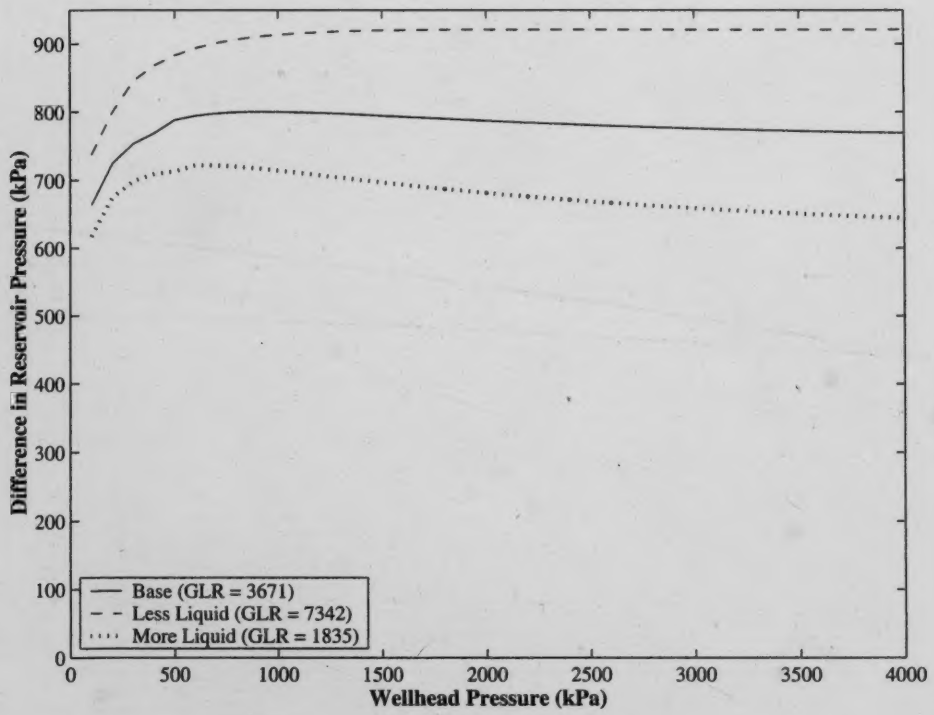


**Figure 2.15: Effect of Changing Gas-Liquid Ratio on $\Delta P_{RES}$**

## 2.6 Summary

The purpose of this chapter was to determine if the concept of producing gas and liquid phases separately, proposed by the Alberta Research Council, in a gas well has any advantage over a conventional two-phase flow configuration. A mathematical model to predict gas well performance in both of these configurations has been presented and tested on a "typical" Alberta gas well.

The mathematical modelling results show that the "typical" Alberta gas well can be operated at a lower reservoir pressure in separate phases flow configuration. Also, it was shown that for increased gas well depth, reservoir resistance and liquid production, that the advantage of utilizing a separate phases flow configuration increases.

The results obtained provide justification for investigation into the applicability of reciprocating pumps, as well as other designs, to operate gas wells in the separate phases flow configuration.

CHAPTER 3

# Mathematical Model of a Reciprocating Pump

The results obtained in Chapter 2 provided justification for further investigation into the applicability of reciprocating pumps to operate natural gas wells in a separate phases flow configuration. This investigation begins here with an introduction to reciprocating pumps, specifically direct acting pumps that are driven by gas pressure. Then a description of the application of a reciprocating pump for use in the ARC pump technology will be given. Finally some equations to model direct-acting, reciprocating pump performance will be developed to gain an understanding of design and operating characteristics.

## 3.1 Direct-Acting Reciprocating Pumps

A reciprocating pump is a displacement pump in which a pumping element (such as a piston or a plunger) reciprocates (moves back and forth). Reciprocating pumps are best suited for high pressure, low volume services where its

capacity is directly related to the rate of reciprocation and the stroke volume of the pumping element [10].

Reciprocating pumps can be classified into two main types:

- Power Pumps
- Direct-Acting Pumps

Power pumps are reciprocating pumps which use a crankshaft driven by a motor, engine or turbine to cycle the pumping element. Alternatively, direct-acting pumps are driven by fluid pressure (either hydraulic or pneumatic). The schematic of a direct-acting reciprocating pump (DARP) is given in Figure 3.1. The drive fluid (at pressure $P_{DRIVE}$) pushes on a piston which subsequently pushes the pumping element (plunger) and the pumped fluid (at pressure $P_{PUMP}$). In most cases the piston has a much larger area in order to magnify the force applied through the plunger. This is advantageous because a low pressure fluid source (such as compressed air) can be used to drive the pumped fluid to very high pressures. A common application of DARPs is in chemical injection into high pressure pipelines.

DARPs can either be single acting (pumps fluid in forward motion only as shown in Figure 3.1) or double acting (fluid is pumped in both the forward and return direction). In a single acting pump, a spring is typically used to return the piston to its original position. In a double acting pump, the driving pressure is switched to the opposite side to return the piston to its starting position and pump the pumped fluid.

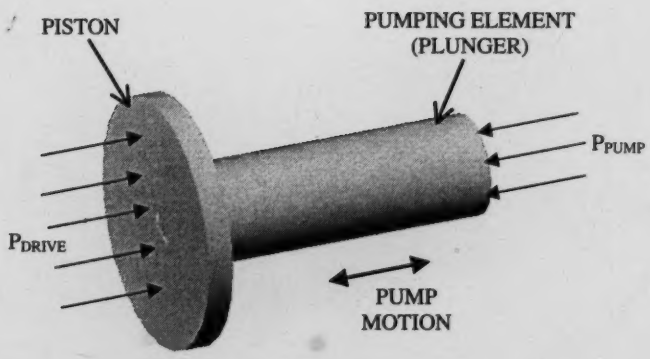


**Figure 3.1: Schematic of Direct-Acting Reciprocating Pump Operation**

## 3.2 Description of a Direct-Acting Pump used in the ARC Pumping Concept

Recall the ARC pumping concept introduced earlier in Figure 1.3. The system consists of a down-hole pump set at the bottom of the production tubing. Gas and liquid enter the bottom of the well and are separated by gravity. The gas and liquid then flow through the down-hole pump and exit up the production and liquid tubing respectively and flow to the surface. Although it is not clearly shown in Figure 1.3, the down-hole pump may be held in place at the bottom of the natural gas well with the use of a packer.

Although any type of pump that uses gas pressure to power it could be used in this application, the DARP appeared to be the most favorable. This is because the DARP has a simple design and its operation resembles the pumpjack used in oilfield production.

### 3.2.1 Description of Pump Operation

A very detailed description of the application of a DARP is given by Ridley et al. [25, 26, 27]. Here, a more general description of the pump application will be given. Within the downhole pump (aptly displayed as a black box in Figure 1.3) there are two main components: the pump itself and a controller. These two components and how they interact with the gas and liquid phases are shown schematically in Figure 3.2. The ARC application of the DARP utilizes a double acting type pump. The reciprocating motion of the pump is enabled through the use of a controller, which consists of a number of a

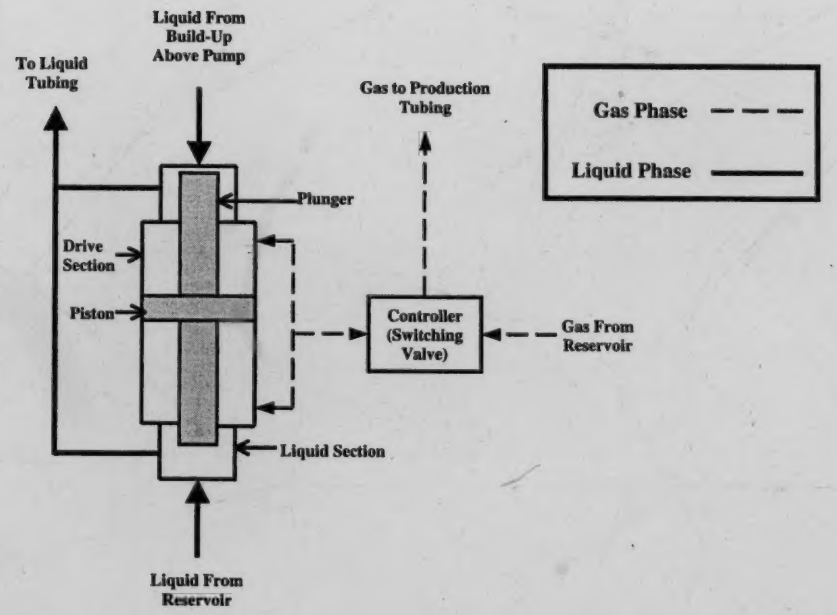


**Figure 3.2: Schematic of Direct-Acting Reciprocating Pump Application in the ARC Technology**

mechanical switching valves that regulate the flow of gas into and out of the drive section of the pump. The pump itself contains a drive section and two liquid sections, one at the top and the other at the bottom. If the need arises, multiple drive sections can be placed in series.

Gas from the reservoir is separated from the liquid phase and enters the controller. The gas is then directed into the drive section and pushes on the pump piston until it reaches the end of its stroke. From here the controller

switches the direction of the pump piston and the gas returns to the controller and is exhausted to the production tubing.

The liquid phase enters the bottom of the gas well and becomes separated from the gas. The liquid travels into the bottom liquid section while the pump stroke is moving upwards. Note that the drive section and liquid sections are sealed between them using some packing or some other means. As the pump piston moves down, the liquid is pumped into a discharge header and subsequently up the liquid tubing.

It is assumed during operation that some of the liquid produced by the gas well will be carried with the gas phase through the pump and will subsequently fall out once the gas has been exhausted to the production tubing. This liquid will build up above the pump and will be enter it through the top liquid section as the pump piston is moving down. Here, this liquid is pumped into the liquid discharge header and up the liquid tubing.

## 3.3 Mathematical Model of the Direct Acting Pump Performance

In order to examine the applicability of direct-acting pumps for use in the ARC pumping concept, a model to predict its performance is required. This model will be used to gain an understanding of design and operating parameters required to best utilize pressure from the gas phase to power the pump.

### 3.3.1 Definitions and Assumptions

In order to describe the pump mathematically, design and operating characteristics need to be defined along with some assumptions about its operation. Referring to Figure 3.3, the schematic of a direct-acting reciprocating pump (DARP) is given. The pump itself consists of a piston driven by gas pres-

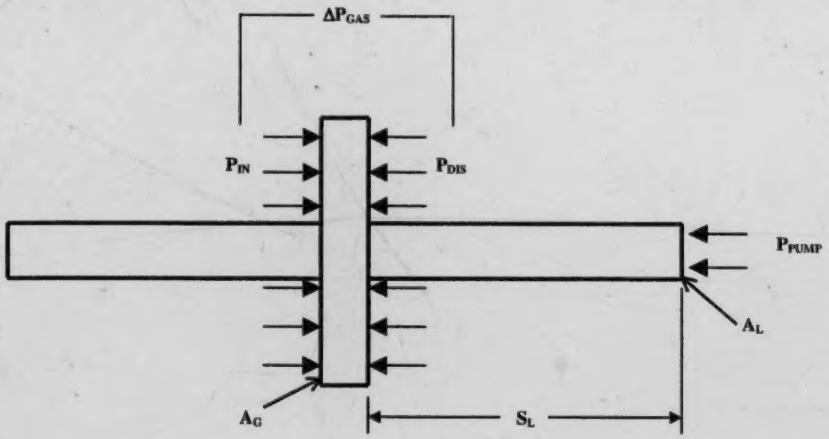


**Figure 3.3: Schematic of Direct-Acting Reciprocating Pump**

sure acting on area $A_G$ to generate a force that pumps the liquid phase to a pressure that acts on area $A_L$, which is the area of the plunger. The Area Ratio ($A_R$) of the pump is the ratio of area of the piston to the plunger and is shown mathematically as:

$$A_R = \frac{A_G}{A_L} \tag{3.1}$$

For each stroke of the pump, the piston and plunger travel length $S_L$. Therefore the volume of the liquid pumped per stroke is:

$$\hat{V}_l = A_L S_L \tag{3.2}$$

The force required is generated on the piston by the gas at the intake pressure $P_{IN}$ and is countered by the gas discharge pressure $P_{DIS}$. The net force on the piston is the difference between the gas intake and discharge pressures and is denoted as $\Delta P_{GAS}$. This net force is then used to deliver the liquid to the pumping pressure $P_{PUMP}$.

It is assumed that the piston moves slowly, and thus gas dynamics within the drive section of the pump can be ignored. To justify this assumption, consider a gas-driven DARP with a plunger with a circular cross-section with diameter of 25 mm. This pump is required to deliver 7 $m^3$/day (the liquid production rate of the "typical" Alberta gas well described in Chapter 2) of an incompressible fluid. The average velocity of the plunger would have to be 0.165 m/s to fulfill the pumping requirement. Compared to a speed of a sound for air at 298 K being approximately 330 m/s, the gas used to drive the pump will behave like an incompressible fluid while it is in the drive section. Using this assumption, the volume of gas used per stroke is:

$$\hat{V}_g = A_G S_L \tag{3.3}$$

at the intake conditions. Utilizing the definition of area ratio, the gas volume at intake conditions is related to the volume of liquid pumped by the equation:

$$Q_g = Q_l A_R \tag{3.4}$$

It is assumed that the mass of the piston is small and thus its weight and inertia are negligible. It is also assumed that for every stroke, the pump starts from rest and is stopped suddenly at the end of the stroke. The liquid is assumed to be incompressible.

### 3.3.2 Gas Utilization

In applying the use of reciprocating pumps for use in natural gas wells it is important to know how much gas is required to drive the pump. This is important because gas flowrate has a significant effect on the amount of reservoir pressure required to keep the gas well flowing. To model gas utilization, Equation 3.4 is used and is converted the volumetric flowrate at standard conditions, the same method as in Equation 2.10 from Chapter 2. The resulting equation becomes:

$$Q_{g,sc} = Q_l \, A_R \frac{P_{IN} T_{sc}}{P_{sc} z T_{IN}} \tag{3.5}$$

Dividing Equation 3.5 by the liquid volumetric flowrate results in a new parameter which will be defined here as the gas-liquid volume ratio which is governed by the equation:

$$R_{gl} = A_R \frac{P_{IN} T_{sc}}{P_{sc} z T_{IN}} \tag{3.6}$$

which has the same definition as gas-liquid ratio of a gas well defined in Chapter 2, but here has a different meaning. Examining Equation 5.2.2, it is apparent that if pump area ratio or intake pressure are increased, the amount of gas required to drive the pump will increase and will require greater pressure from the reservoir to sustain flow.

### 3.3.3 Pump Friction

There appears to be very little modelling work done for gas powered direct-acting reciprocating pumps. In most cases, these pumps are designed using a static analysis (i.e. the forces exerted by the gas pressure are balanced strictly by the liquid pressure forces) and adding a correction to account for friction effects. This is usually adequate because the forces of friction in the pump are generally small compared to the forces required to deliver the liquid to the pumping pressure. Once a pump is designed, it is tested thoroughly to determine its operating characteristics (pump curves).

Here a more general form of the force balance, one that includes a friction term, will serve as the starting point for the pump model:

$$\Delta P_{GAS} A_G = F_{Friction} + P_{PUMP} A_L \tag{3.7}$$

$F_{Friction}$ is the net friction force in the pump. The force balance in Equation 3.7 has the force generated by the gas pressure is balanced by the friction and force of the liquid pressure.

Friction in the pump is generated from a number of sources including:

- Mechanical friction within the drive section due to the reciprocating motion of the piston,
- Friction in the liquid section as the pumped fluid is drawn in and pumped out and
- Pressure losses in drive section due to viscous friction as the gas flows in and out.

Rather than evaluate each of these terms individually, all sources of friction are lumped together as in Equation 3.7. To model the friction, it was assumed that it is proportional to pump speed with the form:

$$F_{Friction} = C_F V_P \tag{3.8}$$

where $C_F$ is a friction coefficient and $V_P$ is the velocity of the piston. This model was chosen because it is assumed that the mechanical friction in the pump drive would be the dominate source. This model corresponds with hydrodynamic lubrication theory, given in texts such as Juvinall and Marshek [15], used to estimate friction in sliding bearings.

Piston velocity is defined here as:

$$V_P = \frac{Q_l}{A_L} \tag{3.9}$$

Using this relation in Equation 3.8 pump friction becomes:

$$F_{Friction} = C_F \frac{Q_l}{A_L} \tag{3.10}$$

An alternatively method of analysis for pump friction is to start with Equation 3.7 and divide through by $A_L$ and recalling the definition of area ration results in:

$$\Delta P_{GAS} A_R = \frac{F_{Friction}}{A_L} + P_{PUMP} \tag{3.11}$$

Introducing a new term called pump friction pressure defined mathematically as:

$$P_{FRICTION} = \frac{F_{Friction}}{A_L} \tag{3.12}$$

converts the friction into an equivalent pumping pressure. Solving for the pump friction pressure results in:

$$P_{FRICTION} = \Delta P_{GAS} A_R - P_{PUMP} \tag{3.13}$$

With this result by Equation 3.13 can be used to solve for the friction coefficient by inserting it into Equation 3.10 and utilizing the definition of pump friction pressure. As a result, friction coefficient can be calculated using the equation:

$$C_F = \frac{A_L^2(\Delta P_{GAS} A_R - P_{PUMP})}{Q_l} \tag{3.14}$$

As well, using this equation, the friction coefficient could be determined using experimental data. Equation 3.13 can also be expressed as:

$$\Delta P_{GAS} = \frac{1}{A_R}\Big(P_{FRICTION} + P_{PUMP}\Big) \tag{3.15}$$

and reduces to the static analysis if friction is negligible. This would be the case if $P_{PUMP}$ was large. However, without sufficient knowledge of the magnitude of friction, the friction term is kept for subsequent analysis.

Since the mass of the piston is neglected, the effect of stroke length is not considered. In general, a longer stroke is desired because it will minimize the occurrence of the transient effects caused by the sudden stop and start at the end of each pump stroke. The maximum stroke length will likely determined by structural and size limits.

### 3.3.4 Thermodynamic Efficiency

The model given previously only considers the forces involved during pump operation. In order to gain an understanding of the the design and operating

conditions where gas pressure is best used to pump liquid, a model for thermodynamic efficiency of the pump is now given. Thermodynamic efficiency ($\eta$) of a direct-acting reciprocating is defined here as:

$$\eta = \frac{W_l}{W_g} \tag{3.16}$$

where $W_l$ is the work done on the liquid during pumping and $W_g$ is the work done by the gas to drive the pump. The liquid work is the product of liquid flow rate and pumping pressure and is defined mathematically as:

$$W_l = P_{PUMP} Q_l \tag{3.17}$$

The work done by the gas pressure is assumed to be the work obtained from the gas if it were expanded isentropically from the intake pressure to the discharge pressure. Using this assumption, Equation 2.56 from Chapter 2 obtained from Moran [22] can be used with some substitutions to show that gas work becomes:

$$W_g = Q_g P_{IN} \frac{k}{k-1} \left(1 - \left(\frac{P_{DIS}}{P_{IN}}\right)^{\frac{k-1}{k}}\right) \tag{3.18}$$

Recognizing that discharge pressure is defined earlier as:

$$P_{DIS} = P_{IN} - \Delta P_{GAS} \tag{3.19}$$

and inserting it into Equation 3.18 yields:

$$W_g = Q_g P_{IN} \frac{k}{k-1} \left(1 - \left(1 - \frac{\Delta P_{GAS}}{P_{IN}}\right)^{\frac{k-1}{k}}\right) \tag{3.20}$$

Inserting Equations 3.17 and 3.20 into Equation 3.16 thermodynamic efficiency becomes:

$$\eta = \frac{k-1}{k} \frac{P_{PUMP} Q_l}{Q_g P_{IN} \left(1 - \left(1 - \frac{\Delta P_{GAS}}{P_{IN}}\right)^{\frac{k-1}{k}}\right)} \tag{3.21}$$

Combining Equations 3.21 and 3.15 efficiency of the pump becomes:

$$\eta = \frac{k-1}{k} \frac{P_{PUMP} Q_l}{Q_g P_{IN} \left(1 - \left(1 - \frac{P_{FRICTION} + P_{PUMP}}{P_{IN} A_R}\right)^{\frac{k-1}{k}}\right)} \tag{3.22}$$

Recall that the volumetric flowrate of liquid is proportional to the volumetric flowrate of gas at the intake conditions, using Equation 3.4 efficiency becomes:

$$\eta = \frac{k-1}{k} \frac{P_{PUMP}}{P_{IN} A_R \left(1 - \left(1 - \frac{P_{FRICTION} + P_{PUMP}}{P_{IN} AR}\right)^{\frac{k-1}{k}}\right)} \tag{3.23}$$

Examining Equation 3.23, the effect of friction serves to reduce the thermodynamic efficiency of the reciprocating pump. Introducing the normalized pumping pressure, defined mathematically as:

$$\tilde{P}_{PUMP} = \frac{P_{PUMP}}{P_{IN} A_R} \tag{3.24}$$

and applying it to the special case where friction is neglected, Equation 3.23 becomes:

$$\eta = \frac{k-1}{k} \frac{\tilde{P}_{PUMP}}{\left(1 - \left(1 - \tilde{P}_{PUMP}\right)^{\frac{k-1}{k}}\right)} \tag{3.25}$$

Thermodynamic efficiency of a gas-powered DARP can be determined simply from one dimensionless value, which is based on operating conditions (pump pressure and intake gas pressure), design conditions (area ratio) and specific heat ratio of the gas used to drive the pump. To examine the effect of normalized pump pressure, a plot of thermodynamic efficiency is given for a pump using air ($k = 1.4$) and the natural gas mixture of the gas well analyzed in Chapter 2 ($k = 1.25$ from Appendix A) is given in Figure 3.4.

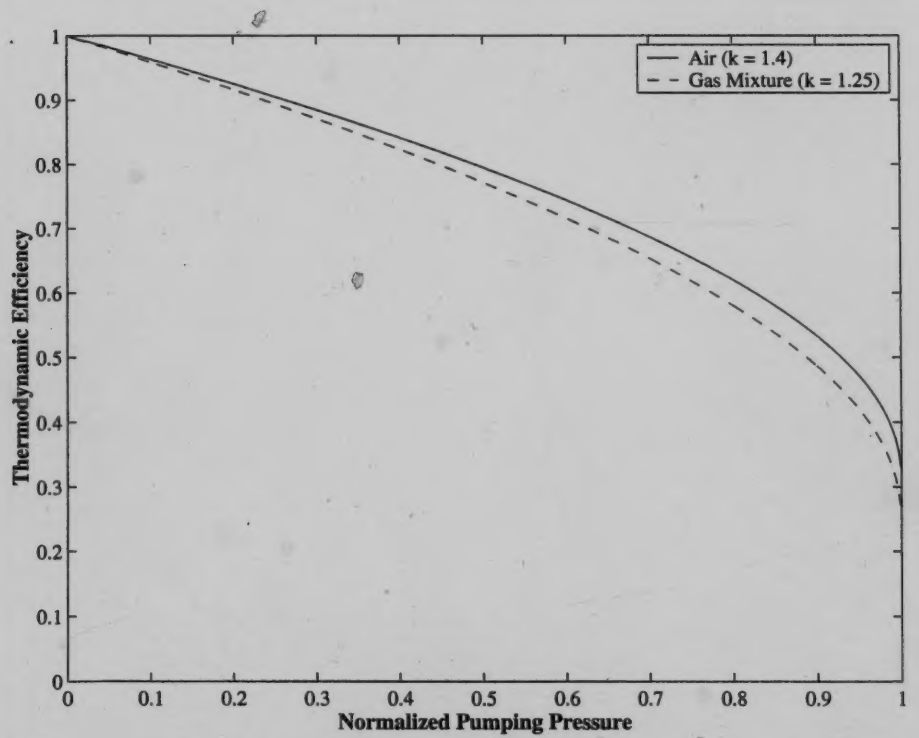


**Figure 3.4: Thermodynamic Efficiency as a Function of Normalized Pressure for a Gas-Powered, Direct-Acting Reciprocating Pump**

The results shown in Figure 3.4 show that the thermodynamic efficiency is maximized at lower normalized pumping pressures. However, the efficiency degrades more at higher normalized pumping pressures when using the gas mixture to power the pump due to its lower specific heat ratio.

The significance of these results is that for a given pumping pressure, the

thermodynamic efficiency can be improved if either the pump area ratio or the gas intake pressure are increased. As well, thermodynamic efficiency decreases more with $\tilde{P}_{PUMP}$ at higher $\tilde{P}_{PUMP}$ values. Therefore, the relative improvement in thermodynamic efficiency with increased area or gas intake pressure is greater at higher initial values of $\tilde{P}_{PUMP}$.

### Effect of Pump Friction

To examine the effect of friction on thermodynamic efficiency the following test case is presented. In this situation, pump friction pressure is increased from 0 to 100 percent of the pumping pressure for normalized pressures of 0.5, 0.25, 0.16 and 0.125. The results of this test case using air ($k = 1.4$) as the drive gas are presented in Figure 3.5. The results show that for all cases that increased pump friction results in lower thermodynamic efficiency. However, thermodynamic efficiency can be improved if pump area ratio and/or gas intake are increased and effectively reducing the normalized pumping pressure. This agrees with the results obtained in Figure 3.4. Also, the effect of friction on degrading thermodynamic efficiency is smaller when normalized pressure is smaller (or area ratio and pump gas intake pressure are larger).

In some cases, thermodynamic efficiency can be improved by increasing the pumping pressure. Referring to point '$A_1$'in Figure 3.5, the pump friction is 80 percent of the pumping pressure for a normalized pressure of 0.125. At point '$A_1$' thermodynamic efficiency is 51 percent. By doubling the pumping pressure, pump friction is reduced to 40 percent of the pumping pressure and the normalized pressure becomes 0.25. This corresponds to point '$B_1$' and a

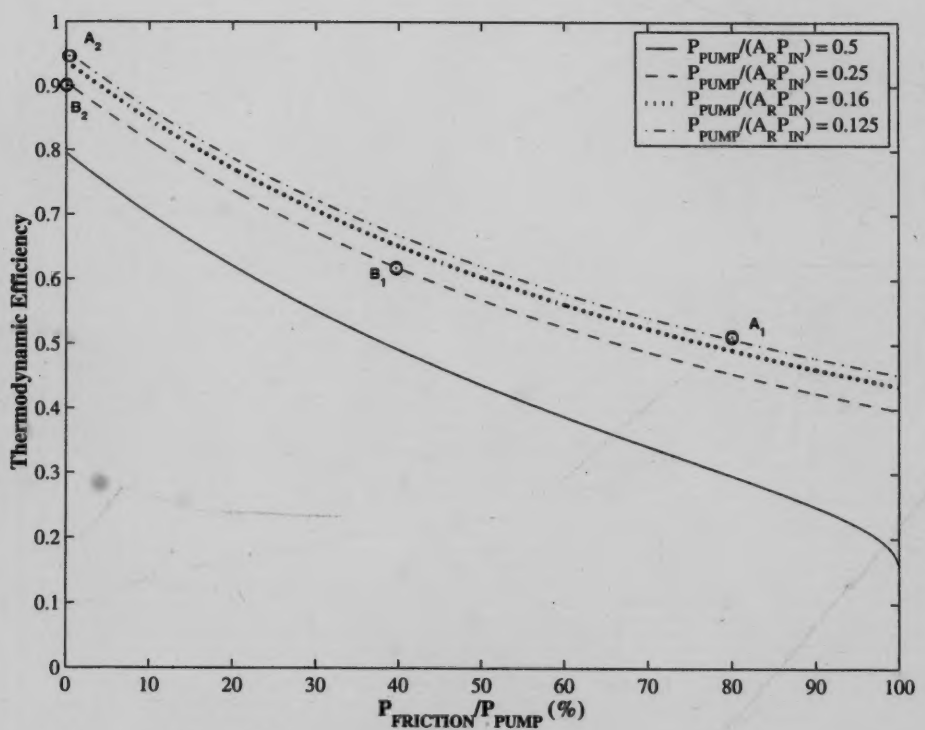


**Figure 3.5: Effect of Friction on Pump Thermodynamic Efficiency**

thermodynamic efficiency 63 percent. However in the case when there is no friction(points '$A_2$' and '$B_1$'), this procedure fails and efficiency is reduced from 95 to 90 percent.

## 3.4 Summary

In this chapter an introduction to reciprocating pumps was given along with a description of its application in the ARC pumping concept. Mathematical

models to predict gas utilization, thermodynamic efficiency and to characterize friction in reciprocating pumps were presented.

Gas utilization for a reciprocating pump is predicted to increase with both area ratio and gas intake pressure. Friction was modelled using a friction coefficient and also expressed in terms of an equivalent pumping pressure. Thermodynamic efficiency can always be improved with increased area ratio and/or gas intake pressure. When friction is present, thermodynamic efficiency can sometimes be improved by increasing the pumping pressure as well. This information can now be used to understand reciprocating pump performance in a physical model.

CHAPTER 4

# Physical Model of a Reciprocating Pump

The purpose of this chapter is to discuss an experimental investigation of a reciprocating test pump. The results from this investigation are compared with pump performance predictions obtained from the mathematical models introduced in the Chapter 3.

## 4.1 Description of the Apparatus

### 4.1.1 Physical Pump Model

A direct-acting reciprocating test pump was designed and manufactured for testing. A schematic of this test pump is shown in Figure 4.1 and a photograph in Figure 4.2. The test pump consists of two parts: the pump itself and a controller to regulate the flow of gas and thus the reciprocating motion of the pump. The controller consists of two proximity probes, a solenoid valve and an electronic control box. The pump itself consists of four different external parts:

- the End Section (2),

- the Liquid Section (2),
- the Drive Section (2) and
- the Coupling (1).

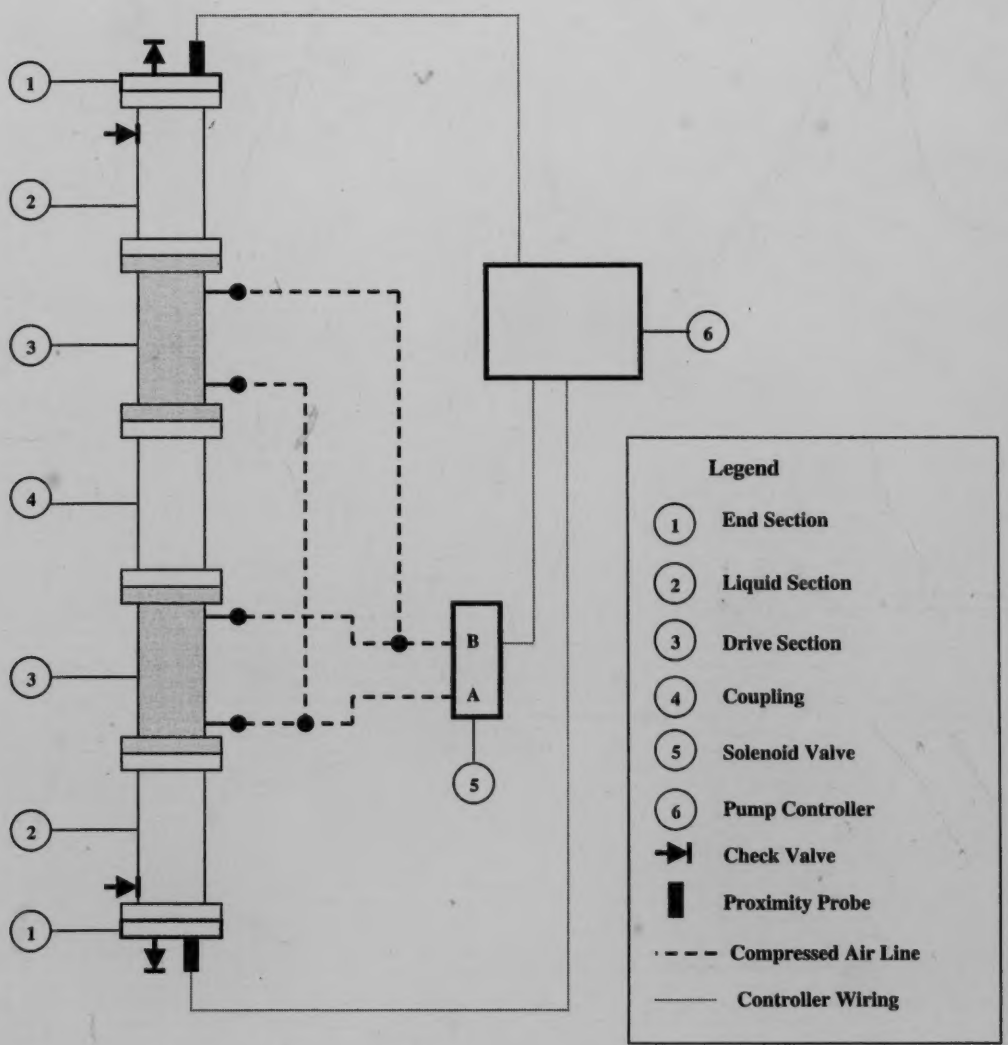


**Figure 4.1: Schematic of Test Reciprocating Pump**

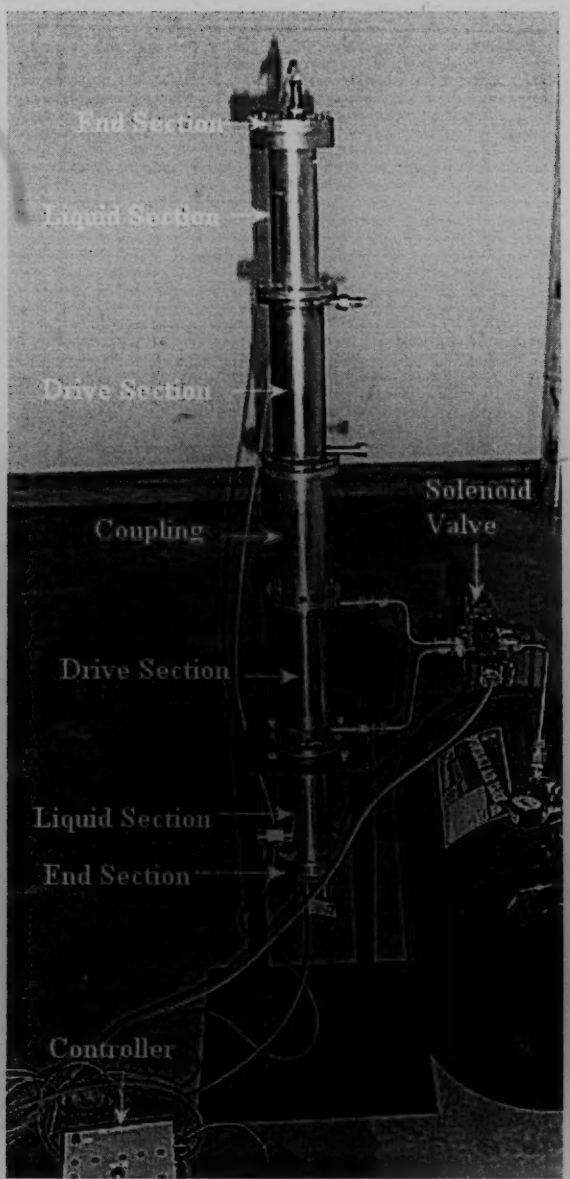


**Figure 4.2: Photograph of Test Reciprocating Pump**

Within the pump there are two pumping elements, with one shown schematically in Figure 4.3. Each pumping element is manufactured from a single

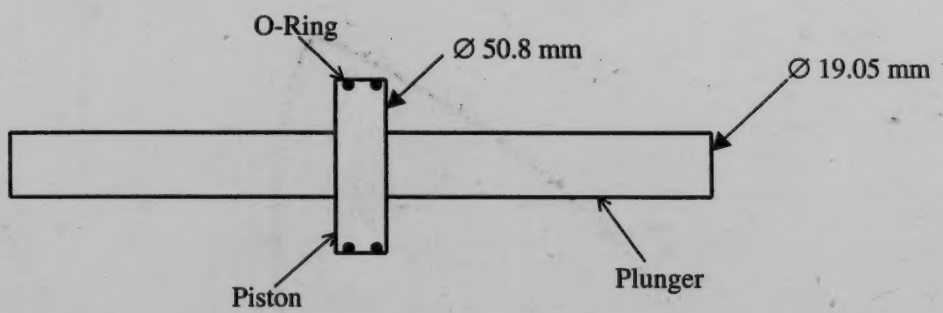


**Figure 4.3: Schematic of Pumping Element in Physical Pump Model**

piece of aluminum and consists of a piston and two plungers. The pumping element was anodized to increase its resistance to wear. This piston has a diameter of 50.8 mm and the plungers have a diameter of 19.05 mm. The pumping element has a stroke length of 111.6 mm. The piston has two O-rings installed to minimize the amount of gas leaking across it while the pump is in operation. Each pumping element weighs approximately 430 g and displaces 31.7 $cm^3$ per stroke.

A photograph of the test pump components is given in Figure 4.4. The piston of each pumping element is set within each drive section of the pump. The drive section is manufactured from stainless steel and has two flow taps

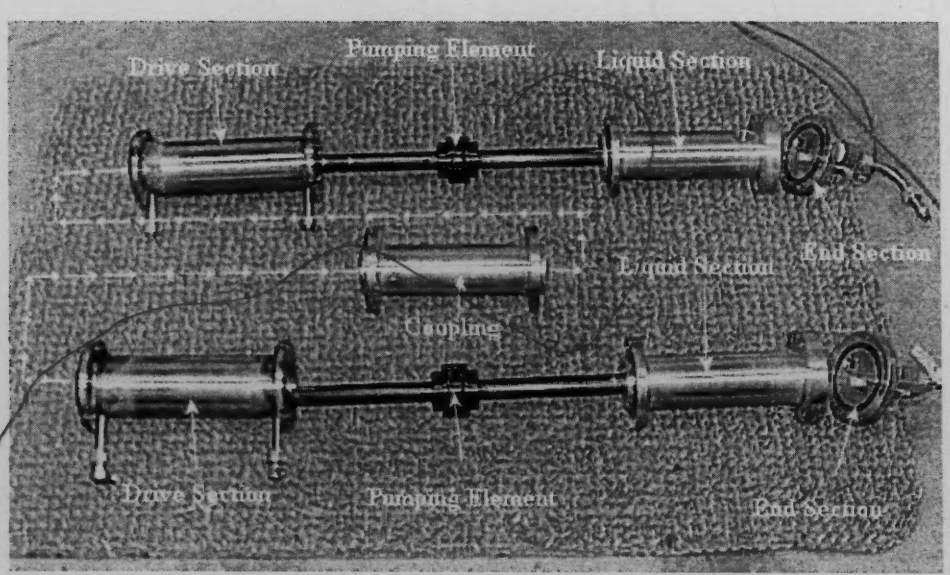


**Figure 4.4: Photograph of Test Pump Components**

to allow gas to flow in and out and drive the pumping element. The two drive sections are joined together using the coupling made of brass. Each end of the coupling is connected to a drive section using six bolts. Inside the coupling, the two pumping elements are connected by nipple that is threaded into a plunger of each element.

Each drive section is also connected to a liquid section, which is made of brass, using six bolts. Here, the plunger reciprocates to pump the liquid. Liquid is brought in from a liquid intake line through a check valve that is threaded into the side of each liquid section. Liquid is discharged through a second check valve that is threaded into the end section of the pump.

The end section connects the liquid section to a discharge line. A proximity probe is also threaded into the end section of the pump. This is shown in the photograph given in Figure 4.5. The proximity probe is used to sense

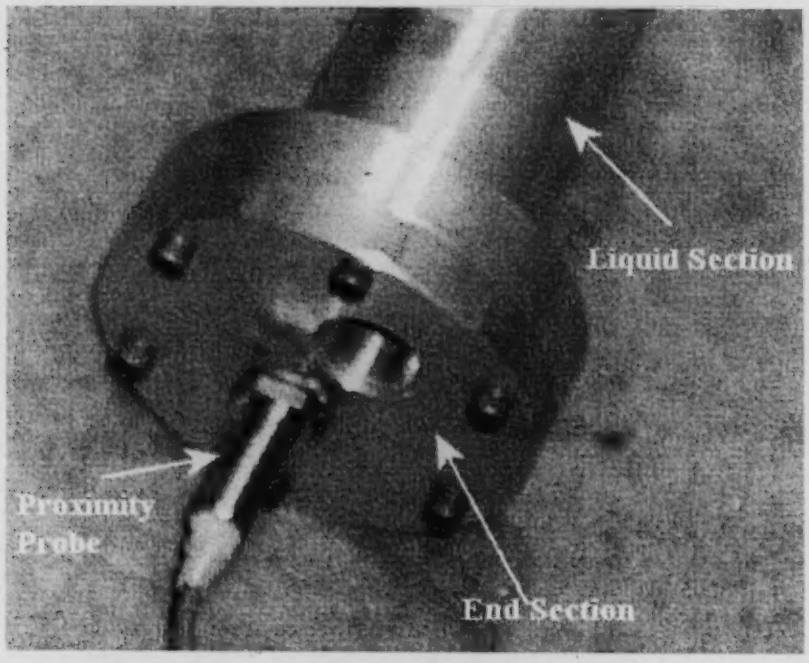


**Figure 4.5: Close-up of Liquid and End Section**

the pumping element when it reaches the end of its pump stroke. The proximity probe energizes and sends a signal to the pump controller which then sends a signal to switch the flow of gas through the solenoid valve (energizes solenoid A or B). The proximity probe threaded into the bottom end section is referred to as probe A and the probe at the top is referred to as probe B.

Proximity probe A and B correspond with solenoid A and B respectively. For example, when solenoid A is energized, gas from an intake pressure is allowed to flow into each drive section (through the bottom tap). At the same time solenoid B is de-energized and gas is allowed to flow out of the drive section (through the solenoid valve) to some discharge pressure. The net pressure difference causes the piston move upwards until it reaches the top of its stroke. The proximity probe at the top end section (probe B) will sense the piston and relay a signal back to the controller and reverse the direction of gas flow by energizing solenoid B and de-energizing solenoid A.

In the patents of Ridley et al. [25, 26, 27] a mechanical gas flow controller is used. Here an electronic controller was used because it was simple to design and could be implemented into a data acquisition system to measure the speed of the pump.

The test pump can be operated using either one or both drive sections. This is referred to as single-stage or two-stage operation. In single stage operation, only one drive section is connected to the solenoid valve to provide gas pressure to its corresponding pumping element. The other drive section operates at ambient conditions with its pumping element carried along as a "dummy" piston. In single stage operation the pump has an area ratio of 6.11 (gas to liquid). In two stage operation, both drive sections are connected to the solenoid valve and each pumping element is driven by gas pressure. In two stage operation the pump has an area ratio of 12.22.

### 4.1.2 Test Facility

The facility used to examine the performance of the test pump consists of two loops: one for gas (compressed air) flow and the other for liquid (water). For the gas flow loop, the system operates at ambient temperature with a maximum pressure of 700 kPag. The liquid flow loop also operates at ambient temperature and the maximum operating pressure was 1000 kPag. The details of each flow loop will now be discussed.

#### Gas Flow Loop

A schematic of the gas flow loop is given in Figure 4.6. In the gas flow loop, compressed instrument air is used as the fluid medium. All air lines were constructed using 1/4 inch (4.5 mm I.D.) Swagelok tubing and fittings.

Compressed air enters the gas flow loop from the building air supply and flows through an air filter (Filter A100) and a coalescer (Filter A101) to remove any dust and condensed water that may be present. The air then flows through a pressure regulator (Regulator A100) and into a 50 L compressed air tank. The compressed air tank is used to dampen gas pressure fluctuations and to provide a large source of compressed air close to the pump apparatus. Here the gas pressure slightly downstream of the compressed air tank is measured (PGT A100). Lines connected to the pressure regulators were filled with water to maximize their response. The air then flows from the tank to the solenoid and valve and its temperature is measured (TC A100).

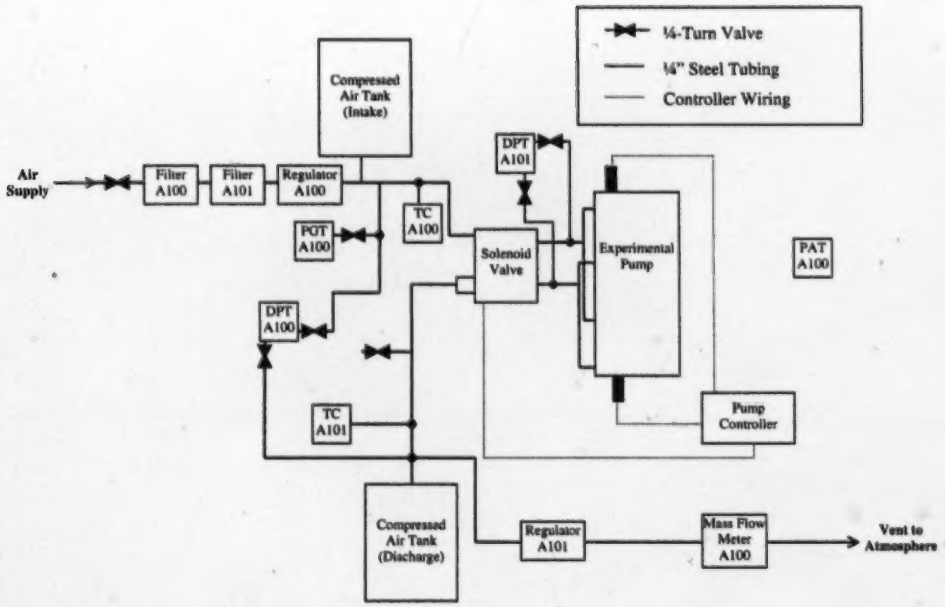


**Figure 4.6: Schematic of Gas Flow Loop**

From the solenoid valve, air flows into the drive section(s) of the test pump, drives the pump until it reaches the end of a stroke and then returns to the solenoid valve. Here the differential pressure between the two outlets of the solenoid valve (recall valves A and B from Figure 4.1) is measured (DPT A101). The air discharges from the drive section of the test pump, through the solenoid valve to a second 50 L compressed air tank and its temperature is measured (TC A101). Also, the approximate differential pressure between the two compressed air tanks is measured (DPT A100). The air flows from the discharge tank to a back-pressure regulator (Regulator A101), which can

be set at various levels. From here the flowrate of the gas is measured as it flows through a mass flow meter (Mass Flow Meter A100) and exhausts to atmospheric pressure.

The gas flow loop is de-pressured by disconnecting the air supply and venting the system at that location and at a vent valve located between the solenoid valve and discharge air tank.

### Liquid Flow Loop

A schematic of the liquid flow loop is given in Figure 4.7. For the liquid loop, the fluid medium is water. Water enters the liquid flow loop from a water supply. The water flows into a 220 L inlet tank to supply the pump. The water flows from the tank to the liquid suction header where the temperature is measured (TC L100). From here the water flows into either the top or bottom liquid section of the experimental pump through a check valve. From the liquid section the water is pumped through a second check valve and into the discharge header where the temperature (TC L101) and pressure (PGT L100) are measured. The pressure in the discharge header is generated partly by a relief valve (RV L100). The water flows through the relief valve and enters a 4 m tall vertical flow line. This flow-line is used to generate additional back-pressure on the discharge line. The water flows to the top of the flow-line and returns down to 20 L bucket (Tank) where it is be collected and its mass measured (Scale L100). Valves are placed along the liquid flow loop to aid in the removal of trapped air and to drain the system.

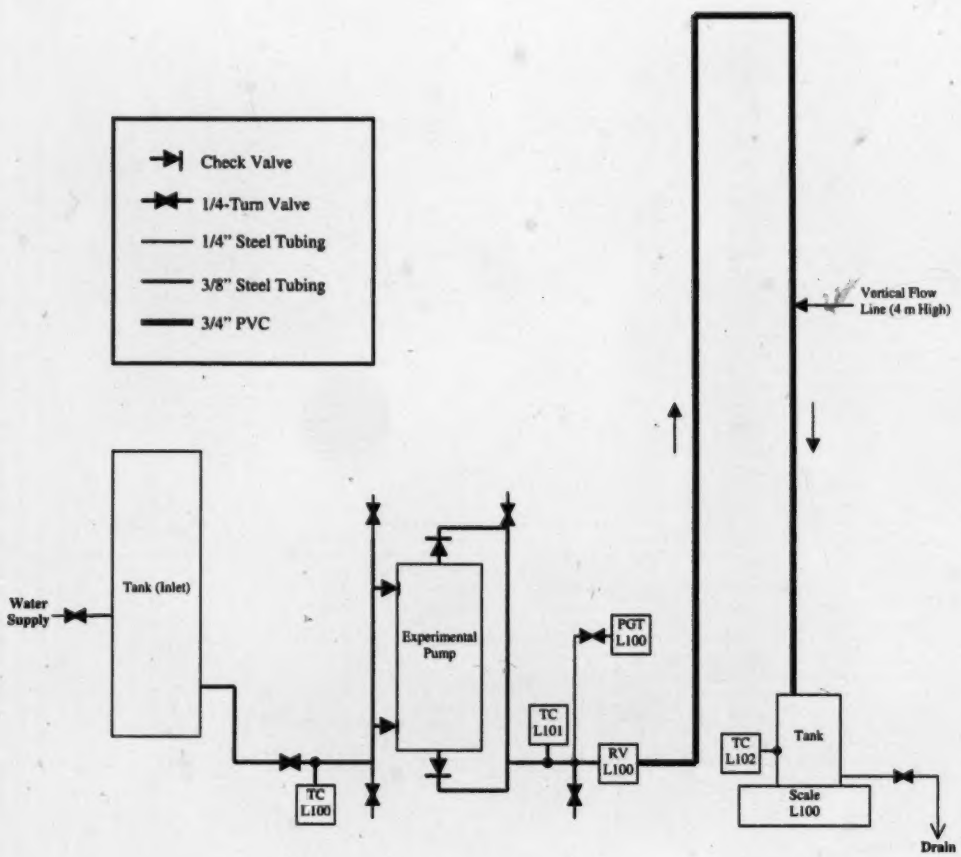


**Figure 4.7: Schematic of Liquid Flow Loop**

### 4.1.3 Instrumentation and Data Acquisition

A list of the instrumentation used in the gas and liquid flow loops is given in Table 4.1. To collect test data for the physical pump model, two data acqui-

**Table 4.1: Gas and Liquid Flow Loop Instrumentation**

| Label | Make | Model | Range | Accuracy |
|---|---|---|---|---|
| PGT A100 | Rosemount | 3051CG4 | -101 to 2070 kPag | ± 2.2 kPa |
| DPT A100 | Rosemount | 3051CD3 | -248 to 248 kPag | ± 0.5 kPa |
| DPT A101 | Rosemount | 3051CD3 | -248 to 248 kPag | ± 0.5 kPa |
| Mass Flow Meter A100 | Hastings | HFM 200 | 0 to 400 SLPM[1] | ± 4 SLPM |
| PAT A100 | Vaisla | PTA 247 | 86 to 105 kPaa | ± 50 Pa |
| PGT L100 | Rosemount | 3051CD3 | -248 to 248 kPag | ± 0.5 kPa |
| Scale L100 | Sartorius | BP 34 | 0 to 34,000 g | ± 0.5 g |
| TC A100-A101 and TC L100-L102 | Omega | Type K Thermocouple | | ± 0.5°C |

sition programs, one referred to here as *Steady* and the other as *Transient*, were written using Labview. The *Steady* data acquisition program was used primarily to measure and monitor variables expected to be static or changing slowly while the pump was running at a set speed. In the *Steady* data acquisition program, the following measurements were taken every second:

[1]Standard conditions for the Hastings Mass Flow Meter is 0° C and 1 Atm.

- Barometric Pressure (PAT A100)
- Air Intake Tank Pressure (PGT A100)
- Air Tank Differential Pressure (DPT A100)
- Liquid Discharge Header Pressure (PGT L100)
- Mass Flow of Gas (Mass Flow Meter A100)
- Mass of Liquid in Bucket (Scale L100)
- Stroke Count (using Proximity Probes A and B)
- Air Intake Temperature (TC A100)
- Air Discharge Temperature (TC A101)
- Liquid Inlet Temperature (TC L100)
- Liquid Discharge Temperature (TC L101)
- Liquid in Bucket Temperature (TC L102)

The *Transient* program was used to measure variables that were changing while the pump was running at a set speed. In the *Transient* program, the following measurements were taken ever 50 milliseconds (12 samples per stroke at max speed of 100 strokes per minute);

- Differential Pressure across drive section (s(DPT A10a)
- Liquid Discharge Header Pressure (PGT L100)
- Solenoid Valve A output (0 Volts off, 5 Volts on)
- Solenoid Valve B output (0 Volts off, 5 Volts on)

## 4.2 Test Procedure

For a given pumping scenario (based on gas intake pressure, liquid discharge pressure and single or two-stage operation), the sequence consisted of 8 to 12 points taken throughout the operating range of the pump. The operating range of the experimental pump investigated here was at a liquid flowrate of about about 5 to 50 mL/s which corresponds to a pump speed of approximately 10 to 100 strokes/minute. A list of tests performed in this research work and their conditions are given in Appendix D.

For each pumping scenario the following test procedure was followed. Refer to Figures 4.6 and 4.7 for details about the apparatus.

1. With the gas flow loop completely decompressed, a 60-second test of the instrumentation was performed using the *Steady* data acquisition program. This was done to determine the offset (if any) of pressure transducers PGT A100, DPT A100 and DPT A101 and the Mass Flow Meter A100 when the gas flow loop is at atmospheric pressure and zero gas flow.

2. The gas flow loop was slowly filled with compressed air until it reached the set operating pressure. This was done to ensure that the pump would not be operated at speed outside of its operating range. As well, this step would minimize the carryover of condensed water that may have been present in the air supply line.

3. Once the gas loop reached the operating pressure, the speed of the pump was set to approximately 50 strokes/minute by adjusting either

the pressure regulator PR A100 or back-pressure regulator PR A101. The experimental pump was then allowed to run for approximately 30 to 40 minutes as a warm-up.

4. After the warm-up stage, the pump was set to a speed in the middle of the flow range (at approximately 50 strokes/min). Using the *Steady* data acquisition program to monitor the instrumentation, the pump was allowed to run until the gas pressures and flowrates stabilizes.

5. With the gas pressures and flowrates stabilized, the valve from the bucket to the drain was closed and the *Steady* data acquisition program was set to log all of its variables every second for selected duration.

6. At the end of the selected duration, the valve to the drain was opened and the *Steady* data acquisition program was paused. The *Transient* data acquisition program was then run for a selected duration, measuring each variable in 50 millisecond intervals.

7. The *Steady* acquisition program was then resumed to monitor the instrumentation and the pump speed was changed by adjusting one or both of the pressure regulators.

8. Steps 6 and 7 are repeated for all data points taken throughout the flow range.

9. After all data points are taken, the gas flow loop was de-pressurized and another 60 second test of the instrumentation was performed to measure the offset of the pressure transducers and flowmeter at null conditions.

## 4.3 Results

Using the apparatus explained earlier, the test pump was tested and compared with the performance models developed in Chapter 3. The test conducted are listed in Appendix D. The results will give insight into the gas utilization, frictional effects and thermodynamic efficiency of a gas powered direct acting reciprocating pump as well as repeatability of the tests.

### 4.3.1 Gas Utilization

In Chapter 3, it was shown mathematically that the volume of the gas at standard conditions is directly related to volume of liquid pumped. This was demonstrated in Equation 3.6 and is given below:

$$R_{gl} = A_R \frac{P_{IN} T_{sc}}{P_{sc} z T_{IN}}$$

For the operating conditions experienced in the gas flow loop mentioned earlier, $z$-factor will be assumed unity. Examining Equation 3.6, the gas-liquid volume ratio increases with intake pressure. Therefore in order to verify this equation, tests were performed with the pump operating at a constant speed of approximately 40 strokes/minute, but varying the intake tank pressure. These tests were performed on both single (Test No. 5) and two-stage (Test No. 6) pump operation.

At each intake tank pressure, the *Steady* data acquisition program was used to capture the data over 150 seconds. The results for temperature, pressure and gas flow were determined by taking their mean values for the entire duration. Liquid flowrate was determined by taking the mass of water collected

in the bucket during each test and dividing it by 150 seconds. The mass of liquid was converted to volume by assuming a density of 1 kg/L. Further details regarding this data analysis is given in Appendix E.

For both the single stage and two-stage pump operation the results are given in Figure 4.8. For comparison, Equation 5.2.2 is plotted for single and two-stage pump operation (area ratios 6.111 and 12.222 respectively) based on an air intake temperature of 291 K (which was the average intake air temperature measured in both experimental results).

The experimental results for single and two-stage operation behave linearly and only differ from the model results. This offset is likely caused by less than ideal volumetric efficiencies in the liquid section of the pump. The reduced volumetric efficiency results in lower than expected volumes of liquid per stroke and would give the measured $R_{gl}$ a higher value. Regardless, the results in Figure 4.8 verify the model for gas utilization for a gas driven, DARP.

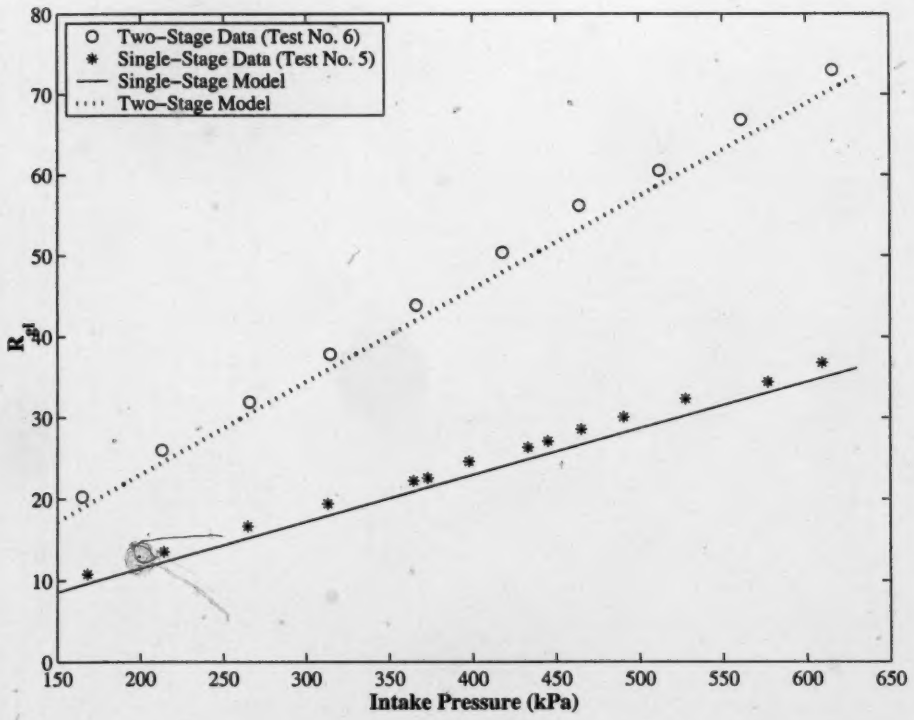


**Figure 4.8: Experimental and Mathematical Model Gas-Liquid Volume Ratios for Physical Pump Model**

### 4.3.2 Friction

The next stage in the experimental investigation was to examine frictional effects in the test pump. Pump friction was characterized in Chapter 3 as an equivalent pumping pressure defined mathematically in Equation 3.13 and given here as:

$$P_{FRICTION} = \Delta P_{GAS} A_R - P_{PUMP}$$

Pump friction, as mentioned in Chapter 3, is the sum of losses in the pump due to:

- mechanical friction as the pumping element is in reciprocating motion,
- liquid flow pressure losses from the pump inlet to the pump discharge header and
- gas flow pressure losses from where $\Delta P_{GAS}$ is measured to the drive section of the experimental pump.

Pump friction pressure ($P_{FRICTION}$) is calculated using transient data (obtained using the *Transient* data acquisition). For each data point the root-mean-square differential pressure across the drive section ($\Delta P_{GAS}$ measured by DPT A101) and the average liquid discharge header pressure ($P_{PUMP}$ measured by PGT L100) was used to calculate pump friction. Details regarding the analysis of raw transient data are given in Appendix E.

To examine pump friction pressure, the results of two sets of single and two stage pump operation tests are presented. These tests were:

- A pair of a single and two-stage configurations deliver water to a pressure of approximately 925 kPag. These results were obtained from tests number 9 (single-stage) and 10 (two-stage) and are given in Figure 4.9.
- A pair of a single and two-stage configurations deliver water to a pressure of approximately 215 kPag. These results were obtained from tests number 19 (two-stage) and 20 (single-stage) and are given in Figure 4.10.

These tests results were selected because each pair was performed consecutively on their respective test dates.

The results in Figures 4.9 and 4.10 show that the pump friction pressure behaves in a similar manner for both pairs of tests. At low liquid flowrates, friction pressure has a finite value and decreases with liquid flow rate. In this region, pump friction pressure for single-stage and two-stage operation are in agreement within measurement accuracy. As liquid flowrates increase, the pump speed increases and pump friction decreases to some minimum value. At higher liquid flowrates, the pump friction increases with liquid flowrate, but the rate of change is higher for two-stage operation. The reason for this difference will be discussed later, but first an explanation for the general friction behavior is given.

At low liquid flowrates the pumping element moves very slowly and periodically stops and starts as it travels the length of its stroke. To demonstrate this consider Figure 4.11, which is a trace for a single up stroke and down stroke of the physical pump operating at at a low liquid flowrate. Figure 4.11

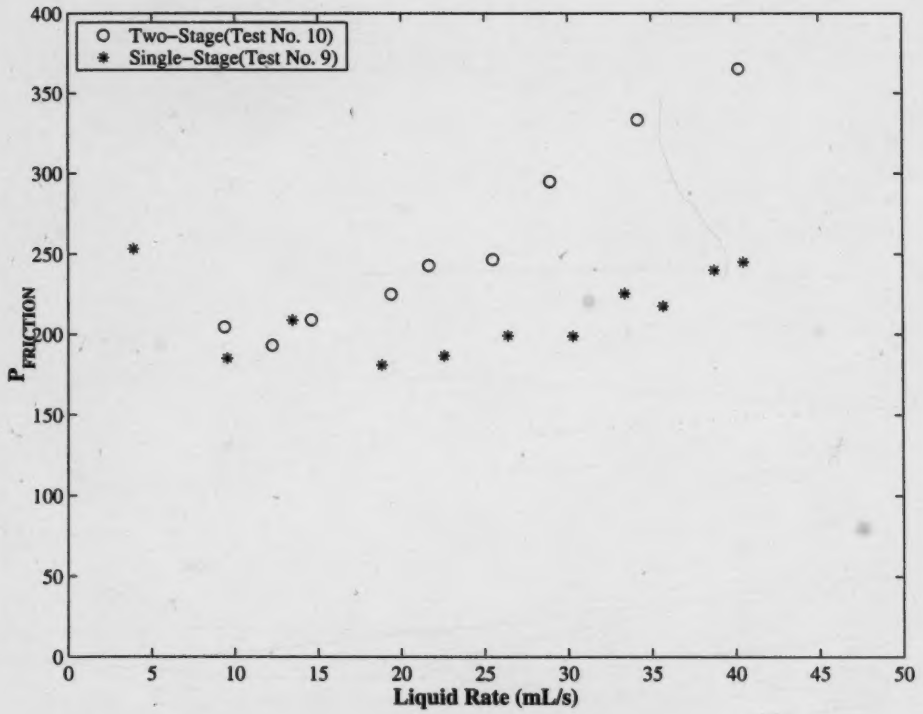


**Figure 4.9: Pump Friction Results for Single and Two-Stage Pump Operation($P_{PUMP}$ = 925 kPag)**

is the trace from test number 19, with a liquid flowrate of 4 mL/s (or 8 strokes/minute). The output voltage for solenoid valve A (5 Volts for on to push the pumping element up) is also given in Figure 4.11. The starting and stopping of the pumping element is indicated by the spikes in $\Delta P_{GAS}$, where differential pressure drops, the pumping element stops, the differential pressure builds up until to generate enough force to get the piston moving again.

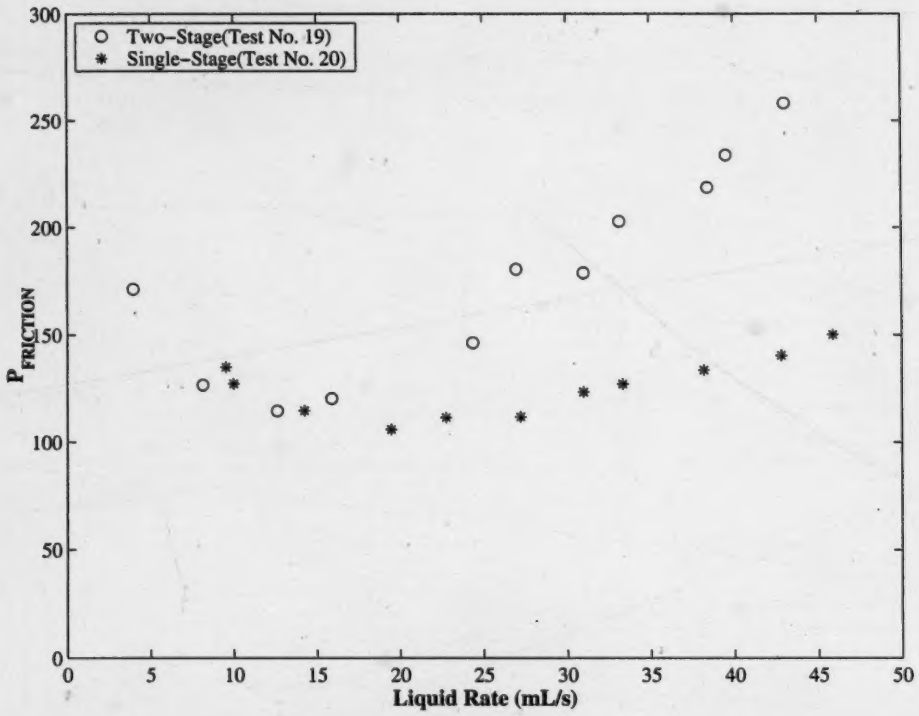


**Figure 4.10: Pump Friction Results for Single and Two-Stage Pump Operation($P_{PUMP}$ = 215 kPag)**

The static friction required to get the pumping element moving at low liquid flowrate is greater than the sliding friction. As the pump stroke frequency increases (corresponding to higher liquid flowrate), the friction decreases because the pump is moving more smoothly (i.e. no longer stopping and starting). This is shown in Figure 4.12, from test number 19 at a liquid flowrate of 12.6 mL/s (24 strokes/min).

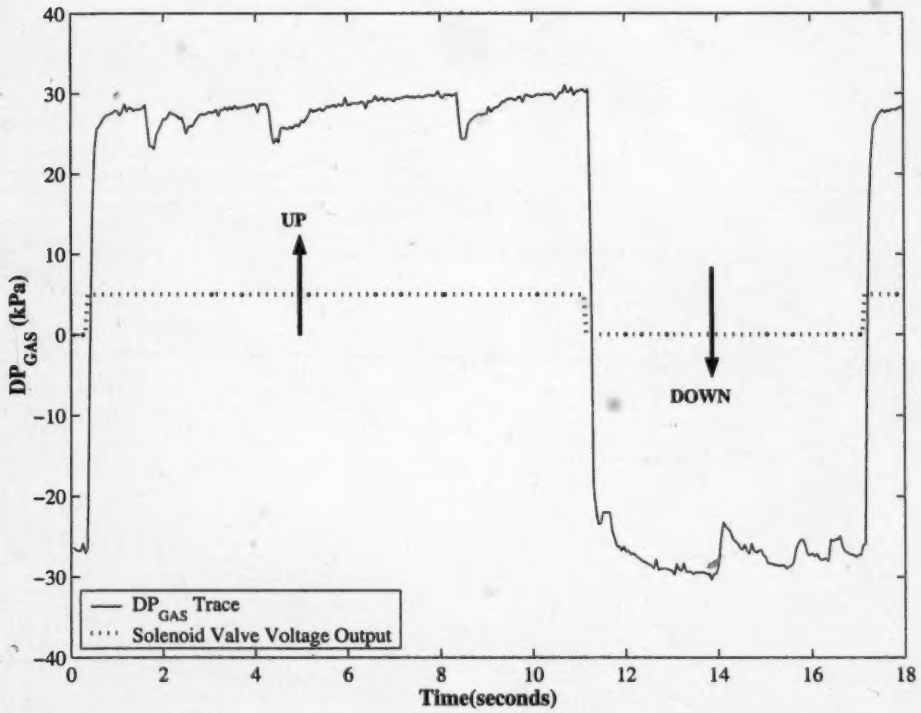


**Figure 4.11: $\Delta P_{GAS}$ Trace For Test No. 19 at a Liquid Flowrate of 4 mL/s**

At higher liquid flowrates the sliding friction becomes greater than the static friction. The effect of static friction no longer is noticeable, and a smoother pressure trace is obtained. This is shown in Figure 4.13 obtained from test 19 at a liquid flowrate of 33 mL/s (65 strokes/min).

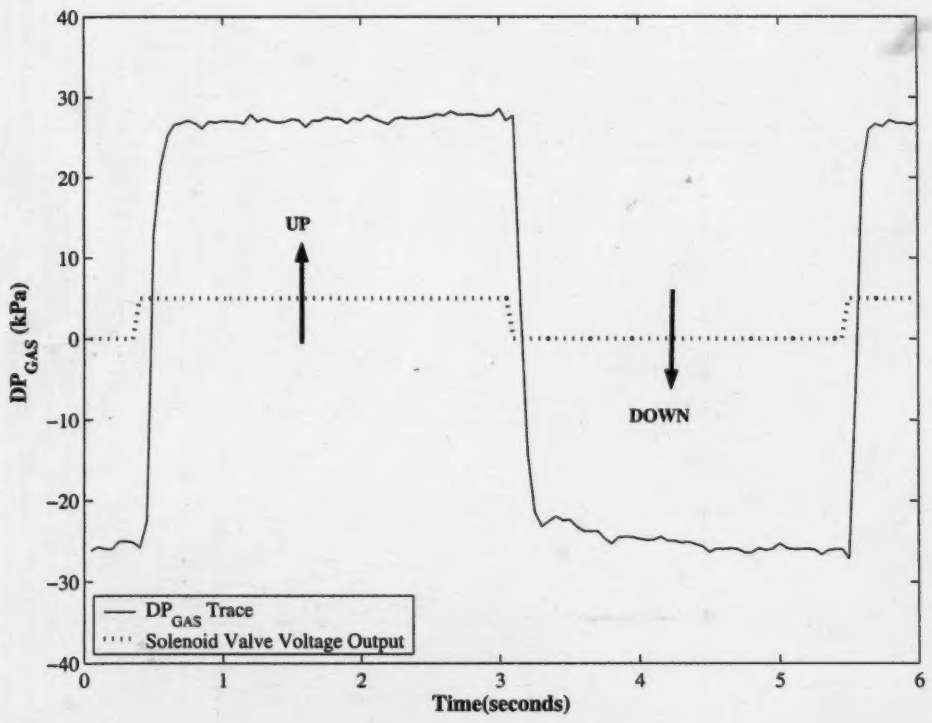


**Figure 4.12: $\Delta P_{GAS}$ Trace For Test No. 19 at a Liquid Flowrate of 12.6 mL/s**

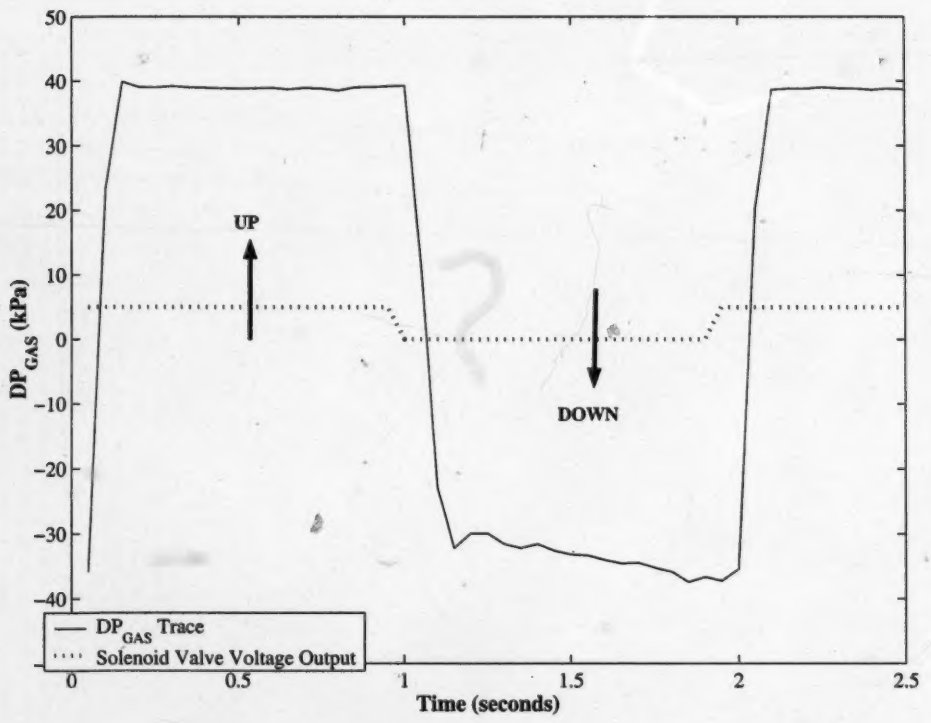


**Figure 4.13: $\Delta P_{GAS}$ Trace For Test No. 19 at a Liquid Flowrate of 33 mL/s**

### Repeatability

To demonstrate the repeatability of the tests performed, results from two sets of pump friction tests are presented in Figures 4.14 (Single Stage) and 4.15 (Two-Stage). The results in both figures show that the pump friction pressures are in agreement and demonstrate repeatability of the tests.

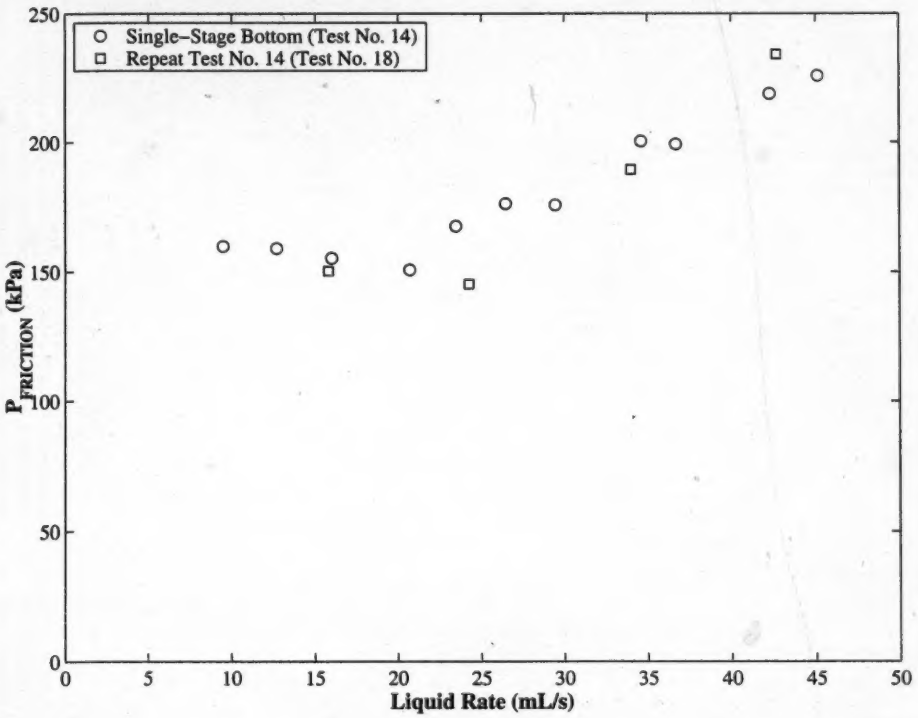


**Figure 4.14: $P_{FRICTION}$ Repeatability Test Results for Single Stage Operation**

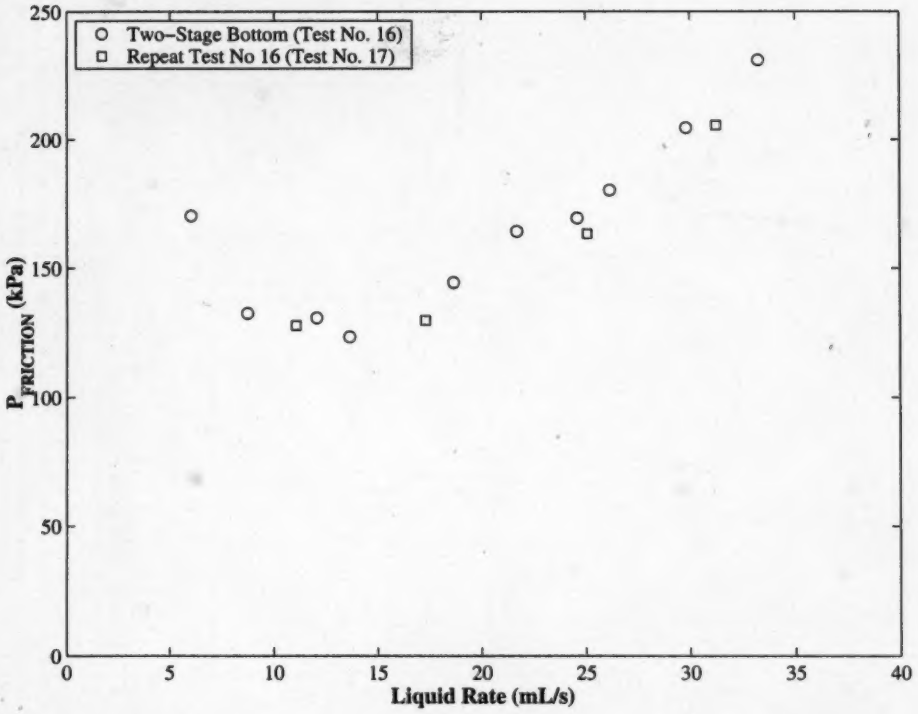


**Figure 4.15: $P_{FRICTION}$ Repeatability Test Results for Two Stage Operation**

### Friction Coefficient

In Chapter 3, pump friction was related to average pumping element velocity using a friction coefficient. Friction coefficient was calculated using Equation 3.14 and is given below:

$$C_F = \frac{A_L^2(\Delta P_{GAS} A_R - P_{PUMP})}{Q_l}$$

Using this equation, the friction coefficient of the pump as a function of liquid flowrate for both pairs of tests (9-10 and 19-20) are given in Figures 4.16 and 4.17 respectively. The results in Figures 4.16 and 4.17 show that at high

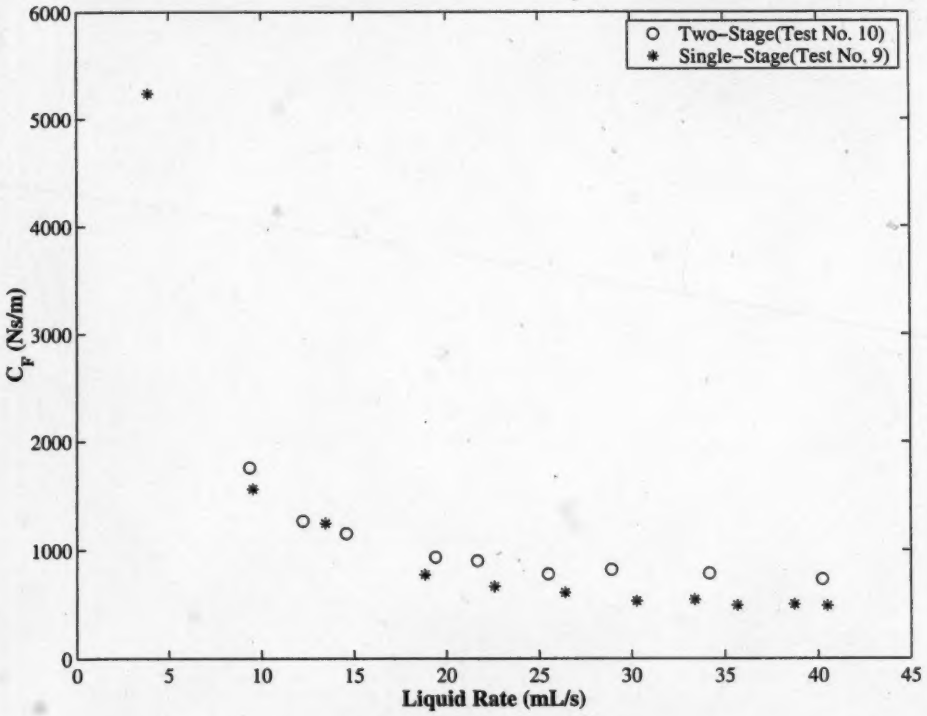


**Figure 4.16: Friction Coefficient Results for Single and Two-Stage Pump Operation ($P_{PUMP}$ = 925 kPag)**

liquid flowrates, that the friction coefficient approaches some constant value. This constant value corresponds with the slope of the pump friction curve at higher liquid flowrates. This indicates that the use of a constant friction coefficient at higher liquid flowrates is reasonable when modelling pump fric-

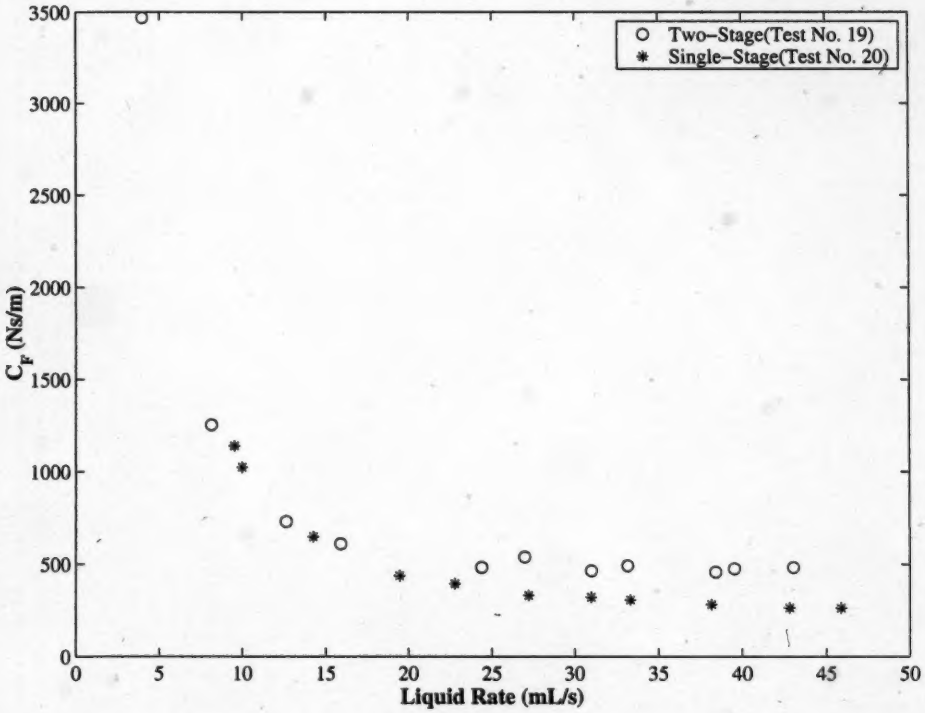


**Figure 4.17: Friction Coefficient Results for Single and Two-Stage Pump Operation ($P_{PUMP}$ = 215 kPag)**

tion.

The results in Figures 4.16 and 4.17 also show that the steady friction coefficient is higher for a two-stage configuration. However, when the pump is operated at a fixed liquid flowrate, the pump element is moved at the same speed in both single stage and two-stage operation. Therefore it is expected that the contribution of pump friction through mechanical friction and liquid

flow friction will be the same. As a result the root cause for the increased friction in two-stage pump operation may be due to gas flow friction.

The reason for the increased gas flow friction in two-stage operation is due to the tubing connections to connect the pump drive sections to the air supply and how the $\Delta P_{GAS}$ is measured. To demonstrate this, a schematic of differential gas pressure measurement for both single and two-stage operation is given in Figure 4.18. In single stage (bottom) operation, gas pressure is

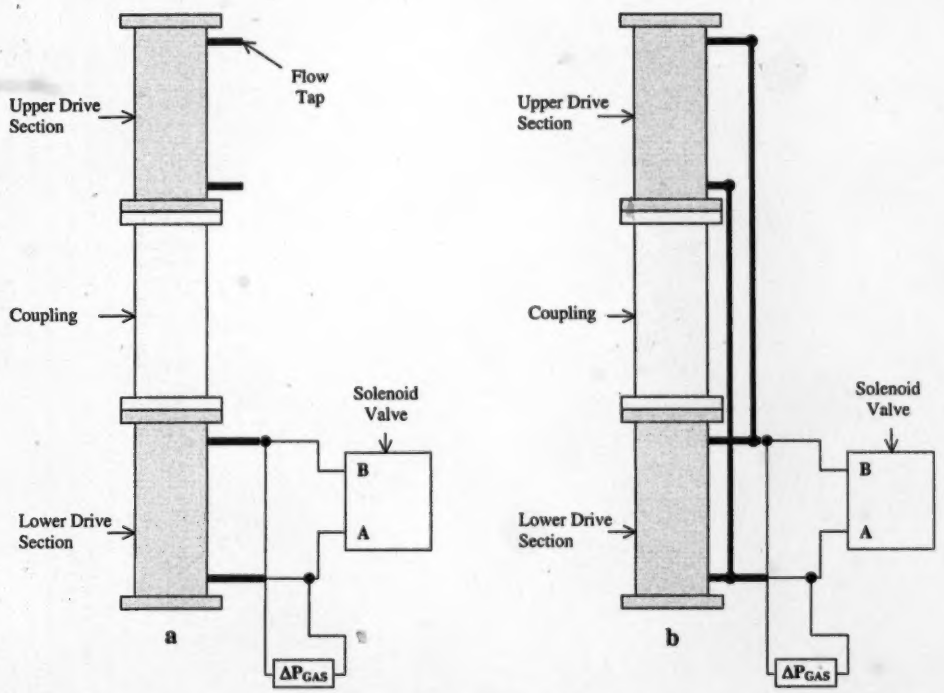


**Figure 4.18: Gas Differential Pressure Measurement for Single Stage(Bottom) (a) and Two-Stage Pump (b) Operation**

applied to the bottom drive section only. This is also shown in Figure 4.2. The flow taps on the top drive section are left open to atmospheric pressure. Differential gas pressure is measured at flow taps approximately 5 cm from the bottom drive section of the pump. In two stage operation, the flow taps on top drive section are connected to the flow taps on the bottom section using two 45 cm long sections of 1/4 inch (4.5 mm I.D.) tubing. Differential gas pressure is measured at the same location as in single stage (bottom) pump operation. Because of the additional gas flow friction in the connection to the upper drive section the differential gas pressure required to drive the pump increases. This is especially true at high liquid flowrates where gas requirements increase. The results in Figure 4.9 demonstrate this.

To further demonstrate this, pumping friction pressure results for a set of single stage (top) and single stage (bottom) are presented in Figure 4.19. The results show that at low liquid flowrates, pump friction pressure for both tests are in agreement. At higher liquid flowrates, the pump friction pressure for the single stage (top) becomes greater than for the single stage (bottom). This is because at higher liquid rates the pump requires greater volumes of friction losses become greater in the single-stage (top) due to the extra piping.

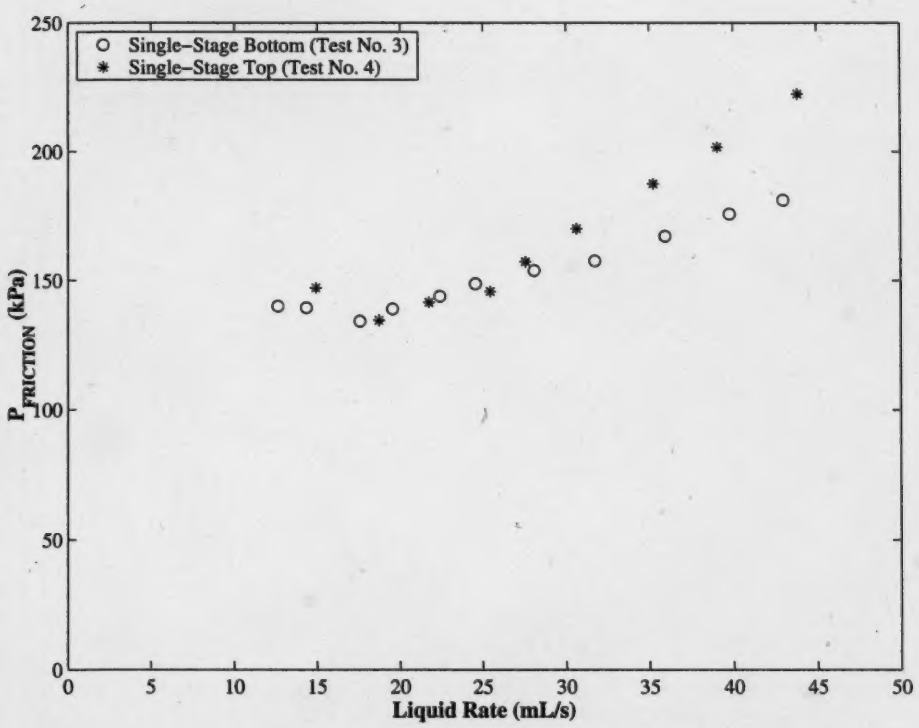


**Figure 4.19: Comparison of Single Stage (Top) and Single Stage (Bottom) $P_{FRICTION}$ Results**

### 4.3.3 Thermodynamic Efficiency

In Chapter 3, it was shown that for a gas driven DARP that its thermodynamic efficiency could be increased by increasing the area ratio and/or increasing the gas intake pressure of the pump. Also, it was shown that in some situations, when friction is present, thermodynamic efficiency could be increased by increasing the pumping pressure. To verify this information, three sets of tests were performed;

1. A low pumping pressure test. In this test, the test pump was set to deliver a pumping pressure of approximately 215 kPag using single-stage operation with a gas intake pressure of 350 kPaa ($\tilde{P}_{PUMP} = 0.1$, Test No. 13). The effect of increasing gas intake pressure was examined by running the same test with a gas intake pressure of 550 kPa ($\tilde{P}_{PUMP} = 0.065$, Test No. 14). The effect of increased area ratio was examined performing the same test with two-stage operation of the pump at a gas intake pressure of 350 kPaa ($\tilde{P}_{PUMP} = 0.05$, Test No. 16).

2. A high pumping pressure test. In this test, the test pump was set to deliver a pumping pressure of approximately 925 kPag single-stage operation with a gas intake pressure of 355 kPaa ($\tilde{P}_{PUMP} = 0.42$, Test No. 8). The effect of increasing gas intake pressure was examined by running the same test with a gas intake pressure of 515 kPa ($\tilde{P}_{PUMP} = 0.3$, Test No. 9). The effect of increased area ratio was examined performing the same test with two-stage operation of the pump at a gas intake pressure of 355 kPaa ($\tilde{P}_{PUMP} = 0.22$, Test No. 7).

3. A constant $\tilde{P}_{PUMP}$ test. In this test, the test pump was set for single-

stage pump operation with gas intake pressure of 240 kPaa and a pumping pressure on 215 kPag ($\tilde{P}_{PUMP} = 0.14$, Test No. 12). For comparison, the test pump was run using two-stage pump operation at a gas intake pressure of 400 kPaa and a pumping pressure of 700 kPag ($\tilde{P}_{PUMP} = 0.14$, Test No. 11).

In Chapter 3, thermodynamic efficiency can be calculated using Equation 3.21 and is given here for convenience:

$$\eta = \frac{k-1}{k} \frac{P_{PUMP} Q_l}{Q_g P_{IN} \left(1 - \left(1 - \frac{\Delta P_{GAS}}{P_{IN}}\right)^{\frac{k-1}{k}}\right)}$$

Gas flow rate in Equation 3.21 is converted to standard conditions using the ideal gas law resulting in the equation:

$$\eta = \frac{k-1}{k} \frac{T_{IN}}{T_{sc}} \frac{P_{PUMP} Q_l}{Q_{g,sc} P_{sc} \left(1 - \left(1 - \frac{\Delta P_{GAS}}{P_{IN}}\right)^{\frac{k-1}{k}}\right)} \tag{4.1}$$

Equation 4.1 is used to calculate thermodynamic efficiency of the test pump in the three sets of tests mentioned above. Gas and liquid flowrates and air intake temperature were obtained from data collected using the *Steady* data acquisition system. Pumping pressure and differential gas pressure were obtained from data collected using the *Transient* data acquisition program. Gas intake pressure was determined by correcting the gas intake tank pressure measured using the *Steady* data acquisition program and the method used in the gas utilization. Details on the procedure used to obtain these variables from results collected using the *Steady* and *Transient* data acquisition programs are given in Appendix E.

### Low Pumping Pressure Test

The thermodynamic efficiency results for the low pressure pumping test are given in Figure 4.20.

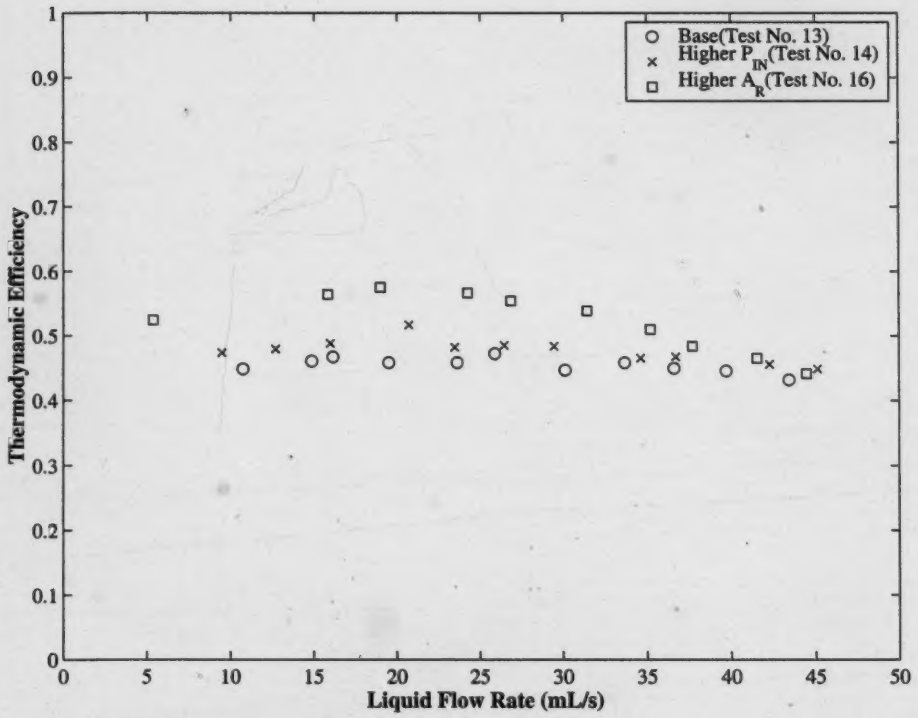


**Figure 4.20: Thermodynamic Efficiency of Experimental Pump at $P_{PUMP}$ = 215 kPag**

The expected increase in thermodynamic efficiency are 3 percent and 2 percent for the area ratio and intake pressure increases respectively. These

increases were calculated using Equation 3.25 from Chapter 3. The results in Figure 4.20 show that if either area ratio ($A_R$) or gas intake pressure ($P_{IN}$) is increased, then thermodynamic efficiency of the pump will increase, but only by a small amount. The effect of higher area ratio was more significant at lower flowrates because it resulted in smaller normalized pumping pressure than the gas intake pressure increase ($\tilde{P}_{PUMP} = 0.05$ for the area ratio change and $\tilde{P}_{PUMP} = 0.065$ for the air intake pressure increase). However, the efficiency of the two-stage pump operation degrades significantly at higher liquid rates. This is because pump friction in two-stage pump operation is higher than single stage operation at higher liquid flow rates.

### High Pumping Pressure Test

The thermodynamic efficiencies for the high pressure pumping test are given in Figure 4.21. The expected increase in thermodynamic efficiency, using Equation 3.25 from Chapter 3, are 12 percent and 8 percent for the area ratio and intake pressure increases respectively. The results in Figure 4.21 show again that if either area ratio ($A_R$) or gas intake pressure ($P_{IN}$) is increased, then thermodynamic efficiency of the pump will increase. In the high pumping pressure case, thermodynamic efficiency does not decrease as significantly at higher liquid flow rate compared with the low pumping pressure results. This is because the higher pumping pressure makes the effect of friction less significant and leads to more efficient pump performance.

In general thermodynamic efficiency of the pump increases with the high pumping pressure. Again, this is because the pump friction becomes propor-

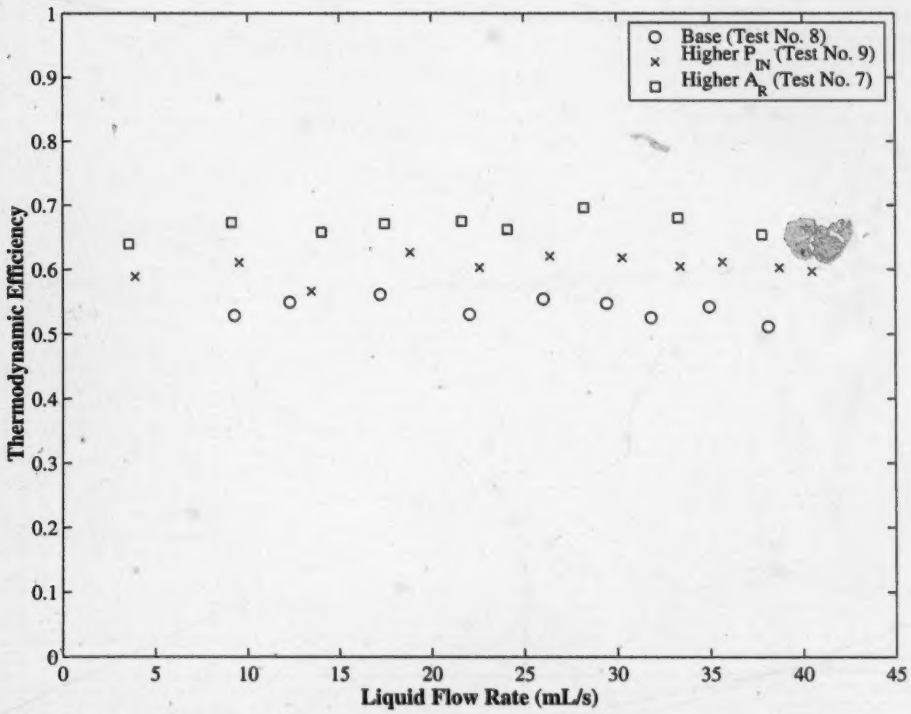


**Figure 4.21: Thermodynamic Efficiency of Experimental Pump at $P_{PUMP} = 925$ kPag**

tionally smaller to the pumping pressure. Also, because the pump is operated at higher normalized pressures ($\tilde{P}_{PUMP}$), it sees much larger efficiency improvements with increased area ratio and gas intake pressure.

### Constant $\tilde{P}_{PUMP}$ Test

The thermodynamic efficiency results for the constant $\tilde{P}_{PUMP}$ test are given in Figure 4.22. In this case, when there is no friction, there should be no

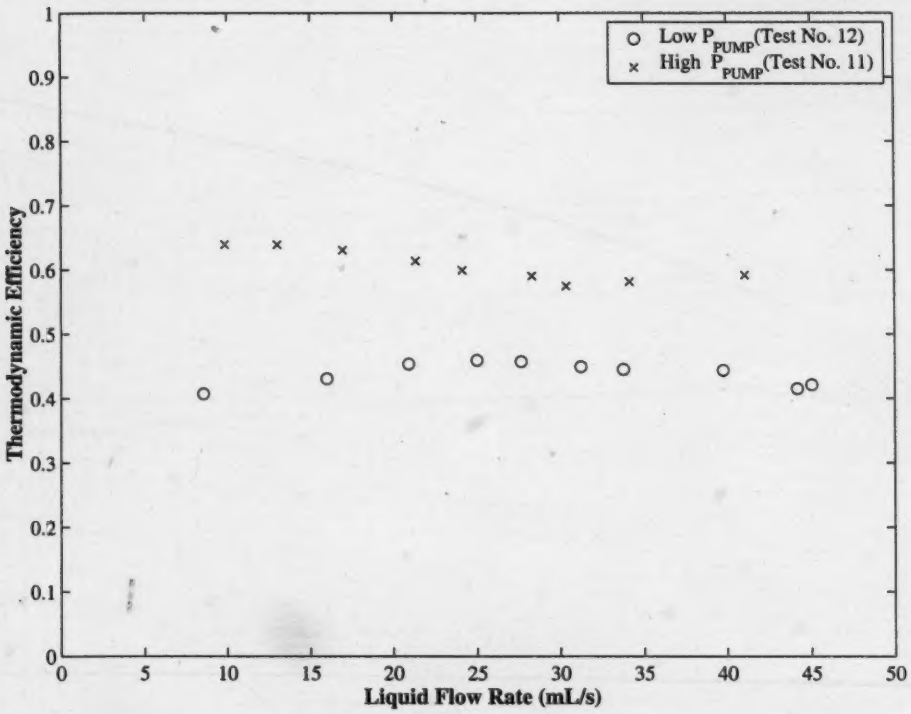


**Figure 4.22: Thermodynamic Efficiency of Experimental Pump at $\tilde{P}_{PUMP} = 0.14$**

change in thermodynamic efficiency. However the results in Figure 4.22 show that higher pumping pressure has greater thermodynamic efficiency than smaller pumping pressure for a constant normalized pumping pressure. By running at a higher pumping pressure, the friction becomes less significant and results in higher thermodynamic efficiency.

## 4.4 Summary

In this chapter the description of a test pump whose performance characteristics were tested, was presented. This test pump was a double-acting DARP, which could be operated in single or two-stage operation. This physical pump model was tested in a gas and water liquid loop and measurements of flow, pressure and temperature were obtained to determine pump performance characteristics that were compared with predictions made by mathematical models presented in Chapter 3.

Gas utilization of the test pump was verified predictions by the mathematical model. Friction in the pump was found to be influenced by static forces at low pump speeds. At higher pump speeds, friction increased linearly with liquid flowrate. This corresponded with a constant friction coefficient, which was deemed appropriate to model friction in the pump when it operates at higher liquid flowrates. It was found that the pump friction measurements for both single and two stage operation can be repeated. Also, at higher flowrates, two-stage pump operation has significantly higher friction due to gas flow friction. This was verified when comparing the measured friction pressure of single stage (top) and single stage (bottom) operation.

The thermodynamic efficiency of the test pump was improved by increasing the pump area ratio and the gas intake pressure. Efficiency increases were larger for systems with higher normalized pumping pressures. As well, because of the presence of friction in the pump, thermodynamic efficiency was higher for systems operating with higher pumping pressures.

# CHAPTER 5

# Application of Reciprocating Pumps in Gas Wells

The purpose of this chapter is to determine the applicability of using reciprocating pumps for use in the pumping concept proposed by the ARC. This is accomplished by utilizing the knowledge gained through through mathematical and physical modelling of reciprocating pump performance described in the previous two chapters and applying it to the natural gas well model developed in Chapter 2. This modified model is used to determine optimum design parameters of a reciprocating pump in application to the "typical" Alberta gas well. In addition, the effect of gas well depth, liquid production rate and reservoir flow resistance are investigated in order to better understand their effect on these design parameters.

## 5.1 Implementation of a Mathematical Model for Reciprocation Pump Application

Recall the ARC pumping concept introduced earlier in Figure 1.3. To reiterate, the concept consists of a down-hole pump set at the bottom of the production tubing. Gas and liquid enter the bottom of the well and are separated by gravity. The gas and liquid then flow through the down-hole pump and exit up the production and liquid tubing respectively and flow to the surface.

### 5.1.1 Mathematical Model of Field Application

A mathematical model for the reciprocating pump application is now presented. This model is based on the mathematical and physical modelling results obtained in Chapters 3 and 4. The model consists of a force balance on the pumping element of a DARP. This force balance is shown schematically in Figure 5.1 and mathematically as:

$$P_{BH}A_G + P_{BH}A_L = P_{DIS}A_G + P_{PUMP}A_L + P_{FRICTION}A_L \tag{5.1}$$

Assuming that the pumping element is moving upwards, the force balance consists of gas pressure and liquid pressure at bottomhole pressure ($P_{BH}$) acting on the piston area $A_G$ and plunger area $A_L$ respectively. This force is resisted by the gas discharge pressure ($P_{DIS}$) acting on the piston area, the pumping pressure ($P_{PUMP}$) acting on the plunger area and the pump friction, which is converted to an equivalent pumping pressure ($P_{FRICTION}$) that acts on the plunger area.

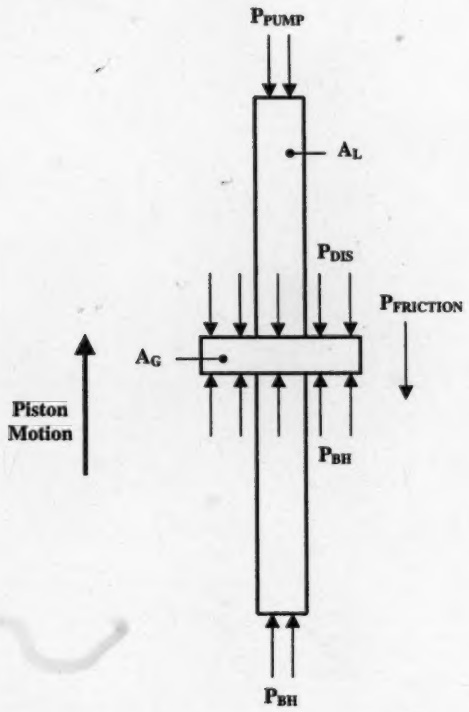


**Figure 5.1: Force Balance on Pumping Element**

The pumping pressure is the pressure required to bring the liquid phase to the surface at a given wellhead (or surface) pressure. Therefore, the pumping pressure can be divided into three terms which are shown in the equation

$$P_{PUMP} = P_{WH} + \Delta P_{TL} + \rho_l g Z_W \tag{5.2}$$

which are the wellhead pressure ($P_{WH}$), friction in the liquid tubing ($\Delta P_{TL}$) and the hydrostatic head ($\rho_l g Z_W$).

### 5.1.2 Simplifying Assumptions

By making some assumptions the model can be simplified.

#### Friction Losses in Liquid Tubing

The first simplification of the model is that friction in the liquid tubing will be neglected. This is because friction in the liquid tubing is assumed to be small compared to the hydrostatic head. This simplification will prevent the need to specify a size for the liquid tubing but assumes that it is large enough for friction to be neglected. To determine the validity of this assumption a simple analysis was performed to compare the magnitude of the friction losses to hydrostatic losses. The friction in the liquid tubing was modelled using the equation:

$$\Delta P_{TL} = f\frac{L_W}{d_t}\frac{\rho_l V_l^2}{2}. \tag{5.3}$$

This analysis is used to determine the liquid tubing size at which friction losses will be one percent of the hydrostatic losses. This criterion is shown mathematically as:

$$0.01 = \frac{f\frac{L_W}{d_t}\frac{\rho_l V_l^2}{2}}{\rho_l g Z_W} = f\frac{L_W}{Z_W}\frac{V_l^2}{2gd_t} \tag{5.4}$$

Converting liquid velocity to a liquid flowrate using the equation:

$$V_l = \frac{4Q_l}{\pi d_t^2} \tag{5.5}$$

and inserting it into Equation 5.4 results in:

$$0.01 = f\frac{L_W}{Z_W}\frac{8Q_l^2}{\pi^2 g d_t^5} \tag{5.6}$$

Rearranging Equation 5.6 and solving for tubing diameter yields:

$$d_t = \left( f \frac{L_W}{Z_W} \frac{8Q_l^2}{0.01\pi^2 g} \right)^{0.2} \tag{5.7}$$

Here it is assumed that the gas well is vertical (i.e. $L_W = Z_W$) and a friction factor of 0.05, which corresponds to a moderate Reynolds number pipe flow regime [34] exists in the pipe. With these assumptions, Equation 5.7 becomes:

$$d_t = \left( \frac{40Q_L^2}{\pi^2 g} \right)^{0.2} \tag{5.8}$$

Using the liquid flowrate of the "typical" Alberta natural gas well given in Appendix A of 7 $m^3$ per day ($8.10 \times 10^{-5}$ $m^3/s$) and gravitational constant of 9.81 $m/s^2$ the minimum diameter is calculated to be 19.3 mm. In a typical Alberta natural gas well, the casing has internal diameter of 103.9 mm and the production tubing has outside diameter of 60.3 mm. The resulting annulus between has a width of 21.8 mm, making the minimum diameter calculated earlier reasonable.

### Pump Friction

Experimental results in the previous chapter revealed that pump friction was significant at the pumping pressures investigated (up to 925 kPa). In a field situation, the pumping pressures are expected to be much higher. For the "typical" Alberta natural gas well, its depth was 715 m and therfore its pumping pressure will be approximately 7 MPa (based on the hydrostatic head). In Chapter 4, physical pump model test results showed that the pump friction pressure was finite for all liquid flowrates, with a maximum on the order of 500 kPa of equivalent pumping pressure. This would correspond to

approximately 7 percent of the field pumping pressure. Pump friction was shown to be a function of speed, and size (area ratio). Because of this it would difficult to accurately predict the frictional effects of a pump placed in a field application. Since pump friction plays a minor role in the forces acting on the pump it was neglected. However, the validity of this assumption will be examined.

### Wellhead and Bottomhole Pressures

With the simplifications made above, Equation 5.1 can be expressed as:

$$P_{BH}A_G + P_{BH}A_L = P_{DIS}A_G + (P_{WH} + \rho_l g Z_W)A_L \tag{5.9}$$

Rearranging Equation 5.9 to solve for $P_{DIS}$ and recalling the definition of area ratio ($A_R$) results in:

$$P_{DIS} = P_{BH} - \frac{(P_{WH} - P_{BH} + \rho_l g Z_W)}{A_R} \tag{5.10}$$

A further simplification can be made if pressure difference between the bottomhole pressure and wellhead pressure is assumed small compared to the hydrostatic pressure term in Equation 5.10. To determine the validity of this assumption results from Chapter 2 will be used. A plot of the difference in pressure between the bottomhole and the wellhead for the constant liquid production rate case is shown in Figure 5.2. The results in Figure 5.2 show that the difference in pressure increases with wellhead pressure with a maximum value of approximately 470 kPa in the range of wellhead pressures examined. Based on this result, this pressure differential is relatively small (approximately 7 percent) compared with the hydrostatic pressure term. This differential pressure term will add mechanical advantage to

the pump, so by neglecting it losses due to mechanical friction in the pump and losses in the liquid tubing are compensated somewhat. Neglecting this differential pressure, Equation 5.10 becomes:

$$P_{DIS} = P_{IN} - \frac{\rho_l g Z_W}{A_R} \tag{5.11}$$

Equation 5.11 shows that pump discharge pressure is a function only of the depth of the gas well ($Z_W$), the pump intake pressure and the area ratio of the pump. The pump model is reduced to a static analysis making it simple, and assumptions about specific pump dimensions are not required.

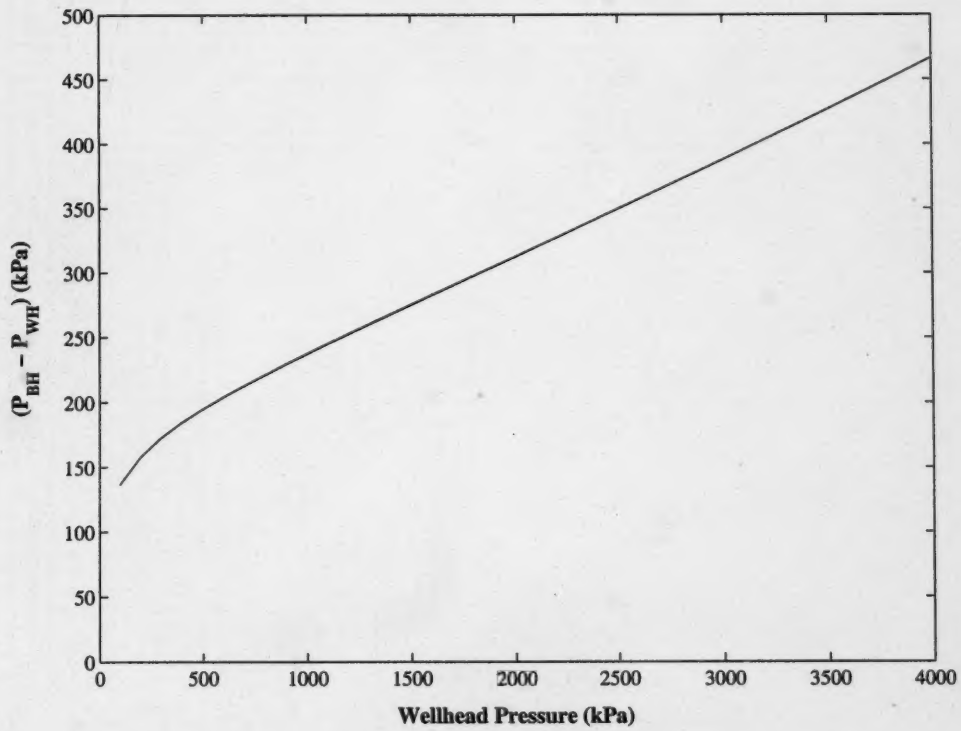


**Figure 5.2: Estimate of Differential Pressure From Pump Intake to Wellhead**

## 5.2 Model Results

The pump model described above was implemented into the original gas well model. This modified model was applied on the "typical" Alberta gas well described in Appendix C. Recall that this gas well was 715 m deep and produced 25,700 $m^3$ of natural gas at standard conditions along with 7 $m^3$ of water per day.

### 5.2.1 Effect of Pump Area Ratio

The revised model was then used to determine the effect of pump area on the minimum reservoir pressure for required to keep the gas well flowing at a certain wellhead pressure. This was done for the same two liquid production conditions examined in Chapter 2:

- Constant Liquid Rate of 7 $m^3$/day and
- Constant Gas-Liquid ratio of 3671.

To examine the effect of pump area ratio on the gas well performance the following calculation procedure and is illustrated in Figure 5.3:

1. Starting from the bottomhole pressure (or pump intake pressure), the liquid production model and a selected area ratio are used in Equation 3.5 to determine the gas requirements for the pump.

2. Reservoir pressure is determined using the calculated gas requirement, the bottomhole pressure and incorporating them into the Reservoir Inflow model (Equation 2.35).

3. The bottomhole pressure and area ratio are then used to calculate the discharge pressure using the Pump Model (Equation 5.11) to calculate the pump discharge pressure.

4. The discharge pressure and gas flowrate are input into the dry gas flow model (numerical integration of Equation 2.50) to obtain the wellhead pressure.

The model was tested for each liquid production scenario using area ratios of 10, 20, 40 and 80 to examine their effect.

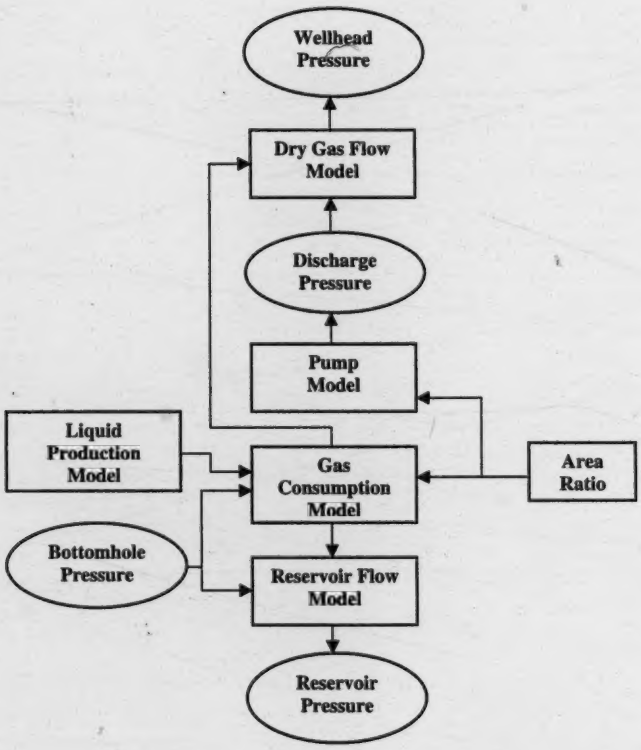


**Figure 5.3: Schematic of Model Solution Procedure to Examine Effect of Area Ratio**

### Constant Liquid Production Rate

For the constant liquid production rate of 7 $m^3$ of water per day, the results from the model are given in Figure 5.4. For comparison, the minimum reservoir pressure required for separate and two-phase gas well operation are also plotted. All of these results are normalized by subtracting the static reservoir pressure at its respective wellhead pressure. The results in Figure 5.4

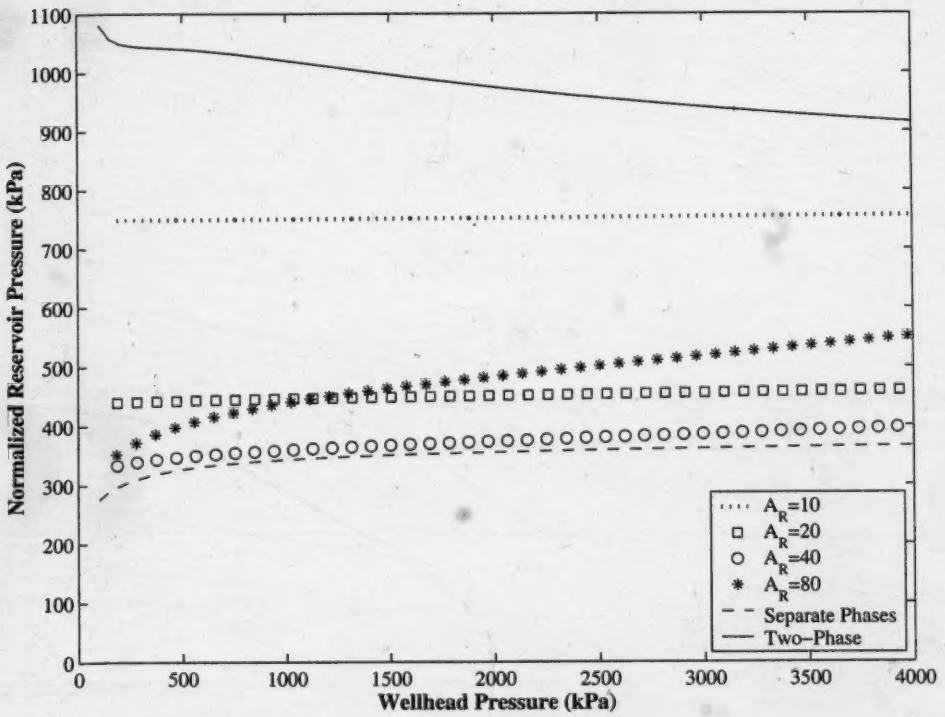


**Figure 5.4: Effect of Area Ratio on Normalized Minimum Reservoir Pressure for Constant Liquid Production Rate of 7 $m^3$/day**

show that higher area ratios lead to better gas well performance. This in agreement with the theory derived in Chapter 3 in that higher area ratios lead to higher thermodynamic efficiency of the pump. However, pumps with higher area ratios also require more gas to drive them and as a result require higher reservoir pressures to provide the required gas flow. This is evident when considering the pump with an area ratio of 80. Therefore there must be some optimum pump area ratio that minimizes the reservoir pressure.

For the four area ratios, 40 seems to be the best choice as it closely follows the separate phases curve. At higher wellhead pressures, higher area ratios deviate from the separate phases curve. This is due to the higher gas flow rates required at higher pressure. Therefore, smaller area ratios perform better at higher pressures. Such is the case with an area ratio of 20 becomes closer to the separate phases curve at higher wellhead pressures.

### Constant Gas to Liquid Production Ratio

For the constant gas to liquid production ratio of 3671, the results for the effect of area ratio is given in Figure 5.5. As in the constant liquid rate case, the minimum reservoir pressure required to operate the gas well in separate and two-phase flow configurations are also presented. As well, the data are normalized in the same manner as previously. The results in Figure 5.5 show that higher area ratios lead to a lower reservoir pressure. Unlike the constant liquid production rate case, the highest area ratio ($A_R = 80$) performs best. This is because in the constant gas to liquid production ratio, the gas well can be operated to a gas flowrate that approaches zero. As a result, the

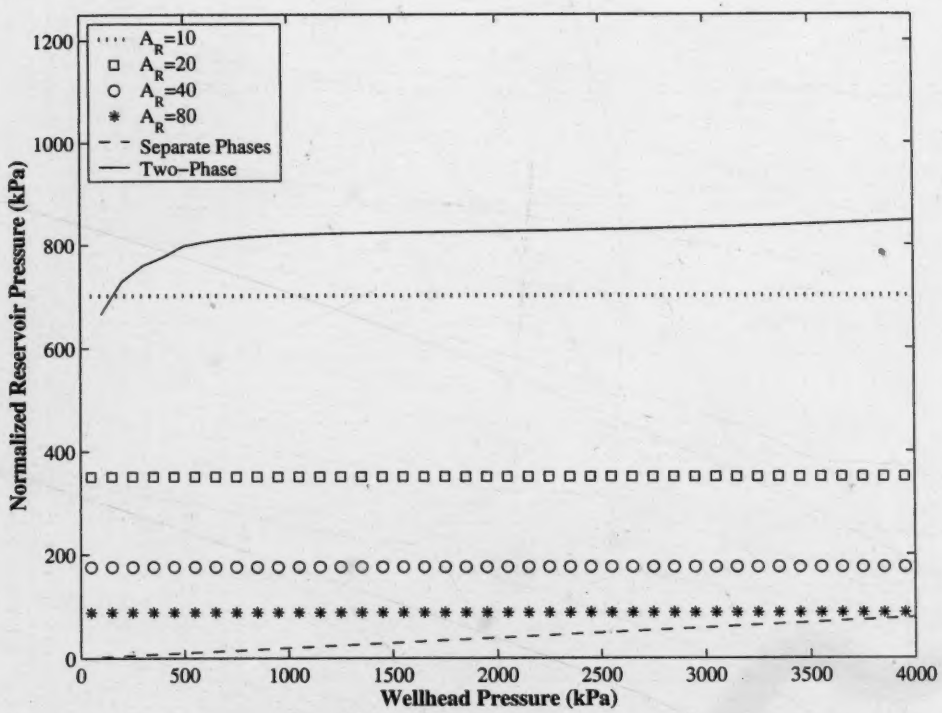


**Figure 5.5: Effect of Area Ratio on Normalized Minimum Reservoir Pressure for Constant Gas Liquid Production Ratio of 3671**

pressure drop from the reservoir to the bottomhole approaches zero for all area ratios.

However, because gas and liquid production is fixed at a constant ratio, there is a maximum (or optimum) area ratio that can be used. As well, if smaller area ratios than this maximum are to be used, then some amount of gas must be diverted around the drive section of the pump.

### 5.2.2 Optimum Area Ratio

As discussed in the previous section, there must exist an optimum area ratio of a reciprocating pump at which for a given wellhead pressure the reservoir pressure can be depleted to a minimum pressure. Alternatively, the optimum area ratio at which the gas well can be operated at a maximum wellhead pressure for a given reservoir pressure.

#### Constant Liquid Production Rate

For the constant liquid rate, the optimum area ratio is determined using the following procedure, which is shown schematically in Figure 5.6. The objective of this model was to determine the maximum wellhead pressure for a given reservoir pressure. This was done by varying the gas flowrate until the wellhead pressure was maximized and corresponded with the optimum area ratio. Details regarding how this wellhead pressure was maximized are given in Appendix C.

Referring to Figure 5.6, the calculating procedure is as follows:

1. Starting from a given reservoir pressure, a chosen gas flow rate is used to determine the bottomhole pressure using the reservoir inflow model.
2. The bottomhole pressure is then used with gas flow rate and the liquid production rate to determine the corresponding area ratio using the gas requirement model.
3. The bottomhole pressure is then used with the calculated area ratio in the pump model to determine the gas discharge pressure.

4. The discharge pressure and the selected gas flow rate are then used in the dry gas flow model to determine the wellhead pressure.

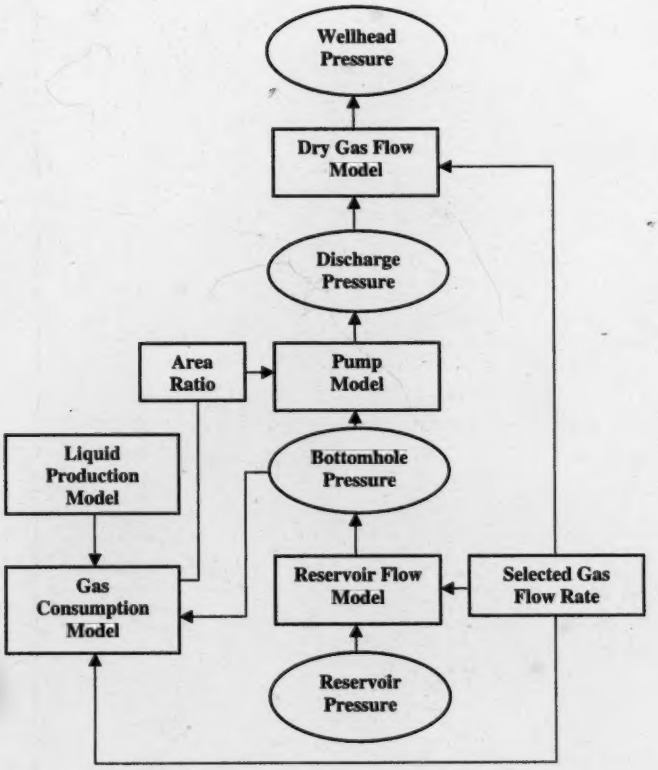


**Figure 5.6: Schematic of Solution Procedure to Determine Optimum Area Ratio for Constant Liquid Rate**

The results for the optimum area ratio for the constant liquid production rate of 7 $m^3$/day is given in Figure 5.7. The results in Figure 5.7 show that

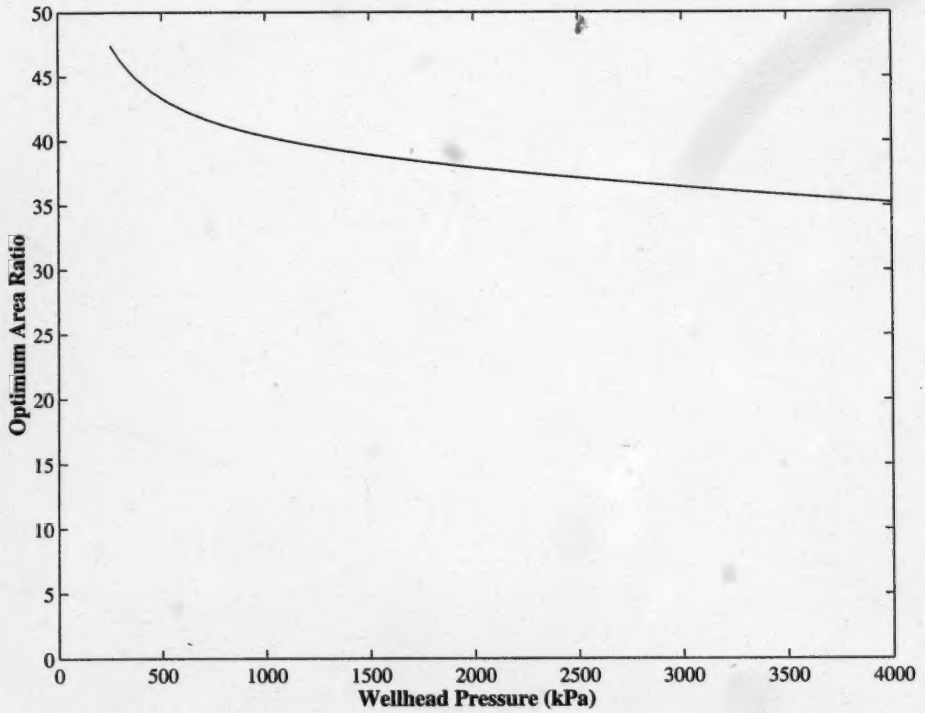


**Figure 5.7: Optimum Area Ratio for Typical Alberta Gas Well at Constant Gas Liquid Production Rate of 7 $m^3$/day**

optimum area ratio decreases with wellhead pressure. This is because at higher pressures, gas utilization increases, and as a result the reservoir pressure required to maintain the flow increases. In order to compensate for the

higher gas flowrates, the optimum area ratio decreases despite the increase in required pressure drop across the pump.

The performance of the optimum area ratio is shown in Figure 5.8. For

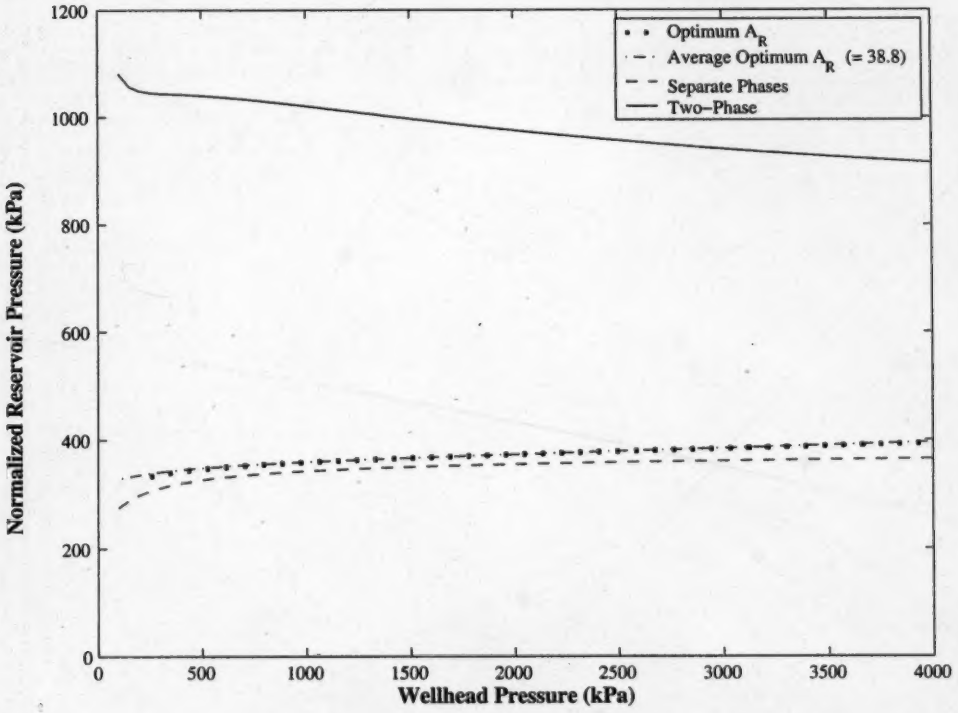


**Figure 5.8: Normalized Reservoir Pressure for Optimum Pump Area Ratio at Constant Gas Liquid Production Rate of 7 $m^3$/day**

comparison, the minimum reservoir pressure to operate the gas well in both separate and two-phase flow configurations are also presented. In practice, it would not be feasible to always operate the gas well at the optimum area

ratio. Therefore, the performance of the average optimum area ratio (which is 38.8) is also plotted for comparison. This average optimum area ratio is the arithmetic average of the optimum area ratio results shown in Figure 5.7. All of these values are normalized by subtracting the static reservoir pressure.

The results in Figure 5.8 show that the optimum area ratio operates at a reservoir pressure approximately 50 kPa higher than the separate phases curve, and the gap appears to increases at higher wellhead pressures. When using the average optimum area ratio of 38.8 is used, the gas well operates nearly as well as the optimum area ratio. Therefore, using the average optimum area ratio would be an appropriate when design choice.

### Constant Gas to Liquid Production Ratio

Because the gas flowrate approaches zero for minimal reservoir pressure in the constant gas to liquid production ratio case, a different technique is used to determine the optimum area ratio. In Figure 5.5 higher area ratios lead to lower reservoir pressure. However there is a limit to the size of the area ratio. Recall Equation 5.2.2 (given below for convenience) which relates the gas to liquid volume ratio of the pump ($R_{gl}$) to the area ratio and the pressure at the intake of the pump.

$$R_{gl}^{\cdot} = A_R \frac{P_{IN} T_{sc}}{P_{sc} z T_{IN}}$$

$R_{gl}$ represents the minimum ratio of gas to liquid required to drive the pump. Therefore the optimum area ratio is solved by equating $R_{gl}$ to the gas-liquid production ratio of 3671 and solving for the corresponding area ratio.

The results for optimum area ratio for the gas well operating with gas to liquid production ratio are given in Figure 5.9. As in the constant liquid rate

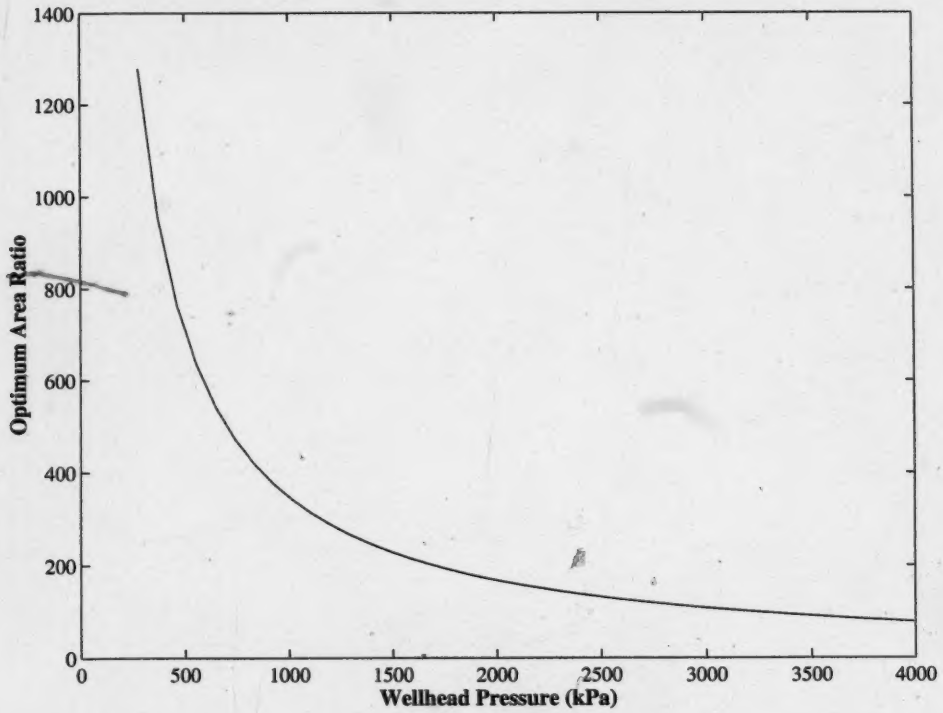


**Figure 5.9: Optimum Pump Area Ratio at Constant Gas Liquid Production Ratio of 3671**

case, the results in Figure 5.9 show that area ratio decreases with wellhead pressure. The reason for this decrease is because gas utilization requirements of the pump increase with higher pressures. Since the ratio of gas to liquid production is fixed, the maximum area ratio must decrease to compensate for the higher gas pressure.

In this case the optimum area ratios are much higher, ranging from 100 to 1300, than the constant liquid rate, which ranged from 30 to 50. Because of this large range and size, it may be more difficult to implement optimum area ratios based on the constant gas to liquid production scenario into a field prototype design.

The performance of the optimum ratio is given in Figure 5.10. For comparison, the results for separate and two-phase flow operation are also given. As well, the performance results for the average area ratio for the constant liquid production rate are give. All of these results are normalized by subtracting static reservoir pressure. The results in Figure 5.10 show that the optimum area ratio operates close to the separate phases curve. However, at higher pressures, the gap between the optimum area ratio and separate phases curve increases. This is because the pump operates at with a finite area ratio and is not 100 percent efficient. The average area ratio from the constant liquid case is higher than separate phases curve, but still a significant improvement over two-phase flow operation. If this average optimum area ratio is used, a means of diverting gas flow past the drive section of the pump will be required in the design.

### 5.2.3 Effect of Pump Friction

Although friction was neglected in the model of the pump, it was determined in Chapter 4 that it played a significant role in the forces acting on the pumping element. To examine the effect of finite friction it was assumed that

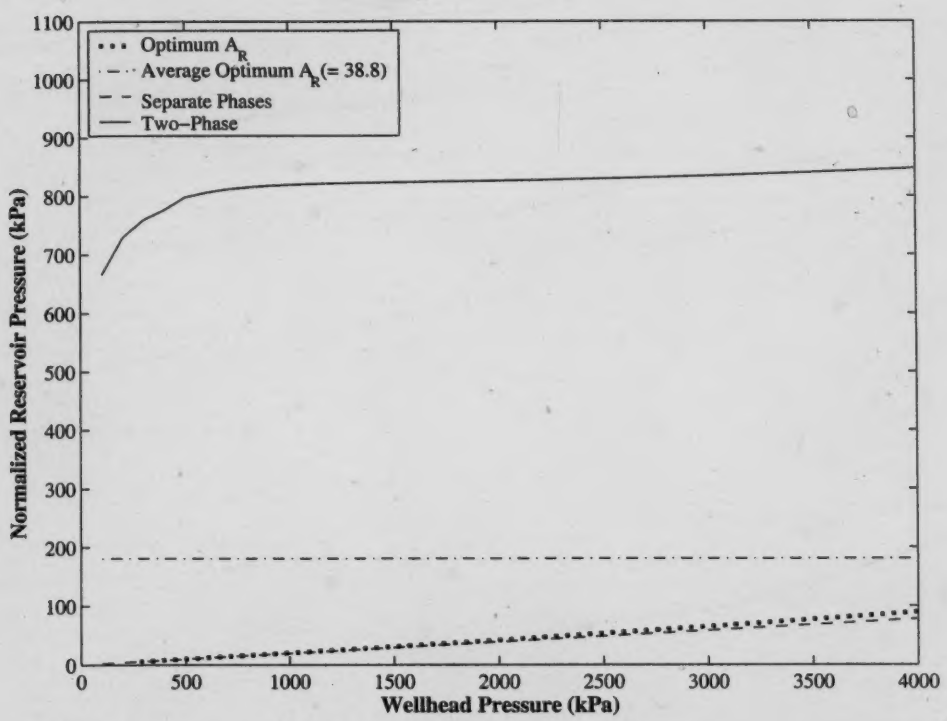


**Figure 5.10: Normalized Reservoir Pressure for Optimum Pump Area Ratio at Constant Gas Liquid Production Ratio of 3671**

it has an value equivalent to 700 kPa of hydrostatic pressure (approximately 10 percent). This value was input into the original model to determine its effect on the optimum area ratio.

### Constant Liquid Production Rate

The results for the effect of friction on optimum area ratio for the constant liquid production rate is given in Figure 5.11. The results in Figure 5.11 show

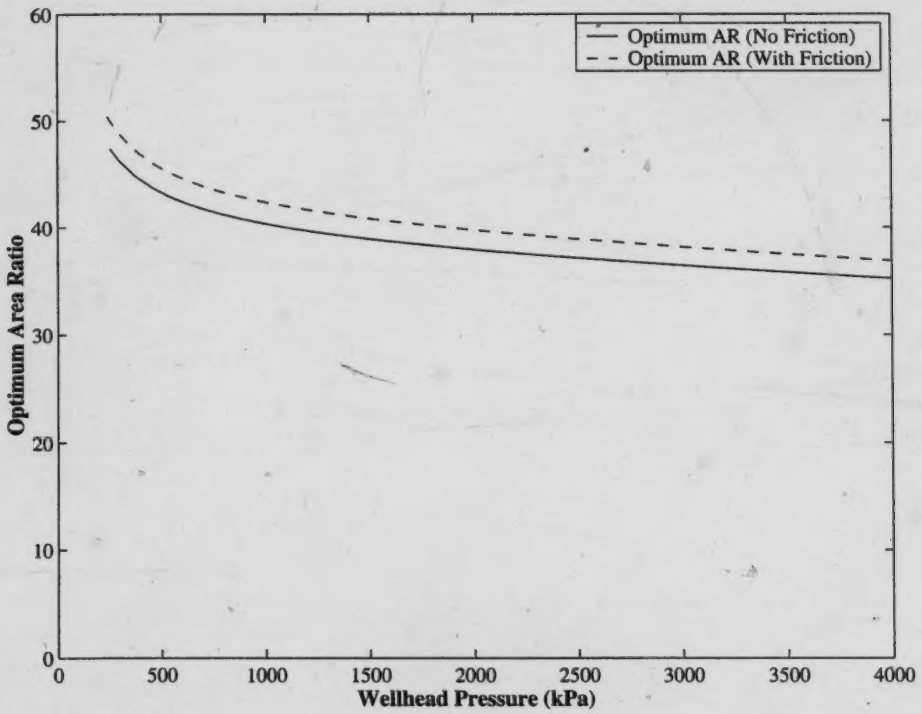


**Figure 5.11: Optimum Area Ratio With and Without Friction at Constant Gas Liquid Production Rate of 7 $m^3$/day**

that the optimum area ratio increases with increased friction. This increase in optimum area ratio is required because of the increased load on the pump due to friction.

The effect of friction and its optimum area ratio on gas well performance is shown in Figure 5.12. For comparison, the results for separate and two-phase flow operation are also given. The performance of the average optimum

area ratio ($A_R = 38.8$) determined for the case with no friction is also given. All of the presented results are normalized by subtracting the static reservoir pressure. The increased friction results in a slightly higher reservoir pressure

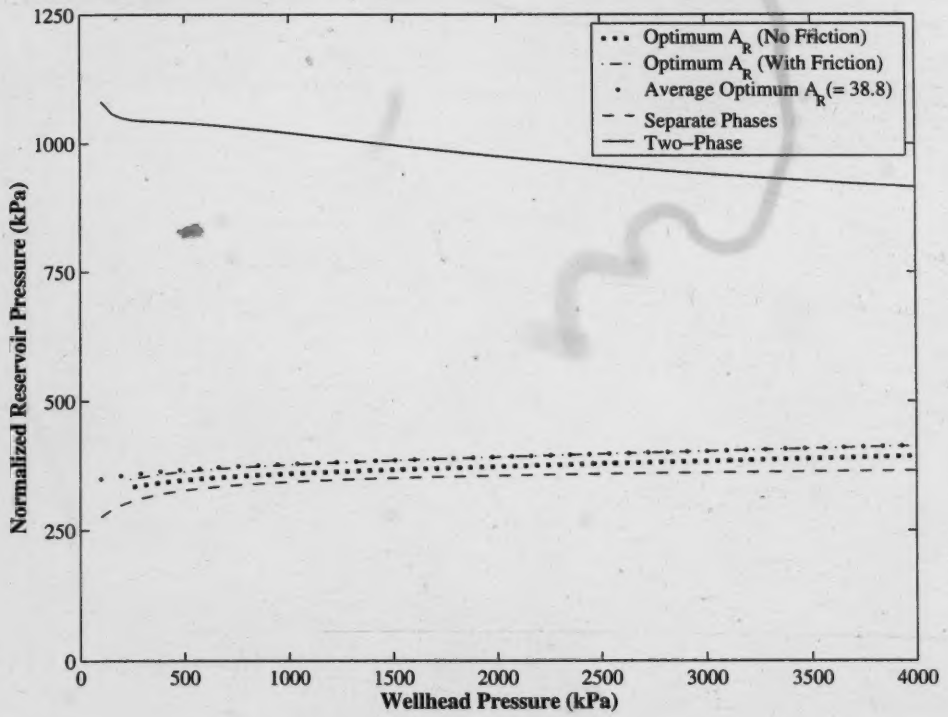


**Figure 5.12: Effect of Friction on Normalized Reservoir Pressure for Optimum Area Ratio at Constant Gas Liquid Production Rate of $7m^3/day$**

compared with the case where friction is neglected. Using the average optimum area ratio of 38.8, the normalized reservoir pressure compares very well with the optimum area ratio with friction present. Therefore, a pump

designed using the assumption of no friction will still perform very well when pump friction is significant.

### Constant Gas to Liquid Production Ratio

In the constant gas to liquid production ratio, an increase in friction will not have an effect on the optimum area ratio of the pump. This is because optimum area ratio is determined only from the gas to liquid production ratio and the pump intake pressure. However, the effect of pump friction will have some effect on the minimum reservoir pressure. To demonstrate this, the gas well performance utilizing the optimum area ratio is shown in Figure 5.13. For comparison, the results for separate and two-phase flow operation are also given. The performance of the average optimum area ratio ($A_R = 38.8$) for the constant liquid production rate is also given. All of the presented results are normalized by subtracting the static reservoir pressure.

As expected, the results in Figure 5.13 the effect of friction increases the minimum pressure required to operate the gas well. The friction effect becomes more significant at higher pressures because the optimum area ratio decreases. The average optimum area ratio ($A_R = 38.8$) requires greater reservoir pressure compared to the optimum area ratio, but still much less than required for two-phase operation.

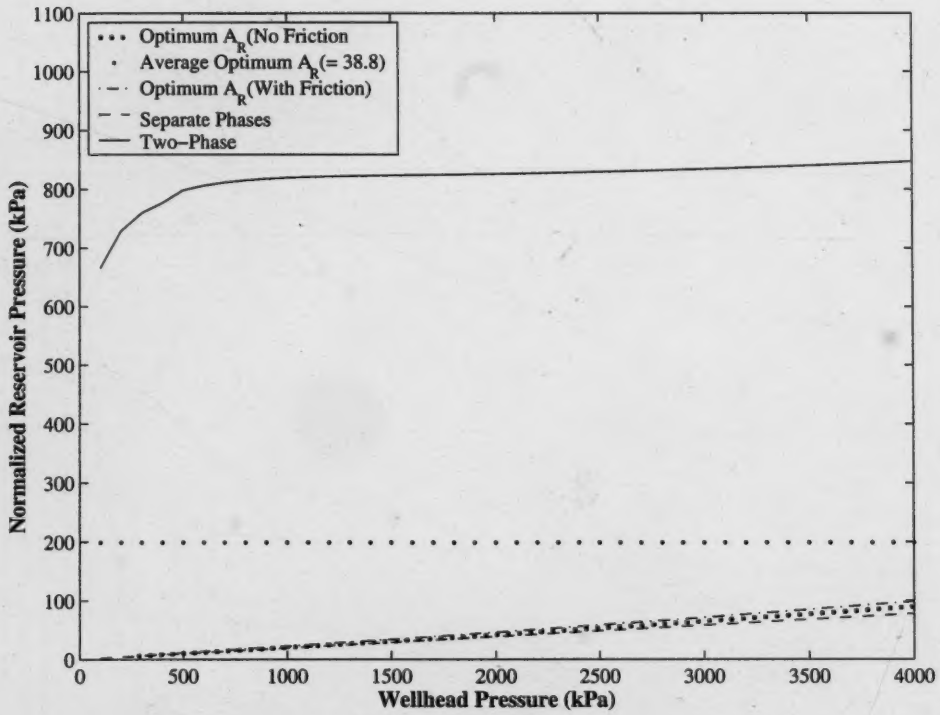


**Figure 5.13: Effect of Friction on Normalized Minimum Reservoir Pressure for Optimum Area Ratio at Constant Gas to Liquid Production Ratio of 3671**

## 5.3 Effect of Field Parameters

To gain greater insight into the applicability of using reciprocating pumps to produce the gas and liquid phases separately, the effect of changing some field variables on optimum area ratio is investigated. The field variables investigated in this research work are:

- Gas Well Depth,
- Reservoir Inflow Resistance and
- Gas Well Liquid Production.

### 5.3.1 Gas Well Depth

As mentioned earlier, the majority of natural gas wells in Alberta range in depth from about 300 m to 1250 m. To investigate this range, the model was tested using a gas well depth 1430 m (twice as deep as 715 m gas well investigated initially) and a gas well with a depth 357 m (half as deep as the inial gas well).

For the constant liquid production scenario, the results for optimum area ratio are given in Figure 5.14. The results in Figure 5.14 show that as gas well depth increases, optimum area ratio increases. This is because deeper wells will have a large hydrostatic pressure that the pump has to overcome, and thus larger area ratios are required to operate at the minimum reservoir pressure, despite the increased gas requirements for the pump.

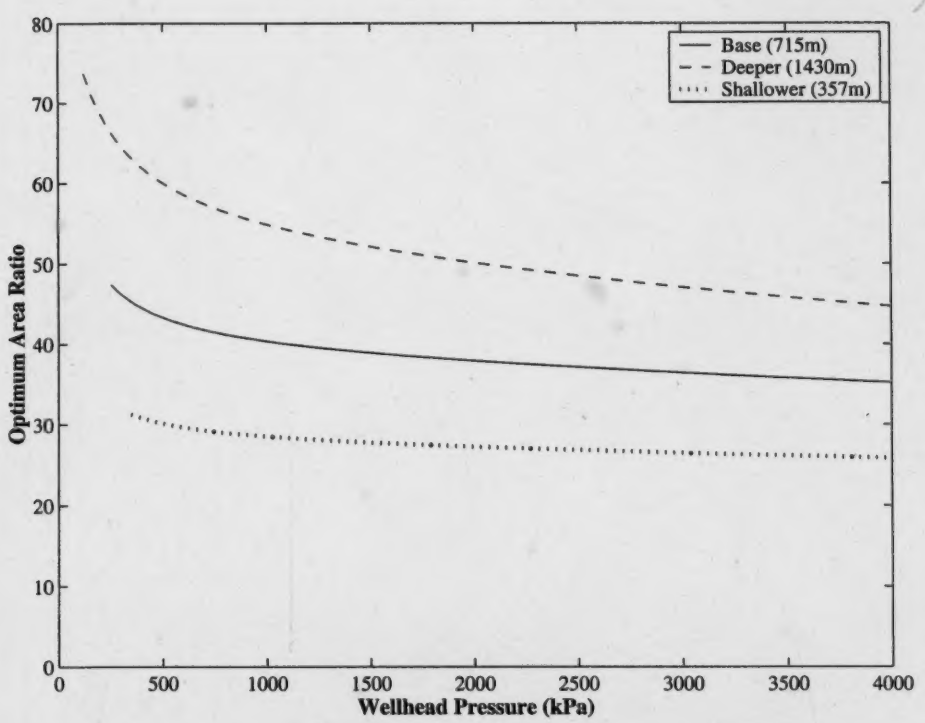


**Figure 5.14: Effect of Gas Well Depth on Optimum Area Ratio for Constant Liquid Production Rate of 7 $m^3$/day**

For the constant gas to liquid production ratio scenario, gas well depth will not have an effect on the optimum area ratio.

### 5.3.2 Reservoir Inflow Resistance

To investigate the effect reservoir inflow resistance, Equation 2.35 was modified. Recall that coefficient 'C' in Equation 2.35 represents an effective gas flow admittance. This coefficient was modified by doubling its original value to examine the effect of smaller inflow resistance, and halved to examine the effect of greater inflow resistance.

For the constant liquid production scenario, the results for optimum area ratio are given in Figure 5.15. The results in Figure 5.15 show that as reservoir inflow resistance decreases, optimum area ratio increases. This is because the incremental gas flow rate required to drive a reciprocating pump with higher area ratio does not require as significant of an increase in reservoir pressure.

Again, for the constant gas to liquid production ratio, the effect of reservoir inflow resistance has no effect on optimum area ratio.

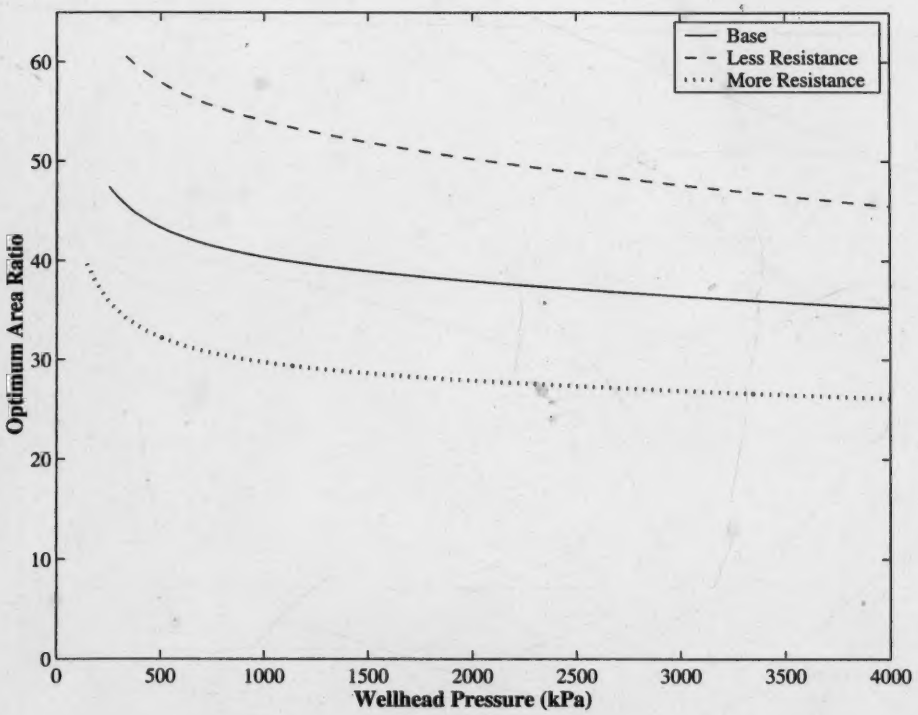


**Figure 5.15: Effect of Reservoir Inflow Resistance on Optimum Area Ratio for Constant Liquid Production Rate of 7 $m^3$/day**

### 5.3.3 Gas Well Liquid Production

To examine the effect of liquid production, changes were made for both the Constant Liquid rate and Constant Gas-Liquid ratio cases. For the Constant Liquid Rate, a liquid production rate of 14 $m^3$ (more liquid) and 3.5 $m^3$ (less liquid) per day were compared to base case of 7 $m^3$/day. Liquid Production will have an effect on the optimum area ratio for the constant gas to liquid production scenario. Therefore, the Constant Gas-Liquid ratio case, a ratio of 7342 (more liquid) and 1835 (less liquid) were compared to the base case of 3671.

For the constant liquid production ratio, the effect of liquid production on optimum area ratio is shown in Figure 5.16. The results in Figure 5.16 show that a decrease in liquid production leads to higher optimum area ratios. This is because at lower liquid production rates, less gas is required from the reservoir to drive the pump. Therefore a higher ratio can be used.

For the constant gas to liquid production ratio, the results are given in Figure 5.17. The results in Figure 5.17 show that that when less liquid is produced, a higher optimum area ratio is obtained. Again, this is because the pump requires less gas (theoretically in this case) to drive the pump.

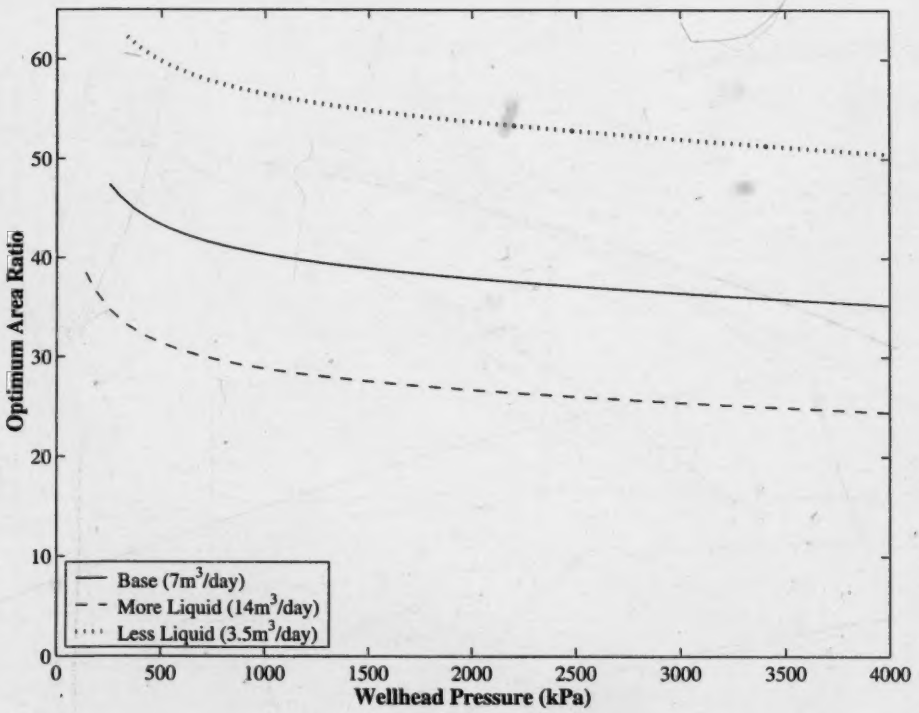


**Figure 5.16: Effect of Liquid Production on Optimum Area Ratio for Constant Liquid Production Rate**

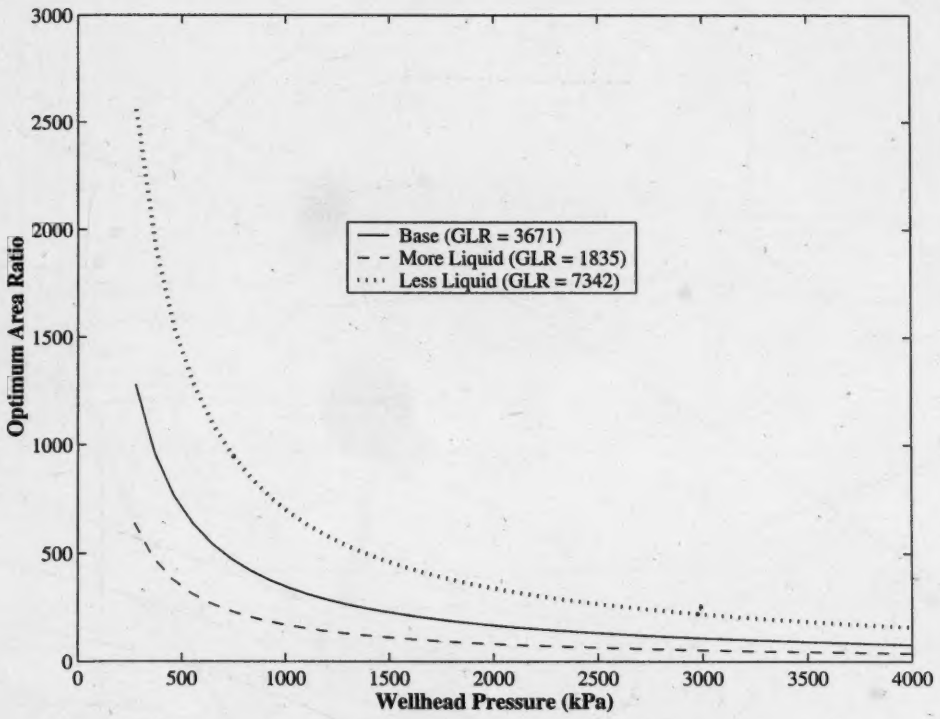


**Figure 5.17: Effect of Liquid Production on Optimum Area Ratio for Constant Gas to Liquid Production Ratio**

## 5.4 Summary

In this chapter, a mathematical model of a field application of reciprocating pump utilized in the ARC concept was presented. This model was based on mathematical and physical modelling results obtained in Chapter 3 and 4 and was reduced to a static force balance. This model was implemented into the gas well model for separate phases flow operation introduced in Chapter 2.

This modified gas well model was used first to examine the effect pump area ratio on the minimum reservoir pressure required to sustain flow. These results were compared to ones obtained in Chapter 2 for separate phase and two-phase flow operation. In general, higher area ratios lead to lower reservoir pressures. However, for the constant liquid production rate, higher area ratios require more gas to operate and thus increase the minimum reservoir pressure. Therefore, there exists an optimum area ratio to operate a gas well with this production case. For the constant gas-liquid production ratio, there is a maximum area ratio that can be utilized. For area ratios below this maximum value, the pump design requires a means of diverting gas past the drive section of the pump.

The revised gas well model was then used to determine the optimum area ratio for each liquid production case. For both cases optimum area ratio decreases with increasing gas pressure. For the constant liquid case, minimum reservoir pressure for the optimum area ratio was compared to the average optimum area ratio ($A_R = 38.8$). It was found that using this constant average optimum area ratio ($A_R = 38.8$) was suitable for design purposes. The

performance of this average optimum area ratio was then compared with the optimum area ratio ($A_R = 38.8$) for constant gas to liquid production ratio. It was found that more reservoir pressure is required to use this average ratio compared to the optimum, but much less than required for two-phase flow operation of the gas well.

The effect of friction was investigated by giving it value of 700 kPa equivalent static pressure. It was found that optimum area ratio increases due to this friction. The reservoir pressure required to sustain also increases, but using the average area ratio ($A_R = 38.8$) from before was suitable for design use even if friction is significant. The results indicate that an area ratio 38.8 will be the best design for this particular gas well.

The effect of field parameters gas well depth, reservoir resistance and liquid production on the optimum area ratio was also investigated using this revised gas well model. It was found that for constant liquid production, increased depth and decreased reservoir resistance increase the optimum area ratio. These two field parameters did not affect results for the constant gas to liquid production ratio. The effect of increased liquid production for both cases decreased the optimum pump area ratio.

CHAPTER 6

# Conclusion

## 6.1 Conclusions

A new technology patented by the Alberta Research Council to address liquid loading problems in gas wells producing from mature reservoirs has been presented. With this technology, the production of the gas and liquid phases is separate, using a pump driven by gas pressure to bring the liquid phase to the surface.

To investigate the applicability of this concept, a model was developed to simulate the performance of a gas well operating with a two phase flow and with gas and liquid phases separately. This model was then tested using data from a "typical" Alberta gas well with a depth of 715 m producing a mixture of natural gas and water. The results show that if the gas well is operated by producing the gas and liquid phases separately, it can be produced to a much lower reservoir pressure compared with the two phase flow. The reason for the lower reservoir pressure is because the gas well can operate at a lower

gas flowrate in a separate phases configuration.

The effect of gas well depth, reservoir inflow resistance and liquid production on gas well performance was also investigated. It was found that the difference in minimum reservoir pressure between the two-phase and separate phases gas well operation is greater with increased gas well depth, increased reservoir inflow resistance and increased liquid production. Therefore this new concept is best applied on deeper gas wells that produce large volumes of liquid and have higher reservoir inflow resistance.

Although any type of pump can be used to bring the liquid phase to the surface, a direct-acting reciprocating pump appeared to be ideal due to its simple design. In order to determine the applicability of reciprocating pumps, some mathematical models were developed to predict its performance. It was found that area ratio, or ratio of area driven by gas pressure to area driving the liquid, was the most important design characteristic. Thermodynamic efficiency of the pump was modelled and it was determine that the pump will operate most efficiently at higher gas intake pressures and higher area ratios. Improvement in thermodynamic efficiency by increasing gas intake pressure or the pump area ratio is greatest when the normalized pumping pressure is higher. When friction is present, thermodynamic efficiency can also be increased using higher pumping pressures to decrease the relative magnitude of friction. This holds true when normalized pressure is low. Gas utilization of the pump increases with both gas intake pressure and pump area ratio.

Experiments were performed on a reciprocating pump manufactured in-house in order to verify the mathematical models for pump performance and to examine the friction forces in this type of pump. The experimental results agreed with the model for gas utilization, where higher intake pressure and area require greater amounts of gas to drive the pump.

Friction in the pump was shown to behave in two different ways. At low pump speeds friction is dominated by static friction forces. At higher flowrates, friction is dominated largely by dynamic forces and friction increases linearly with pump speed. This indicates that pump friction can be modelled using a constant friction coefficient at higher pump speeds. Also, at higher flowrates higher area ratios, (generated with two pump drive sections) have increased friction. This is because higher area ratios require more gas to drive the pump and minor losses within the piping will increase.

Thermodynamic efficiency was also examined experimentally. It was determined that for a constant pumping pressure, the efficiency increases when gas intake pressure and/or area ratio is increased. Efficiency increases obtained in this manner were greater when the normalized pumping pressure is larger. It was also shown that because of the friction in the pump, thermodynamic efficiency can also be increased by increasing the pumping pressure to minimize the relative losses due to the friction.

Using the verified mathematical models, the original model for flow in a gas well was modified with a new pump model. The pump model was based on

the mathematical and physical modelling done previously and was reduced to a static analysis of the forces on the pumping element neglecting friction. This was advantageous as the pump performance is calculated strictly from the area ratio of the pump and assumptions about physical sizes of pump dimensions and liquid tubing sizes are not required.

This modified gas well model was used first to examine the effect pump area ratio on the minimum reservoir pressure to sustain flow. In general, higher area ratios lead to lower reservoir pressures. However, for the constant liquid production rate, higher area ratios require more gas to operate and thus increase the minimum reservoir pressure. Therefore, there exists an optimum area ratio to operate a gas well with this production case. For the constant gas-liquid production ratio, there is a maximum area ratio that can be utilized. For area ratios below this maximum value, the pump design requires a means of diverting gas past the drive section of the pump.

The modified model was used to determine the optimum area ratio for a given wellhead pressure. It was shown that the optimum pump area ratio decreases with higher wellhead pressures. It was also shown for the constant liquid production rate case that the average optimum area ratio performs nearly as well as the local optimum area ratio.

The effect of pump friction on the optimum area ratio was investigated and the results indicated that a higher area ratio is required and that the gas well will require a higher reservoir pressure in order to operate. The average area

ratio obtained for the case when friction is neglected was found to perform as well as the optimum for the case with friction present. Therefore, an area ratio of approximately 40 would be the best choice for the "typical" Alberta gas well investigated here.

The effect of gas well depth, reservoir inflow resistance and liquid production on the optimum area ratio was also investigated. It was found that a higher optimum area ratio was obtained for gas wells with greater depth, decreased reservoir inflow resistance and decreased liquid production. Since smaller pump area ratios are expected to be easier to implement, reciprocating pumps used in this new technology are best applied to gas wells with higher reservoir inflow resistance and liquid production.

## 6.2 Recommendations for Future Work

The implementation of reciprocating pumps into the ARC pumping concept needs to be proven in a field application. Therefore, the following process is recommended:

1. A gas well needs to be selected using the model developed in Chapter 2.

2. Based on the characteristics of the selected gas well, a prototype pump should be designed using the method shown in Chapter 5. The pump should be designed using the average optimum area ratio for a constant liquid production rate for the range of wellhead and reservoir pressures, at which the gas well is expected to operate. A means of diverting gas

flow past the drive section of the pump should also be designed and implemented to handle irregularities in gas to liquid production ratios.

3. If the selected gas well is shallow and friction effects within the pump are expected to be significant, a constant friction coefficient can be used to model the friction forces in the pump. In general, friction can be compensated by increasing the area ratio slightly, but neglecting friction in the design should still yield satisfactory results.

4. Friction in the pump was found to increase with higher area ratios due to pressure losses due caused by higher gas flow requirements. Therefore, the pump should be designed to minimize these pressure losses.

5. The prototype pump should be tested in the selected gas well and the results from these tests should be used to improve the model as necessary.

Further recommended research work is as follows:

1. Extension of the model to investigate gas wells that produce gas and hydrocarbon condensate. Here, the effect of vaporization and condensation needs to be included in the model.

2. The applicability of other pump designs, such as turbine drive, should be examined and their optimum design parameters determined.

3. The effect of directing some amount of the reservoir gas phase into the liquid tubing in order to reduce the hydrostatic pressure. This will have an effect on the optimum area ratio of a reciprocating pump applied to the gas well.

4. Investigate the concept of separate phases operation for gas wells that are not experiencing liquid loading problems. Operating a gas well with separate phases utilizes gas pressure more efficiently. Thus, for a given reservoir pressure, the same volumes of gas and liquid could be produced to the surface at a higher wellhead pressure in a separate phases operation compared with two-phase flow operation.

5. In this work, the reservoir inflow model used was based on the 715 m deep "typical" Alberta gas well. However, petroleum reservoirs behave differently at various gas well depths and this may have an affect on the results. Therefore in order to ensure proper selection of optimum design parameters for other gas well depths, the corresponding reservoir inflow model should be used.

6. In this work, optimum design parameters were determined for a single gas well. Production of natural gas comes from a number of wells connected to a pipeline network. Therefore research opportunities exist to determine optimum design parameters for an entire gas well network. This optimization also could be performed in conjunction with field compression optimization studies. As well, the effect of changing wellhead pressure on pump operation should also be investigated, as this is suspected to cause some controllability problems.

# Appendix A

# Selection of a "Typical" Alberta Natural Gas Well

The purpose of this appendix is to describe the process used to select a typical Alberta natural gas well. The properties of this "typical" Alberta gas well were incorporated into the gas well mathematical model described in Chapters 2 and 5..

## A.1 Classification of Alberta Gas Wells

Currently there are over 60,000 gas wells flowing in Alberta [3]. Based on this large number of natural gas wells, further work was done to categorize them. Since all gas wells are relatively unique in terms of their production characteristics, the simplest and most meaningful comparison was to categorize Alberta gas wells by depth.

In order to categorize these gas wells, the database program GeoVista was used. GeoVista is a database program that uses data submitted to regula-

tory bodies (such as the Alberta Energy and Utilities Board or AEUB) by petroleum producers. This database was accessed in July 2001 which had gas well data available up to February 2001. Using this database, the number of flowing gas wells in Alberta (63,000), British Columbia (3,000) and Saskatchewan (7,000) was determined. Alberta natural gas wells were sorted by depth are given in Table A.1 and shown graphically in Figure A.1. The results in Table A.1 and Figure A.1 show that the majority of gas wells have a depth between 300 and 1200 m. Therefore, a gas well approximately 700-750 m would most likely be considered a typical gas well for Alberta in terms of depth.

For comparison,in the United States, the average depth of a gas well is estimated to be approximately 1,700 m. This value is based on the number of wells drilled each year and the total drilling footage as reported by the American Petroleum Institute (API) [1].

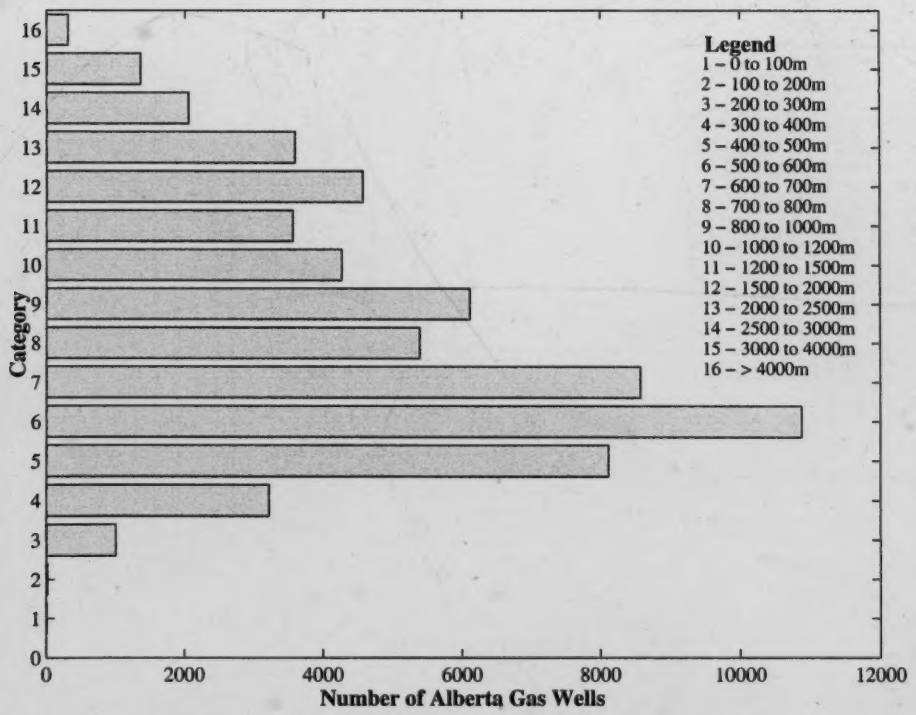


**Figure A.1: Number of Alberta Gas Wells by Depth**

**Table A.1: Alberta Gas Wells Sorted by Depth**

| Depth Range (m) | Number of Gas Wells |
|---|---|
| 0 to 100 | 10 |
| 100 to 200 | 19 |
| 200 to 300 | 1013 |
| 300 to 400 | 3221 |
| 400 to 500 | 8114 |
| 500 to 600 | 10870 |
| 600 to 700 | 8572 |
| 700 to 800 | 5391 |
| 800 to 1000 | 6111 |
| 1000 to 1200 | 4264 |
| 1200 to 1500 | 3556 |
| 1500 to 2000 | 4569 |
| 2000 to 2500 | 3586 |
| 2500 to 3000 | 2053 |
| 3000 to 4000 | 1358 |
| Greater than 4000 | 313 |

## A.2 Selection of a "Typical" Alberta Gas Well

With a typical depth in mind, the GeoVista database program was then used to select the "typical" Alberta gas well. In order to be chosen for the model, certain gas well specifications and data were required to be available from GeoVista database. This information consisted of:

- Stable and consistent production to indicate that the gas well was flowing without any production problems.
- A recent productivity test (4-point Isochronal) in order to determine reservoir inflow characteristics.
- A detailed list of the reservoir fluid composition in order to predict properties of the natural gas mixture.

### A.2.1 Gas Well Properties

Based on this criteria, the properties of a gas well with a depth of 715 m was selected to be used in the mathematical model. At the time of access, the gas well was owned by Newquest Seal and its LSD was 4-4-83-13W5/0. The properties of this gas well are given in Table A.2.

### A.2.2 Reservoir Inflow Properties

A 4-point Isochronal back-pressure test was performed on the natural gas well in March of 1997. The results of the test are given in Table A.3 and were used to determine inflow constants 'C' and 'n' in the equation of Rawlins

and Schellhardt [24]:

$$Q_{g,sc} = C(P_{RES}^2 - P_{BH}^2)^n \tag{A.1}$$

**Table A.2: Properties of "Typical" Alberta Gas Well**

| Property | Value | Comments |
|---|---|---|
| Gas Production Rate | 25.7 $10^3 m^3$/day | |
| Liquid(Water) Production Rate | 7 $m^3$/day | |
| Casing Size (O.D.) | 114.3 mm | |
| Casing Size (I.D.) | 103.9 mm | Assumed and Typical |
| Tubing Size (O.D.) | 60.3 mm | Assumed and Typical |
| Tubing Size (I.D.) | 50.6 mm | Assumed and Typical |
| Reservoir Temperature | 300K | |
| Wellhead Temperature | 288K | Assumed |

AOF refers to absolute open flow which is the maximum volume of gas the well can produce at a certain reservoir pressure. The coefficient 'C' is calculated using Equation A.1 by setting the gas well flowing pressure ($P_{BH}$) to zero and setting the gas flowrate ($Q_{g,sc}$) to the AOF value.

### A.2.3 Composition of Natural Gas Mixture

The composition of the gas mixture for the "typical" gas well is given in Table A.4. The properties of the produced water were not available so the properties (density, viscosity etc.) of pure water were used. In general, water

**Table A.3: Reservoir Inflow Properties**

| Property | Value | Comments |
|---|---|---|
| AOF | $87.94 \times 10^3$ $m^3$/day | |
| Reservoir Pressure | 3500 kPa | |
| 'n' | 1 | Given |
| 'C' | $7.179 \times 10^{-6}$ | Calculated from Equation A.1 |

from petroleum reservoirs has some amount of dissolved components that will effect the properties of the water.

**Table A.4: Composition of Gas Mixture**

| Component | Mole Fraction |
|---|---|
| $CH_4$ | 0.9170 |
| $C_2H_6$ | 0.0014 |
| $C_3H_8$ | 0.0002 |
| i-$C_4H_{10}$ | 0.0001 |
| $CO_2$ | 0.0789 |
| $H_2S$ | 0.0001 |
| He | 0.0001 |
| $N_2$ | 0.0022 |

### A.2.4 Properties of Gas and Liquid Phases

The properties of the gas mixture used in modelling are given in Table A.5.

**Table A.5: Gas Mixture and Liquid Properties**

| Property | Value | Obtained From |
|---|---|---|
| Gas Molecular Weight | 19.86 | Method in Appendix B |
| Gas Pseudocritical Pressure | 4580 kPa | Method in Appendix B |
| Gas Pseudocritical Temperature | 213.4K | Method in Appendix B |
| Gas Specific Heat Ratio | 1.25 | Method in Appendix B |
| Gas Viscosity | Function of Temperature | Method in Appendix B |
| Liquid Density | 1000 $kg/m^3$ | Assumed |
| Liquid Surface Tension | 0.072 N/m | Assumed |
| Liquid Viscosity | 0.001 Pa s | Assumed |

Some of these properties were assumed and are constant, others are functions of temperature and pressure and their calculation is given in Appendix B.

# Appendix B

# Estimation of Properties of Natural Gas Mixture

The purpose of this appendix is to describe the models used to estimate various properties of a natural gas mixture. These properties include:

- molecular weight of gas mixture,
- pseudocritical properties (pseudo-critical Temperature and Pressure),
- z-factor (deviation from ideal gas behavior),
- gas viscosity and
- gas specific heat ratio.

## B.1 Molecular Weight of Gas Mixture

The molecular weight of the gas mixture is calculated by using Kay's mixing rule, given by Kumar [17], which has the form:

$$M_{W,mix} = \sum Y_i M_{Wi} \tag{B.1}$$

$Y_i$ is the mole fraction of component $i$ and $M_{Wi}$ is the molecular weight of component $i$.

## B.2 Pseudocritical Properties

The pseudocritical properties of a gas mixture are used here primarily to determine the deviation from ideal gas behavior at higher pressures and temperatures. For a purely hydrocarbon mixture, Kay's mixing rule are used to estimate the critical properties of the mixture. Using Kay's rule, pseudocritical pressure ($P_{pc}$) is:

$$P_{pc} = \sum Y_i P_{ci} \tag{B.2}$$

and pseudocritical temperature ($T_{pc}$) is:

$$T_{pc} = \sum Y_i T_{ci} \tag{B.3}$$

where $Y_i$ is the mole fraction of component i and $P_{ci}$ and $T_{ci}$ are the critical pressure and temperature of component i respectively.

If the gas mixture contains some amount of hydrogen sulphide ($H_2S$) or carbon dioxide ($CO_2$), the pseudocritical properties must be corrected. This correction is made by utilizing the method of Wichert and Aziz [35]. In this method the pseudocritical temperature is corrected using the equation:

$$\bar{T}_{pc} = T_{pc} - \varepsilon \tag{B.4}$$

where $\bar{T}_{pc}$ is the corrected pseudocritical temperature and $\varepsilon$ is a correction determined using a correlation with the form:

$$\varepsilon = 120((Y_{H_2S} + Y_{CO_2})^{0.9} - (Y_{H_2S} + Y_{CO_2})^{1.6}) + 15(Y_{H_2S}^{0.5} - Y_{H_2S}^{0.4}) \tag{B.5}$$

where $Y_{CO_2}$ and $Y_{H_2S}$ are the mole fractions of carbon dioxide and hydrogen sulphide respectively in the gas mixture. The correction in Equation B.5 has units in degrees Rankine. Pseudocritical pressure is corrected using the equation:

$$\bar{P}_{pc} = \frac{P_{pc}\bar{T}_{pc}}{T_{pc} + \varepsilon Y_{H_2S}(1 - Y_{H_2S})} \tag{B.6}$$

where $\bar{P}_{pc}$ is the pseudocritical pressure. The correction in Equation B.6 has temperature in units Rankine and pressure in psia.

For convenience, the molecular weight and critical properties of common components in natural gas mixtures, given by Katz and Lee [16], is shown in Table B.1.

## B.3 Calculation of z-Factor

The z-factor is used primarily to correct the ideal gas equation of state when it is used to determine the density of the gas mixture. In this work, z-factor was calculated using the method of Dranchuk and Abou-Kasem [7]. This method uses an implicit model to estimate z-factor as a function of reduced temperature and pressure. The equation has the form:

$$\begin{aligned} z \;=\; & 1 + (A_1 + \frac{A_2}{T_r} + \frac{A_3}{T_r^3} + \frac{A_4}{T_r^4} + \frac{A_5}{T_2^5})\rho_r \\ & + (A_6 + \frac{A_7}{T_r} + \frac{A_8}{T_r^2})\rho_r^2 - A_9(\frac{A_7}{T_r} + \frac{A_8}{T_r^2})\rho_r^5 \\ & + A_{10}(1 + A_{11}\rho_r^2)(\frac{\rho_r^2}{T_r^3}) \exp(-A_{11}\rho_r^2) \end{aligned} \tag{B.7}$$

where $T_r$ is the reduced temperature, $\rho_r$ is the reduced density and $A_1$ to $A_{11}$ are coefficients with values given in Table B.2. Reduced density is calculated

**Table B.1: Critical Properties of Natural Gas Components**

| Component | $M_{Wi}$ | $P_{ci}$ (kPa) | $T_{ci}$ (K) |
|---|---|---|---|
| Air | 28.97 | 3771 | 132.4 |
| $CH_4$ | 16.04 | 4641 | 196.7 |
| $C_2H_6$ | 30.07 | 4883 | 305.4 |
| $C_3H_8$ | 44.09 | 4257 | 370.0 |
| i-$C_4H_{10}$ | 58.12 | 3648 | 408.2 |
| n-$C_4H_{10}$ | 58.12 | 3797 | 525.2 |
| i-$C_5H_{12}$ | 72.15 | 3330 | 461.0 |
| n-$C_5H_{12}$ | 72.15 | 3375 | 469.8 |
| $C_6H_{14}$ | 86.18 | 2976 | 503.0 |
| $C_7H_{16}$ | 100.21 | 3014 | 542.1 |
| $CO_2$ | 44.01 | 7398 | 304.3 |
| $H_2S$ | 34.08 | 9005 | 1210.3 |
| He | 4.0 | 228 | 5.2 |
| $N_2$ | 28.02 | 3392 | 132.4 |

by the equation:

$$\rho_r = \frac{0.27 P_r}{z T_r} \tag{B.8}$$

where $P_r$ is the reduced pressure.

Reduced temperature and pressure are determined using the equations:

$$T_r = \frac{T}{T_c} \tag{B.9}$$

**Table B.2: Values of Coefficients in Equation B.7**

| Coefficient | Value |
|---|---|
| $A_1$ | 0.3265 |
| $A_2$ | -1.0700 |
| $A_3$ | -0.5339 |
| $A_4$ | 0.01569 |
| $A_5$ | -0.05165 |
| $A_6$ | 0.5475 |
| $A_7$ | -0.7361 |
| $A_8$ | 0.1844 |
| $A_9$ | 0.1056 |
| $A_{10}$ | 0.6134 |
| $A_{11}$ | 0.7210 |

and

$$P_r = \frac{P}{P_c} \tag{B.10}$$

respectively where $P$ and $T$ are the pressure and temperature of the gas mixture. In utilizing Equation B.7, the corrected pseudocritical pressure and temperature are used to approximate the critical temperature and pressure.

Since Equation B.7 is implicit, an iterative technique is required to solve it. This equation is easily solved using a Newton-Raphson root-finding technique, described in most numerical methods textbooks such as Loney [21],

with an initial guess for z-factor being 1.

## B.4 Viscosity of Natural Gas Mixture

The viscosity of the natural gas mixture is estimated using the method of Lee et al [19]. This method consists of an analytic expression for viscosity with the form

$$\mu_g = K \exp(X \rho_g^y) \tag{B.11}$$

where $K$ is a coefficient calculated by the equation:

$$K = \frac{10^{-4}(9.4 + 0.02 M_{W,mix}) T^{1.5}}{209 + 19 M_{W,mix} + T} \tag{B.12}$$

$X$ is a coefficient calculated by the equation:

$$X = 3.5 + \frac{986}{T} + 0.01 M_{W,mix} \tag{B.13}$$

$y$ is a coefficient calculated by the equation:

$$y = 2.4 - 0.2X \tag{B.14}$$

and $\rho_g$ is the density of the gas mixture given by the equation:

$$\rho_g = \frac{P M_{W,mix}}{zRT} \tag{B.15}$$

Equation B.11 solves for viscosity in units centipoise. Temperature in these equations is in degrees Rankine and gas density is g/cm$^3$. Kumar [17] notes that the limitation of the Lee et al method [19] is that it does not correct for gas impurities such as carbon dioxide ($CO_2$), nitrogen ($N_2$) and hydrogen sulphide ($H_2S$).

## B.5 Specific Heat Ratio for Gas Mixture

The specific heat ratio ($k$) of the gas mixture is estimated using an equation given by Ikoku [13] with the form:

$$k = \frac{2.738 - \log_{10}\left(\frac{M_{W,mix}}{M_{W,air}}\right)}{2.328} \tag{B.16}$$

# Appendix C

# Numerical Techniques Used in the Gas Well Model

The purpose of this appendix is to discuss some of the numerical techniques used in the gas well model described in Chapters 2 and 5. The techniques described in this appendix are:

- Numerical integration of two-phase flow pressure gradient (Chapter 2).
- Numerical integration of dry gas flow pressure gradient (Chapter 2).
- Determining the minimum reservoir pressure for the constant liquid production rate (Chapter 2).
- Determining the optimum area ratio for constant liquid production rate (Chapter 5).

## C.1 Numerical Integration of Two-Phase Flow Pressure Gradient

For a natural gas well in a standard configuration (gas and liquid flowing together in a two-phase flow), the pressure at the bottom of the gas well is estimated by integrating the two-phase flow pressure gradient from the wellhead to the bottom of the well. The two-phase flow pressure gradient used in this work is given in Equation 2.32 shown below:

$$\frac{dP}{dL} = \Phi_{lo}^2 \left(\frac{dP}{dL}\right)_{lo} + \frac{Z}{L}\Big(\alpha\rho_G + (1-\alpha)\rho_L\Big)g \tag{C.1}$$

Consider the pipeline element given in Figure C.1. Numerical integration was performed on a large number of pipeline segments using an iterative implicit method. This is shown in the following equation:

$$P_2 = P_1 + \Delta L \frac{dP}{dL} \tag{C.2}$$

This implicit method used the average pressure of each pipeline segment to determine fluid properties which were used to calculate the void-fraction ($\alpha$) and friction multiplier ($\Phi_{lo}^2$) to estimate the pressure gradient used in Equation C.2. The procedure used to calculate $P_2$ for each pipeline element consists of:

1. The void fraction and friction multiplier are calculated at pressure $P_1$.
2. The pressure gradient is then calculated and used to calculate pressure $P_2$.
3. Void fraction and friction multiplier are calculated at the average of pressures $P_1$ and $P_2$. The pressure gradient is then calculated again to determine a new $P_2$.

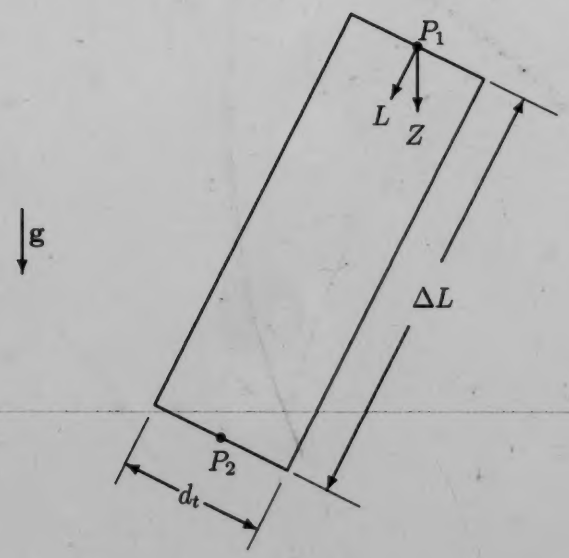


**Figure C.1: Diagram of a Pipeline Element**

4. This procedure is repeated until the calculated $P_2$ reaches convergence with a tolerance of $10^{-6}$.

In applying this technique, the gas well model was applied to 715 m gas well described in Appendix A. At a wellhead pressure of 1000 kPa, 8 pipeline elements were sufficient to reach a tolerance of 0.01 kPa for estimating the pressure at the bottom of the well. However to ensure minimum errors due to step sizes at all pressures, 50 pipeline elements were used in all of the gas well modelling.

## C.2 Numerical Integration of the Dry Gas Flow Pressure Gradient

For the flow of dry gas (no liquid phase present), the pressure gradient was modelled using Equation 2.50 and has the form:

$$\frac{dP}{dL} = -\frac{\frac{8fQ_{g,sc}^2P_{sc}^2}{T_{sc}^2\pi^2d_t^5} + g(\frac{P}{zT})^2\frac{\Delta Z}{\Delta L}}{\frac{PR}{zM_WT} - \left(\frac{4Q_{g,sc}P_{sc}}{T_{sc}\pi d_t^2}\right)^2\frac{1}{P}} \tag{C.3}$$

To determine the pressure at the bottom of the well, this pressure gradient was numerically integrated from the wellhead to the bottom using an implicit technique. This technique was performed in the same manner as for numerical integration of the two-phase flow pressure gradient. As with the two-phase flow pressure gradient, 8 pipeline elements were sufficient for modelling a 715 m gas well, but 50 were used to ensure minimal errors due to integration step sizes.

## C.3 Minimum Reservoir Pressure for Constant Liquid Production Rate

In Chapter 2, when modelling a gas well in a separate phases configuration with a constant liquid rate, there exists a reservoir pressure for a given wellhead pressure for any finite positive gas flow rate. However, in this model the purpose was to determine the minimum reservoir pressure for a given wellhead pressure. To achieve this, the gas flow rate corresponding to the minimum pressure drop from the wellhead to the reservoir was determined.

The pressure drop between the wellhead and the reservoir is calculated using three models shown schematically in Figure C.2. The three models used to calculate the reservoir pressure are the Dry Gas Flow model (numerical integration of Equation 2.50), the Pump model (Equation 2.58) and the Reservoir Inflow model (Equation 2.35). For each of these models, the pressure change calculated is a function of gas flowrate. For the Dry Gas Flow and Reservoir Inflow models, the pressure change increases with gas flowrate. For the Pump model, the pressure change decreases with gas flowrate. Therefore, there must be some gas flowrate where the pressure difference between the wellhead and reservoir is minimized.

To understand how these three models interact, reservoir pressure as a function of gas flowrate for the "typical" Alberta gas well described in Appendix A is given in Figure C.3. The results in Figure C.3 show that as gas flowrate goes to zero reservoir pressure approaches an infinite value. Also, it is seen

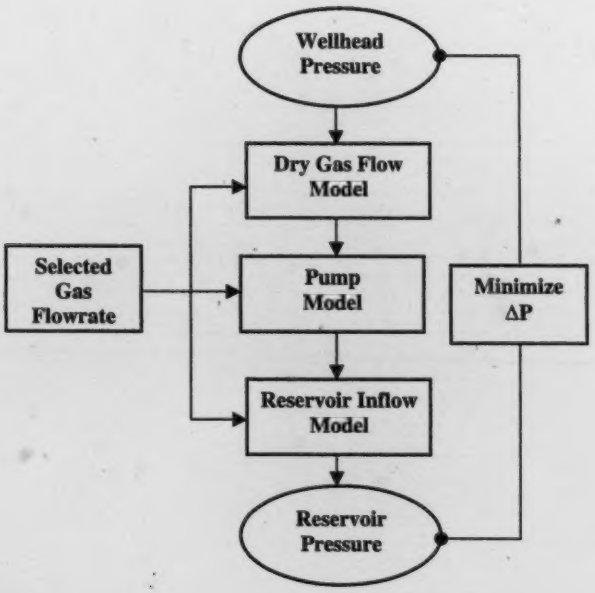


**Figure C.2: Schematic of Models Used to Calculate Reservoir Pressure**

that reservoir pressure increases as gas flow rate increases. In the middle their lies a single optimum gas flow rate of approximately $3 \times 10^3 m^3$/day where the reservoir pressure is at a minimum.

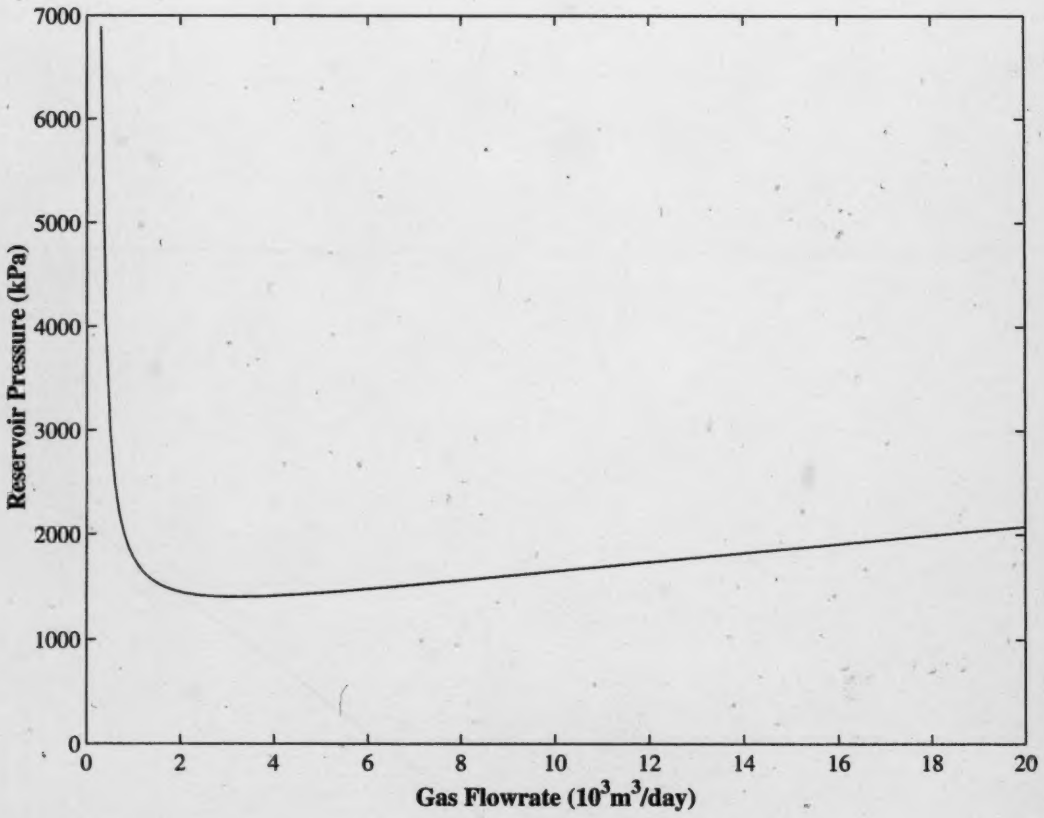


**Figure C.3: Reservoir Pressure as a Function of Gas Flowrate for the Typical Alberta Gas Well at $P_{WH} = 1000$ kPa**

To determine this optimum value in the gas well model, an algorithm was developed. Using the knowledge gained from Figure C.3, gas flowrates below the optimum value, reservoir pressure decreases with increasing flowrate. As well, at gas flowrates above the optimum value, reservoir pressure increases with gas flowrate. A schematic of this minimization algorithm is shown in Figure C.4. The algorithm consists of a marching scheme, that starts from

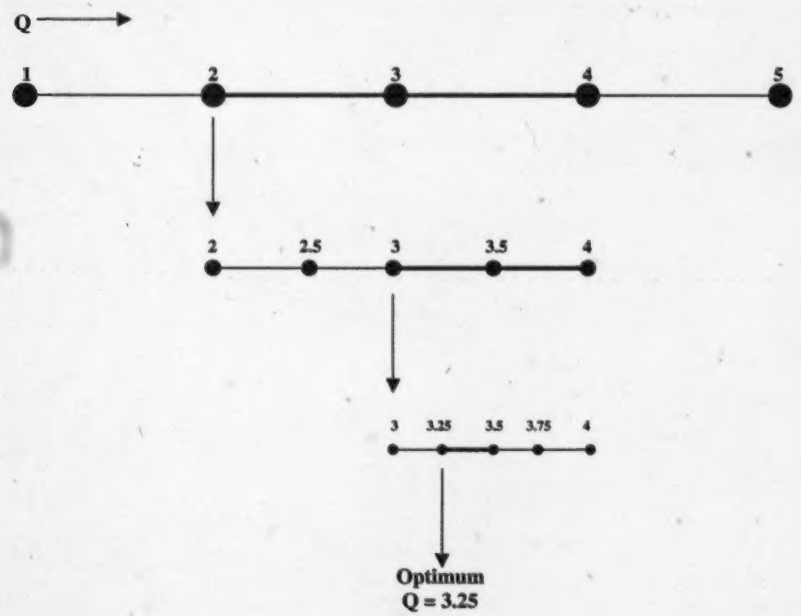


**Figure C.4: Schematic of Minimization Algorithm to Determine Minimum Reservoir Pressure**

a very small flow rate (Q = 1) and calculate its corresponding reservoir

pressure. The gas flowrate is then increased in steps of $\Delta Q = 1$, until the calculated reservoir pressure is higher than the value at the previous step (Q = 4). At this point the current gas flowrate is above the optimum gas flowrate.

The scheme then moves back two steps (Q = 2), and begins marching forward with a smaller steps ($\Delta Q = 0.5$) until the current reservoir pressure is greater then at the previous flowrate (Q = 4). The scheme again moves back two steps (Q = 3) and starts marching with steps of $\Delta Q = 0.25$ until reservoir pressure is greater than the previous step (Q = 3.5). The scheme moves back one step (Q = 3.25), and this becomes the optimum flowrate/minimum reservoir pressure. However, this process repeated using smaller step sizes to obtain a higher level of convergence.

For this research work, this optimization algorithm starts at a gas flowrate of $0.5\times10^3 m^3$/day. The initial step size is $1\times10^3 m^3$/day and is refined by a factor of 10 (although step sizes were refined by a factor of 2 in Figure C.4) every time the marching scheme is restarted. The step size is refined four times for each wellhead pressure resulting in an optimized gas flowrate converged to a value $0.0001\times\ 10^3 m^3$/day.

## C.4 Optimum Area Ratio for Constant Liquid Production Rate

In Chapter 5, a similar optimization technique was used to determine the optimum area ratio. The objective of this optimization was to determine the gas flowrate when the pressure difference between the wellhead and the reservoir is minimized. For a given reservoir pressure, this occurs when the calculated wellhead pressure is maximized. The optimum gas flowrate will then correspond with the optimum area ratio. The calculation procedure used to calculate wellhead pressure is shown in Figure C.5.
Referring to Figure C.5, the calculating procedure is as follows:

1. Starting from a given reservoir pressure, a chosen gas flow rate is used to determine the bottomhole pressure using the reservoir inflow model (Equation 2.35).

2. The bottomhole pressure is then used with gas flow rate and the liquid production rate to determine the corresponding area ratio using the gas requirement model (Equation 3.5).

3. The discharge pressure and the selected gas flow rate are then used in the dry gas flow model to determine the wellhead pressure (numerical integration of Equation 2.50).

Using this model, the wellhead pressure as function of gas flowrate for the same well conditions used in Figure C.3 is given in Figure C.6. The results in Figure C.6 show that a single maximum wellhead pressure exists for gas flowrates greater than zero. Therefore the optimization algorithm described

in the previous section was used. The only difference is that marching scheme only moves forward until the current wellhead pressure is less than the value at the previous step (as opposed to marching until the pressure at the current step is greater than the previous step).

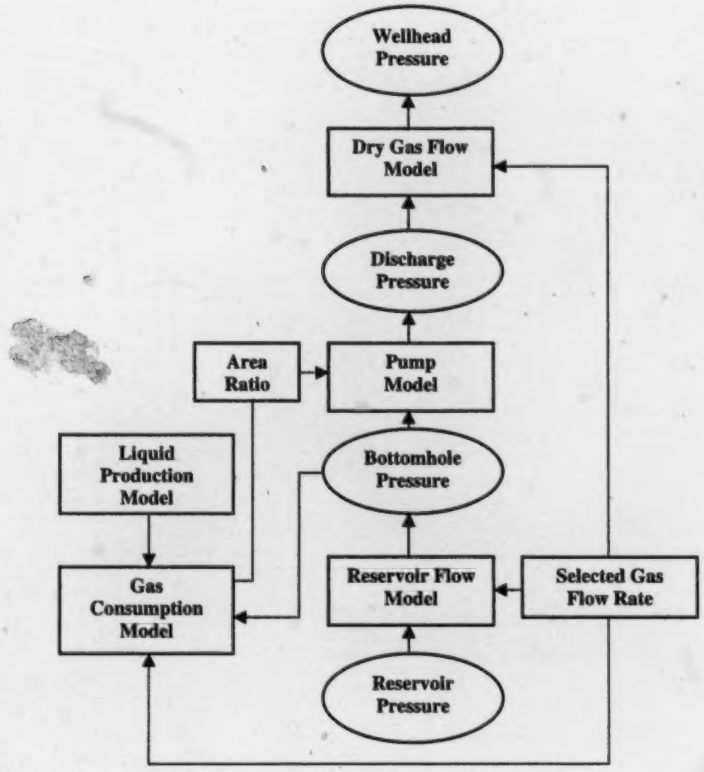


**Figure C.5: Schematic of Solution Procedure to Determine Optimum Area Ratio for Constant Liquid Rate**

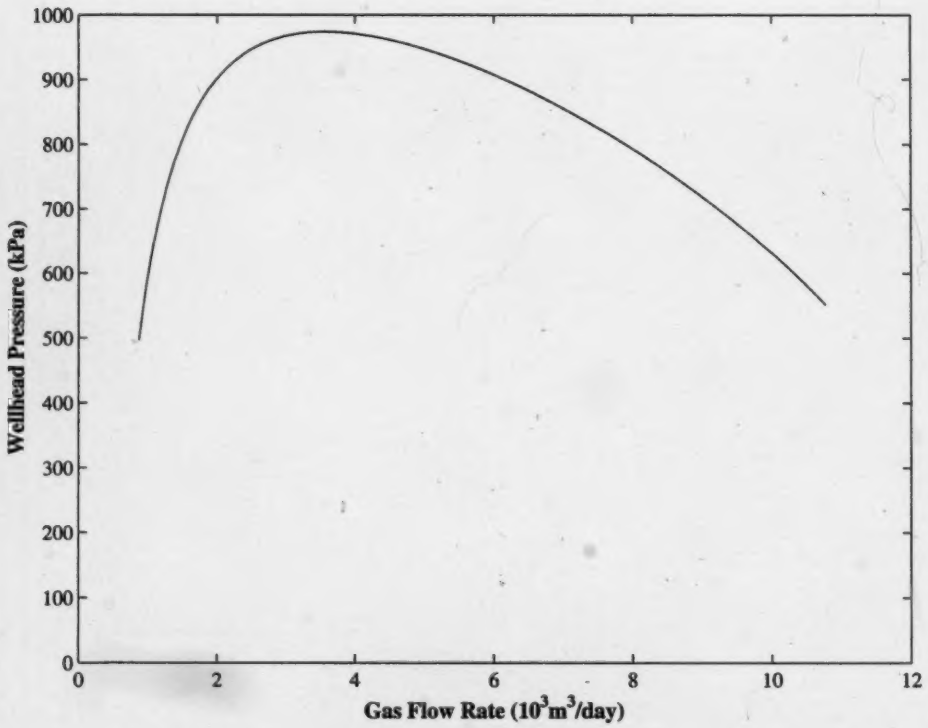


**Figure C.6: Wellhead Pressure as a Function of Gas Flowrate for Gas Well in Appendix B at Reservoir Pressure of 1200 kPa**

# Appendix D

## Tests Performed

In this research work, over 50 tests were performed. Once commissioning and de-bugging tests were completed, the tests listed in Table D.1 were performed for subsequent analysis. This table consists of the following:

- The test number.
- The date the test was performed.
- The approximate gas intake Pressure of the pump ($P_{IN}$).
- The approximate pumping pressure of the liquid ($P_{PUMP}$).
- The number of stages used in the pump operation (1 or 2). If only one is used, distinction of which stage is driven gas (Top or Bottom) is given.
- The estimated average operating temperature of the pump. This is the average liquid discharge temperature measured during the test.

Also, comments regarding the test are also given as necessary.

**Table D.1: Test Matrix**

| Test No. | Date | $P_{IN}$ (kPaa) | $P_{PUMP}$ (kPag) | No. of Stages | Pump Temp(°C) | Comment |
|---|---|---|---|---|---|---|
| 1 | 12-04-02 | 360 | n/a | n/a | n/a | Gas Friction Test |
| 2 | 12-04-02 | 620 | n/a | n/a | n/a | Gas Friction Test |
| 3 | 12-09-02 | 360 | 215 | 1 (Bottom) | 14.1 | |
| 4 | 12-09-02 | 360 | 215 | 1 (Top) | 13.2 | |
| 5 | 12-10-02 | Varies | 215 | 2 | 16.3 | GLR Test |
| 6 | 12-10-02 | Varies | 215 | 1 (Bottom) | 16.7 | GLR Test |
| 7 | 01-13-03 | 355 | 925 | 2 | 14.1 | |
| 8 | 01-13-03 | 355 | 925 | 1 (Bottom) | 12.9 | |
| 9 | 01-14-03 | 515 | 925 | 1 (Bottom) | 15.3 | |
| 10 | 01-14-03 | 420 | 925 | 2 | 13.7 | |
| 11 | 01-14-03 | 410 | 700 | 2 | 12.6 | |
| 12 | 01-15-03 | 250 | 215 | 1 (Bottom) | 14.7 | |
| 13 | 01-15-03 | 350 | 215 | 1 (Bottom) | 13.0 | |
| 14 | 01-15-03 | 550 | 215 | 1 (Bottom) | 11.3 | |
| 15 | 01-16-03 | 360 | 215 | 2 | 12.6 | |
| 16 | 01-22-03 | 550 | 215 | 2 | 16.8 | |
| 17 | 01-29-03 | 550 | 215 | 2 | 18.5 | Repeat Test No. 16 |
| 18 | 01-29-03 | 575 | 215 | 1 (Bottom) | 15.4 | Repeat Test No. 14 |
| 19 | 02-10-03 | 360 | 215 | 1 (Bottom) | 7.7 | Cold Temp Test |
| 20 | 02-10-03 | 360 | 215 | 2 | 6.6 | Cold Temp Test |

# Appendix E

# Test Data Analysis

The purpose of this appendix is to describe the techniques used to analyze the test data obtained in the experiments described in Chapter 4 of this research work. The techniques described here are:

- Analysis of Steady Data.
- Analysis of Transient Data.
- Correction to Determine Pump Intake Pressure.

## E.1 Analysis of Steady Data

Steady data was obtained using the *Steady* data acquisition program described in Chapter 4. The *Steady* data acquisition program measures 14 variables, 11 that are expected to remain constant and 3 expected to increase slowly through the duration of each test point. For each test point, 120 measurements are taken for each variable at a frequency of 1 Hz. The raw data from a test point for Test No. 14 (given in Appendix D) is shown graphically in Figure E.1.

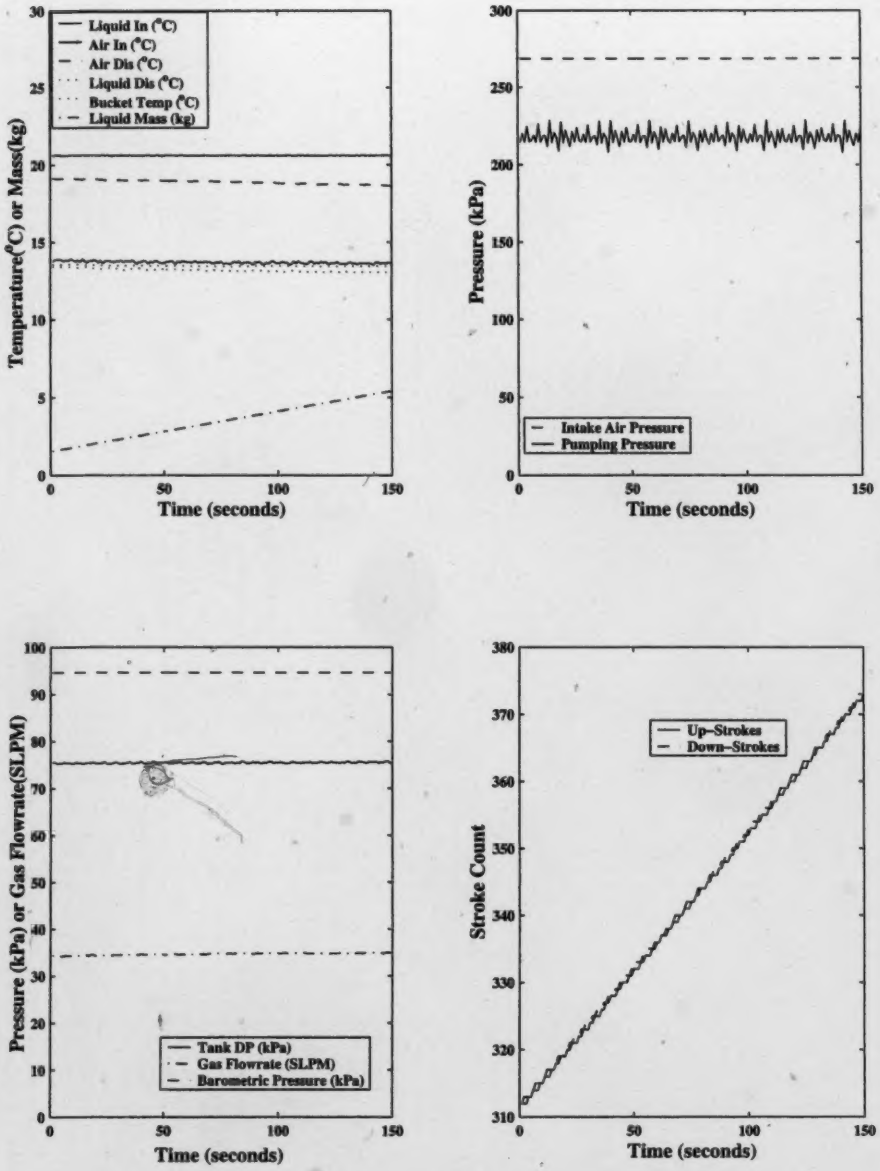


**Figure E.1: Typical Sample of Steady Raw Data**

With the exception of liquid mass and stroke counts, all of the data is analyzed by taking the arithmetic mean of each variable. This is shown in the following equation:

$$\bar{y} = \frac{\sum_{i=1}^{150} y_i}{150} \tag{E.1}$$

where $y$ is any of the measured variables. The liquid mass measurements were used to calculate the liquid flowrate. This is done by taking the amount of liquid accumulated during the test interval and dividing it by 150 seconds. Here it was assumed that water has a density of 1 kg/L.

Stroke count measurements were used as a diagnostic test for the pump. Taking the amount of liquid accumulated during the test interval and dividing it by the total number of strokes. The result should be within 5 percent of 31.7 mL/stroke to indicate proper pump operation. Deviations from this range indicated that some air was trapped in one or both or of the liquid sections.

## E.2 Analysis of Transient Data

Transient data was measured using the *Transient* data acquisition program described in Chapter 4. The *Transient* data acquisition program measures 4 variables that are constantly changing at a frequency of 20 Hz for an interval of 100 seconds. The raw data from the same test point shown in Figure E.1 is shown graphically in Figure E.2.

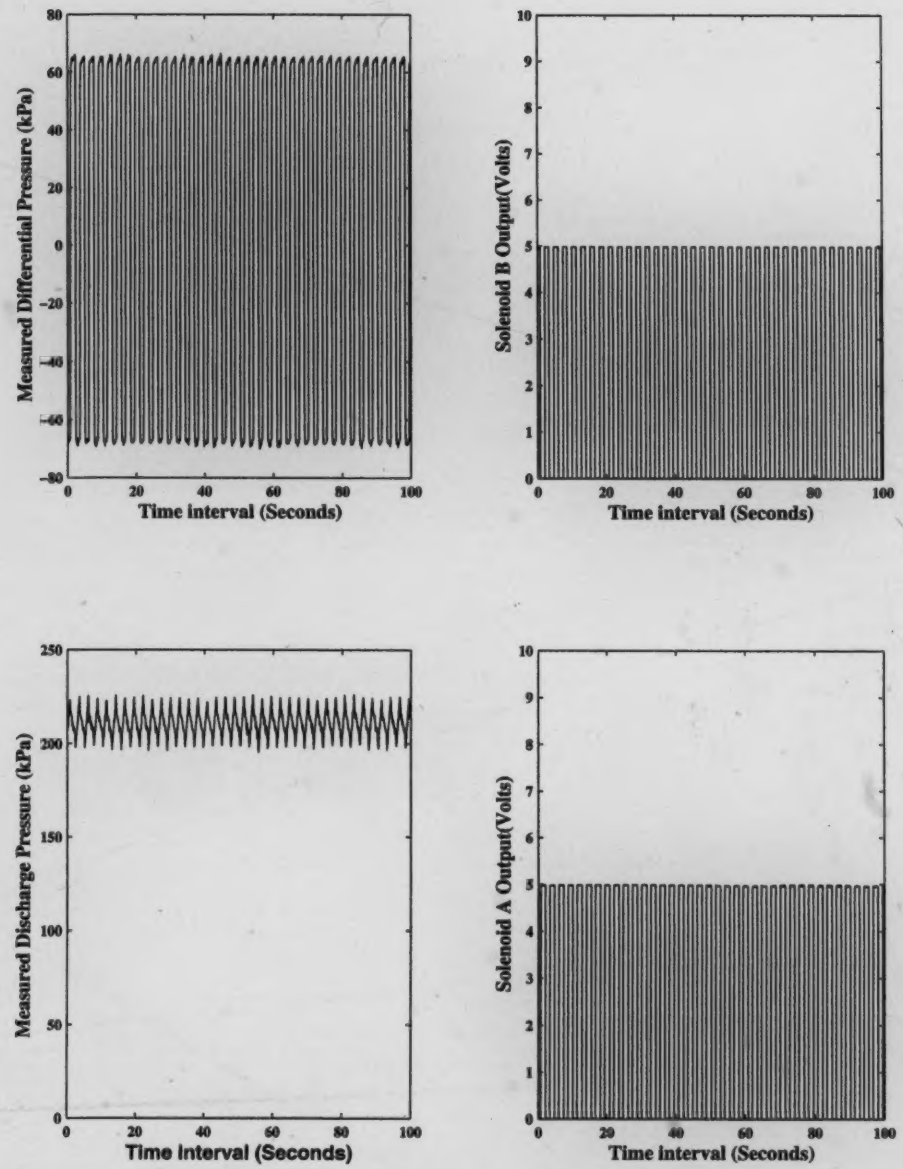


**Figure E.2: Typical Sample of Transient Raw Data**

Because of its periodic nature, differential gas pressure is analyzed by taking the root mean square of the entire trace. Root mean square is defined mathematically as:

$$y_{rms} = \sqrt{\frac{\sum_{i=1}^{2000} y_i^2}{2000}} \tag{E.2}$$

again where $y$ is a measured variable. Pumping pressure was analyzed by taking its arithmetic mean using Equation E.1. Solenoid A and B output voltage were used to indicate when pump strokes begin and end.

## E.3 Correction to Determine Pump Intake Pressure

The gas intake pressure is measured upstream of the drive section of the test pump described in Chapter 4. However, this measured pressure is not equal to the gas intake pressure in the drive section of the pump because of gas flow friction. Therefore, a correction for this measured pressure was required. For isothermal flow of an ideal gas through a duct, White [34] relates mass flow as a function of the pressures between each end of the duct. This equation has the form:

$$\dot{m}^2 = M_W \frac{P_1^2 - P_2^2}{RT(2\frac{fL}{d_t} + ln\frac{P_1}{P_2})} \tag{E.3}$$

Mass flow rate is related to the flow rate at standard conditions by the equation:

$$\dot{m} = Q_{g,sc}\frac{P_{sc}M_W}{RT_{sc}} \tag{E.4}$$

Using this relation in Equation E.3 it becomes:

$$Q_{g,sc}^2 = \frac{RT_{sc}^2(P_1^2 - P_2^2)}{P_{sc}^2 M_W T(2\frac{fL}{d_t} + ln\frac{P_1}{P_2})} \tag{E.5}$$

It was assumed that relative change in pressure from $P_1$ to $P_2$ is small. Therefore Equation E.5 can be simplified. It was also assumed that the $f\frac{L}{d_t}$ term was constant for all flow rates. As well, experience in using the experimental apparatus has found the gas temperature $T$ does nor vary significantly and was assumed constant. All remaining terms except, $P_1$, $P_2$ and $Q_{g,sc}$ are constant and can be lumped together. Therefore Equation E.5 can be reduced to:

$$Q_{g,sc}^2 = B(P_1^2 - P_2^2) \tag{E.6}$$

where $B$ is a constant determined empirically. Here $P_1$ corresponds with the measured intake pressure ($P_{meas,IN}$) and $P_2$ is the gas intake pressure of the drive section ($P_{IN}$). To determine $B$ tests were performed on a modified form of the gas flow loop shown in Figure E.3. In this flow loop, gas is allowed to flow continuously from the intake tank through the solenoid valve and to the discharge tank. $P_{meas,IN}$ is determined by adding the pressures measured using PGT A100 and PAT A100. $P_{IN}$ is obtained by subtracting the pressure measured by DPT A101 from $P_{meas,IN}$. $Q_{g,sc}$ is determined from the measurement made by Mass Flow Meter A100. Empirical constant $B$ is then determined by plotting $Q_{g,sc}^2$ as a function of $P_{meas,IN}^2 - P_{IN}^2$. $B$ will be the slope of the line of best fit through the data points.

This process was carried out at an tank intake pressure of approximately

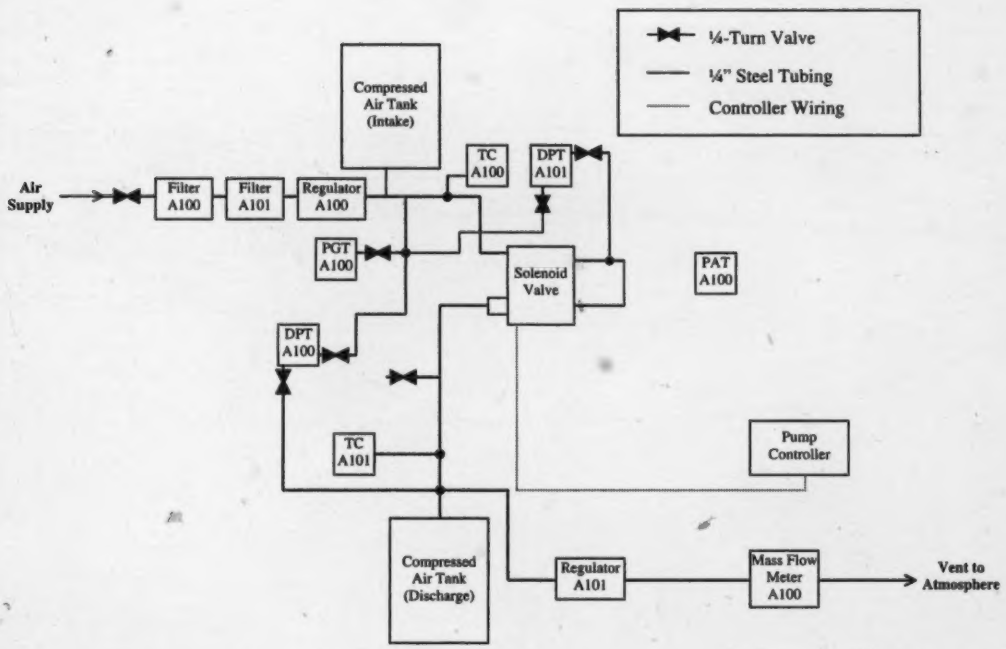


**Figure E.3: Schematic of Gas Flow Loop used to Determine Pressure Correction**

370 kPa and gas flow rates from 15 to 105 SLPM . The results of these tests is shown in Figure E.4. As expected the results in Figure E.4 are linear. Using a least squares approach, the slope, and hence coefficient $B$, was determined to be 0.44.

To verify the model is applicable at other gas pressures, the same test was carried out at a tank intake pressure of approximately 620 kPa. The results from these experiments are shown in Figure E.5 with the empirical model

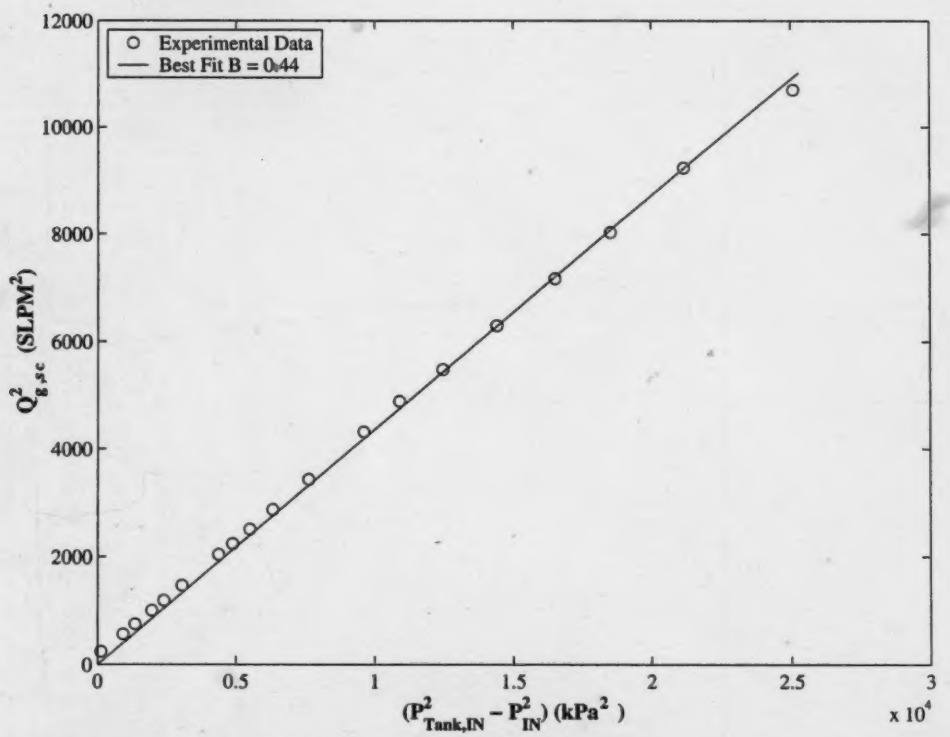


**Figure E.4: Experimental Results for Determining Empirical Constant 'B' to Correct the Gas Tank Intake Pressure**

for comparison.The results in Figure E.5 indicate excellent agreement with the empirical model. Therefore the empirical model was deemed appropriate for correcting the measured intake pressure. Re-arranging Equation E.6 and inserting empirical constant $B$ the correction for gas intake pressure has the form:

$$P_{IN} = \sqrt{P^2_{meas,IN} - \frac{Q^2_{g,sc}}{0.44}} \tag{E.7}$$

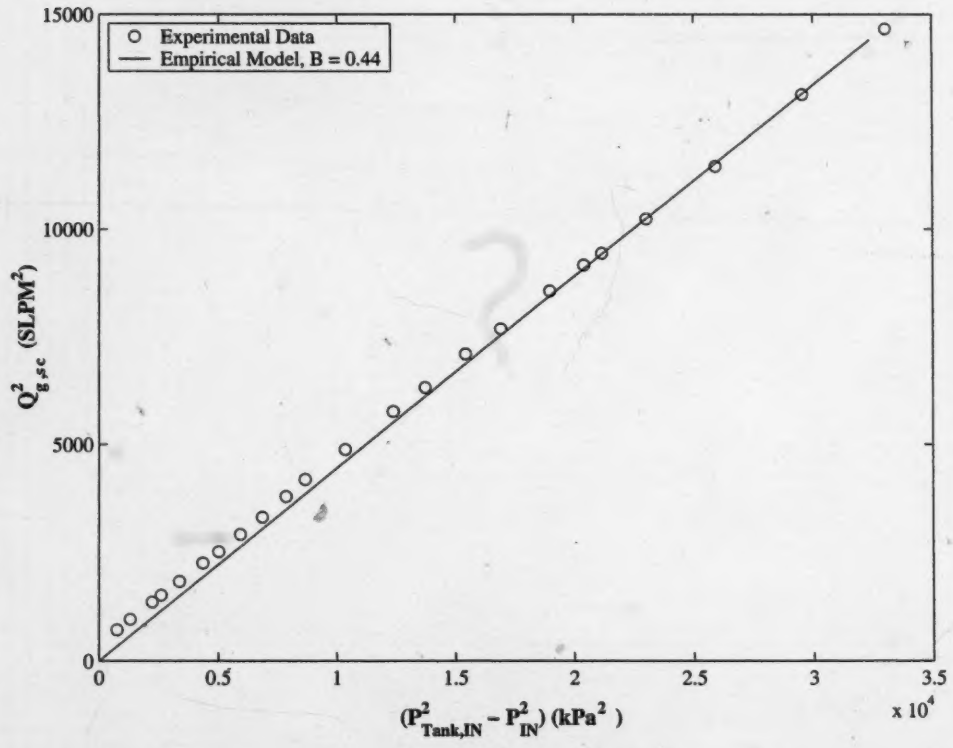


**Figure E.5: Experimental Results for Validating Empirical Constant 'B' to Correct the Gas Tank Intake Pressure**

# BIBLIOGRAPHY


[1] American Petroleum Institute, 1999, Basic Petroleum Data Book, Petroleum Industry Statistics **19**(1) January, API, Washington D.C., U.S.A.

[2] Beauregard, E. and Fergurson, P.L., 1982, "Introduction to Plunger Lift: Applications and Limitations," Society of Petroleum Engineers 1982 Rocky Mountain Regional Meeting, Billings MT USA, SPE 10882.

[3] Bott, R., 1999, "Our Petroleum Challenge: Exploring Canada's Oil and Gas Industry," Petroleum Communication Foundation, Calgary.

[4] Brodkey, R. S. and Hershey, H.C., 1988, Transport Phenomena: A Unified Approach, McGraw-Hill, New York, Chap. 9.

[5] Coleman, S.B., Clay, H.B., McCurdy, D.G. and Norris, H.L., 1991, "A New Look at Predicting Gas-Well Load-Up," Journal of Petroleum Technology, **43**(3)

[6] Cullender, M.H. and Smith, R.V., 1956, "Practical Solution of Gas-Flow Equations for Wells and Pipelines with Large Temperature Gradients," Transactions of the AIME, **207**, pp. 281-287

[7] Dranchuk, P.M., Abou-Kasem, J.H. 1975, "Calculation of Z-factor for Natural Gases Using Equations of State", Journal of Canadian Petroleum Technology, **14**(3)

[8] Friedel, L., 1979, "Improved Friction Pressure Drop Correlations for Horizontal and Vertical Two-Phase Flow", European Two-Phase Flow Group Meeting, Ispra, Italy (quoted by Hewitt [11]).

[9] Gasbarri S. and Wiggins W.L., 1997, "A Dynamic Plunger Lift Model for Gas Wells," Society of Petroleum Engineers 1997 Production Operations Symposium, Oklahoma City, OK USA, SPE 37422.

[10] Henshaw, T. L., 1987, Reciprocating Pumps, Van Nostrand Reihnhold, New York, Chap. 1.

[11] Hewitt, G.F., 1982, "Pressure Drop and Void-fraction", Handbook of Multiphase Systems, G. Hestroni eds, McGraw-Hill, New York.

[12] Hinze, J.O., 1949, "Critical Speeds and Sizes of Liquid Globules," Applied Scientific Research **A-1**(4), pp. 273.

[13] Ikoku, C. U., 1984, Natural Gas Production Engineering, John Wiley and Sons, New York, Chap 5, 8.

[14] Ilobi, M.I. and Ikoku, C.U., 1981, "Minimum Gas Flow Rate for Continuous Liquid Removal in Gas Wells," Society of Petroleum Engineers 56th Annual Fall Technical Conference and Exhibition, San Antonio, Texas USA, SPE 10170.

[15] Juvinall, R.C. and Marshek, K.M., 1991, Fundamentals of Machine Component Design, 2nd Edition, John Wiley and Sons, New York, USA, Chap. 13.

[16] Katz, D.L, and Lee, R.L., 1990, Natural Gas Engineering, Production and Storage, McGraw-Hill Publishing Company, New York, Chap 4.

[17] Kumar, S., 1987, Gas Production Engineering, Gulf Publishing Company, Houston Texas, Chap. 3.

[18] Lea, J.F and Tighe, R.E., 1983,"Gas Well Operation With Liquid Production," Society of Petroleum Engineers 1983 Production Operation Symposium, Oklahoma City, OK USA, SPE 11583.

[19] Lee, A.L., Gonzalez, M.H. and Eakin, B.E., (1966), "The Viscosity of Natural Gases", Journal of Petroleum Technology, **18**( 8).

[20] Lockhart, R.W. and Martinelli, R.C., 1949, "Proposed Correlation of Data for Isothermal Two-Phase Two-Component Flow in Pipes," Chem. Eng. Prog. **45**, pp. 39-48.

[21] Loney, N.W., 2001, Applied Mathematical Methods for Chemical Engineers, CRC Press, New York, Chap. 9.

[22] Moran, M.J., Shaprio, H.N., 1996, Fundamentals of Engineering Thermodynamics 3rd Ed, John Wiley & Sons, USA, Chap. 6

[23] Premoli, A., Francesco, D. and Prina, A., 1970, "An Empirical Correlation for Evaluating Two-Phase Mixture Density under Adiabatic Condi-

tions", European Two-Phase Flow Group Meeting, Milan, Italy (quoted by Hewitt [11])

[24] Rawlins E.L., and Schellhardt, M.A., 1936, Back-Pressure Data on Natural Gas Wells and Their Application to Production Practices, United States Bureau of Mines Monograph 7,

[25] Ridley, R.K., DeRocco M., "Method for Underground-Reservoir Fluids Production with Pump Drive Contained within the Wellbore", United States Patent #5,860,795, Issued January 19, 1999 to the Alberta Research Council.

[26] Ridley, R.K., DeRocco M., "Reservoir Fluids Production Apparatus and Method", United States Patent #6,234,770, Issued May 22, 2001 to the Alberta Research Council.

[27] Ridley, R.K., DeRocco M., "Reservoir Fluids Production Apparatus and Method", Canadian Patent CA2200665, Issued July 31, 2001 to the Alberta Research Council.

[28] Saleh, S. and Jamae'y, M., 1997, "Foam-Assisted Liquid Lifting in Low Pressure Gas Wells," Society of Petroleum Engineers 1997 Production Operation Symposium, Oklahoma City, OK USA, SPE 37425.

[29] Turner, R.G., Hubbard, M.G. and Dukler A.E., 1969, "Analysis and Prediction of Minimum Flow Rate for the Continuous Removal of Liquids from Gas Wells", Journal of Petroleum Technology **21** (11),pp. 1475-1482.

[30] Vosika, J.L., 1983, "Use of Foaming Agents to Alleviate Liquid Loading in Greater Green River TFG Wells," Society of Petroleum Engineers 1983 Symposium on Low Permeability, Denver, CO USA, SPE 11644.

[31] Wallis, G.B., 1969, One-Dimensional Two-Phase Flow, McGraw-Hill, New York, Chap 11.

[32] Whalley, P.B., 1987, Boiling, Condensation and Gas- Liquid Flow, Oxford University Press, New York, Chap 6.

[33] White, F. M., 1994, Fluid Mechanics 3rd Ed, McGraw-Hill, USA, Chap. 6.

[34] White, F. M., 1991, Viscous Fluid Flow 2nd Ed, McGraw-Hill, Boston, Massachusetts, Chap. 3.

[35] Wichert, E. and Aziz, K., 1972,"Calculation of Z's for Sour Gases," Hydrocarbon Processing,**51**(5), 119-122.

[36] Young, K.L., 1967, "Effect of Assumptions Used to Calculate Bottom-Hole Pressure in Gas Wells" Journal of Petroleum Technology, **19**(4), pp. 547-550